Uranium metallogeny in the North Flinders Ranges region of South Australia

Pierre-Alain Wülser

Department of Geology and Geophysics
Adelaide University

This thesis is submitted in the fulfilment of the requirements for the degree of Doctor of Philosophy in the Faculty of Science, Adelaide University

June 2009

THE UNIVERSITY OF ADELAIDE
AUSTRALIA

PART ONE

The Sandstone-hosted Beverley Uranium Deposit:

MINERALOGY, GEOCHEMISTRY AND TIME-CONSTRAINED MODEL FOR ITS GENESIS

(Paralana High Plains, Lake Frome basin, South Australia)

1 Introduction & Location

The Beverley uranium deposit is located on the Eastern piedmont flanking the North Flinders Ranges towards the Lake Frome. It lies approximately 13 km away from the crystalline basement of the Mt Painter Inlier in the Paralana High Plains on the Wooltana Station (Fig.4). Beverley was the first sedimentary uranium deposit to have been discovered in Australia and since 2000 it is mined using in-situ acid leaching techniques (ISL). The Transoil-Petromin Group identified a radioactive anomaly extending over 50 km^2 in November 1969. Following this first hit, they started a drilling campaign, which resulted in the definition of the Beverley deposit, in join venture with Western Uranium Ltd. Regional prospecting in the Tertiary sediments of the Lake Frome basin resulted in the discovery of numerous additional uranium occurrences or deposits (e.g. Honeymoon, Gould's Dam, Oban and East Kalkaroo). Uranium exploration drilling programs also resulted in the first studies of the stratigraphy and sedimentology of the basin (Callen, 1974, Callen, 1975, Callen and Tedford, 1976, Wopfner *et al.*, 1974). In the following years, several syntheses on the sediment-hosted uranium deposits of the Lake Frome basin were published: (Brunt, 1978, Curtis *et al.*, 1990, Ellis, 1980). Finally, in November 2000, after 25 years of political tribulations, the Beverley deposit started producing, operated by Heathgate Resources Pty Ltd. By the end of 2006 remaining reserves were estimated at ~13,000 tons of U_3O_8 at a grade of 0.25% U_3O_8 and ~5,200 tons had been produced (Heathgate Resources Pty Ltd, 2005). Uranium is recovered through the In-Situ Leaching (ISL) method, using an acid, oxidising (H_2SO_4-$O_{2(g)}$) liquor to extract U from the permeable, poorly reactive sediments. Recent exploration in the immediate vicinity of Beverley has lead to the discovery of a new mineralised zone to the west of the mine: the Four Mile Creek prospect. The new prospect is divided into Four Mile West and Four Mile East deposits.

The aim of this study is to establish the genesis of the Beverley deposit in its geological framework. The approach is essentially based on the study of the mineralogy and geochemistry of the hosting and surrounding sediments. We also provide the first U-Pb analytical data on the timing of the Lake Frome basin uranium mineralisations. In addition, we discuss some geological features in the Mount Painter Domain to document the sources of uranium. The recent tectonic event in the North Flinders Ranges (Neotectonics) is integrated in the regional geology for a better understanding of the formation of the successive basins (subsidence) and the uplift of the ranges. This work fills a gap in the literature on uranium deposits in South Australia and provides new ideas and tools for their study and for prospecting (zircon provenance, carnotite dating, mineralogy and geochemistry).

This study has been conducted using a drill core available for study at the Primary Industries and Resources South Australia (PIRSA) core library facility. The drill core Nr 137-058, named WC2, was collected by Western Nuclear in the central ore zone of the Beverley deposit in February 1972. Using this core has the advantage to eliminate possible contamination or alteration by several leaching tests that were conducted early on.

2 Geological setting

2.1 General geology

The northern tail of the Flinders Ranges has the particularity of showing two unique tectonic windows on the underlying crystalline Proterozoic basement of the Adelaide Geosyncline (AG) or Adelaide Rift Complex (Fig. 1). The so-called Mt Painter and Mt Babbage Inliers are together named the Mt Painter Domain (MPD) (Brugger *et al.*, 2005). A major tectonic fault crosscuts and delimitates the inliers on its Eastern border: the Paralana Fault Zone; this structural corridor forms a cluster of fault ramifications along a general NE-SW trend. The basement rocks in the MPD are Mesoproterozoic and not older than ~1590 Ma (Fanning *et al.*, 2003); the formations interpreted to be Paleoproterozoic by (Teale, 1995) are in fact younger. The granitoids of the MPD are unusually rich in uranium and thorium, with frequent metasomatic enrichments reaching ~100 ppm U at a kilometre scale (Wülser *et al.*, 2005), and numerous primary uranium occurrences are widespread throughout the basement rocks (Coats and Blissett, 1971). The MPD belongs to the Curnamona Province, forming its north-east corner. Most parts of the Curnamona Province are recovered by the Adelaide Geosyncline rifting volcano-sedimentary sequences deposited from the Neoproterozoic (~830 Ma) to the Cambrian. The end of the sedimentation in the Adelaide Geosyncline marks the beginning of the Delamerian orogeny (514 to 490 Ma) (Foden *et al.* 2006). Both Mesoproterozoic basement and the volcano-sedimentary rift sequences were subject to metamorphism (amphibolite facies in most of MPD (Sandiford *et al.*, 1998)). Delamerian magmatism in the MPD is restricted to pegmatite and small leucogranite intrusions. A second period of magmatism begins, clearly after the end of the orogenesis (~440 Ma), with granitic intrusions at (Mudnawatana tonalite, Paralana granodiorite and British Empire granite) (Fig. 1) (Elburg *et al.*, 2003). The central area of the province is represented by the Lake Frome basin, beneath which a thick sequence of sediments were deposited in a number of evolving sub-basins. The sedimentary record extends from Cambrian to present but a major unconformity marks the basis of the Cretaceous. The Beverley deposit is hosted in Miocene formations. For a good comprehension of its regional environment and later its genesis, we will detail the underlying Mesozoic formations to the Quaternary formations as well as the history of the successive basins.

2.1.1 Cretaceous formations

The Lower Cretaceous formations are present both in the Lake Frome and Eyre basins (Fig. 5) (Cadna-owie Formation) and on the basement in the MPD or Adelaide Rift Complex sediments (Parabaranna Sandstone) (Krieg *et al.*, 1995). The lower Cretaceous is mainly composed of detrital quartz-rich sandstones to conglomerates with quartzite/quartz pebbles. The recent discovery of glacial diamictite at the basis of the Cadna-owie formation, West of the Petermorra Springs at Trinity Well (Fig. 4), is the first definitive evidence for an Early Cretaceous glaciation (Alley and Frakes, 2003) for which palynology data give ages ranging from Berriasian to Valanginian (144 to 131 Ma). Paleolatitudes around the North Flinders Ranges are ~66°S during the Lower Cretaceous. Other evidences for cool climate previously mentioned in the area include: (1) a striated pebble found at the basis of the Parabaranna Sandstone near Moolawatana (David, 1950); (2) a volcanic pebble of Devonian age from the basal conglomerates of the Bulldog formation, north of the Mount Babbage Inlier (Teale *et al.*, 1995). This pebble has been interpreted to have originated from the Lachlan Fold belt and been carried by glaciers during the Permo-Carboniferous glaciation; (3) polished basement outcrops with overlying Devonian boulders found in the MBI have also been attributed a glacial origin (Sheard and Flint, 1992). The polished surfaces have been preserved by later burial and were only recently exhumed together with the associated erratics.

The post-glacial environment of deposition is fluviatile and the area bordering the North Flinders form the edge of the basin. The Parabaranna Sandstone marks the transitional facies to a terrestrial environment (Ludbrook, 1966) and probably contains abundant Early Cretaceous morainic materials. The so-mapped Cretaceous mesa near the Paralana Hot Springs sits directly on the local basement and shows large silicic volcanic pebbles and cobbles, whose provenance is still uncertain (Campana *et al.*, 1961a). However they clearly were deposited in fluvial or fluvioglacial environments.

The depositional environment changes into marine conditions during the Aptian for most of the basin. The widespread related formation (Bulldog Shale) (Fig. 5) is essentially formed of grey mudstones, siltstones with clays, pyrite, carbonaceous matter and classic detrital minerals. The depositional environment was shallow in the southern part of the basin. The Bulldog formation is overlain by the Coorikiana Sandstone, a tidal to intertidal formation. This latter formation is present south west of the basin but has not been confirmed around the North Flinders Ranges area (Krieg *et al.*, 1995).

The Upper Cretaceous sedimentation in the Eromanga basin (Winton formation) is a non-marine shale, siltstone, sandstone with minor coal layer sequence (Krieg *et al.*, 1995). Although this formation has not been described in the Southern part of the basin, we mention it here because it generally forms the substrate of the following Cainozoic sediments. Ferromagnesian minerals of volcanic origin are present in the sandy fractions of the Winton Formation as well of large amounts of organic matter. The environment of sedimentation is interpreted as low-energy fluvial to lacustrine, with marshes and lakes accumulating organic matter. Sediments contain dolomite, and paleowaters are

thought to have been magnesium-rich. The ultimate source of the volcanic material is interpreted to be coming from the volcanoes in eastern Australia but probably relates to the Early Cretaceous reworked fluvioglacial materials.

The final stage of the Upper Cretaceous times is dominated by erosion and weathering and the basin is shallowing, with drainages flowing towards the south-west, perhaps even as far as into the active rift system between Antarctica and Australia (Bight Basin) (Senior and Mabbutt, 1979). Concerning the neighbourhood of Beverley, we cannot clearly state whether Upper Cretaceous formations are still present or not. Geochronology data are scarce and the vicinity of the sub-outcropping and locally outcropping crystalline basement of the MPD makes lateral correlation difficult. As mapped on the 1 mile Geological Map Series (1:63360) (Campana *et al.*, 1961a, Campana *et al.*, 1961b), some outcrops in the Four Mile Creek bed and next to the ranges could be possibly Upper Cretaceous members, but palynology data is lacking. These outcrops have been omitted from the Figure 4.

2.1.2 Palaeocene to Oligocene (Eyre Formation, silcretes and ferricretes)

The Cainozoic sedimentation around the North Flinders Ranges area takes place in a non-marine environment. Following a ~30-50 Ma period of weathering and erosion, sedimentation starts again in the Lake Eyre Basin during the Late Palaeocene (Callen *et al.*, 1995a, Wopfner *et al.*, 1974). The Eocene Eyre Formation is widespread overall the basins and present west, north, and east of the North Flinders Ranges. There is no clear evidence whether the Eocene sedimentation extended continuously over the position of the actual Ranges or not. The two distinct basins: the Lake Frome area (Callabonna sub-basin) and the Lake Torrens area (Torrens basin) were most likely separated by a high standing level during the Eocene. Some potential remnants of Eocene sediments are recognised between the two basins on Adelaide Geosyncline series (Coats, 1973), and an E-W or NE-SW Cainozoic drainage across the Flinders Ranges could have existed south of the MPD. The sediments are composed mostly of carbonaceous pyritic mature sands, locally intercalated with clays and gravels beds (Wopfner *et al.*, 1974); they are interpreted to have been deposited in braided rivers during the epeirogenic uplift of the North Flinders ranges and the Olary Ranges and synchronous subsidence of the Lake Eyre basin (Callen *et al.*, 1995a). Evidence of active faulting and uplift is recorded by fission-track ages around the Paralana Fault Zone, East of the Paralana High Plains and Beverley (Foster *et al.*, 1994, Mitchell *et al.*, 2002).

Numerous silcrete levels occur in the North Flinders Ranges (Gammon Ranges) and in the Sturt Ranges sediments. They have been interpreted to be part of or the upper Eyre Formation (Callen *et al.*, 1995a, Krieg, 1985). However, there is no strong evidence to exclude a younger age such as Miocene, and the mentioned authors also interpret silcrete as a possible Miocene shoreline facies. However, these silcrete have never been described in drill-holes.

2.1.3 Late Oligocene to Miocene (Namba, Neuroodla and Etadunna formations)

Sedimentation during the Miocene still operates in lacustrine, alluvial environment. Around the Lake Eyre, sediments are calcareous and dolomitic, overlain by green and grey magnesium-rich claystone and fine sand. There is also evidence of Eyre formation remobilisation (Callen *et al.*, 1995a). The Namba formation, in the Callabonna sub-basin, shows similar sediments, with angular sand, silts, and clay. Dolomite is also present and clay is black. Sediments thicken towards the Flinders Ranges, where the maximum subsidence is observed. Kaolinite is present in the upper part of the formation. West of the Flinders, the Neuroodla formation also shows green and grey, black clay sediments and also dolomitic mudstones. Clays are smectite-rich and Mg-rich in the basal part. Miocene formations frequently lie directly on the Cretaceous sediments and are generally unconformable. In most of the cases Miocene sediments contain reworked Cretaceous to Eocene underlying materials. According to the predominance of dolomite and/or palygorskite in the sediments, the waters of the lake were of hydrogeno-carbonated type, with $Ca \leq Mg$ and $HCO_3 \geq (Ca + Mg)$ (Cojan and Renard, 1997). At the Beverley deposit, two Namba sub-units are defined: the alpha-mudstone and the Beverley Sands, incised in the previous one. A third sub-unit called the Beverley Clays caps the Beverley Sands over the mineralisation. The age of this layer is unclear.

The deposition centre of the Namba formation is located on the eastern part of the basin, not far away from the Beverley Mine and the formation shows the thickest sequences (90 to 170 m) near Wooltana. This period is tectonically quiet and the north-eastern part of the craton subsides along a network of NNE-SSW faults bordering its margin (Wooltana, Poontana, Arrowie faults). The age of the Namba Formation deposition varies depending on the studied locations, but generally goes from Late Oligocene to Pliocene, extending possibly to the end of the Pliocene. Geographically, the closest dating information is from the Wooltana 1 drillcore (Martin, 1990) where palynology records a Late Oligocene to Pliocene age (indicative ages from ~25 to ~6-4 Ma).

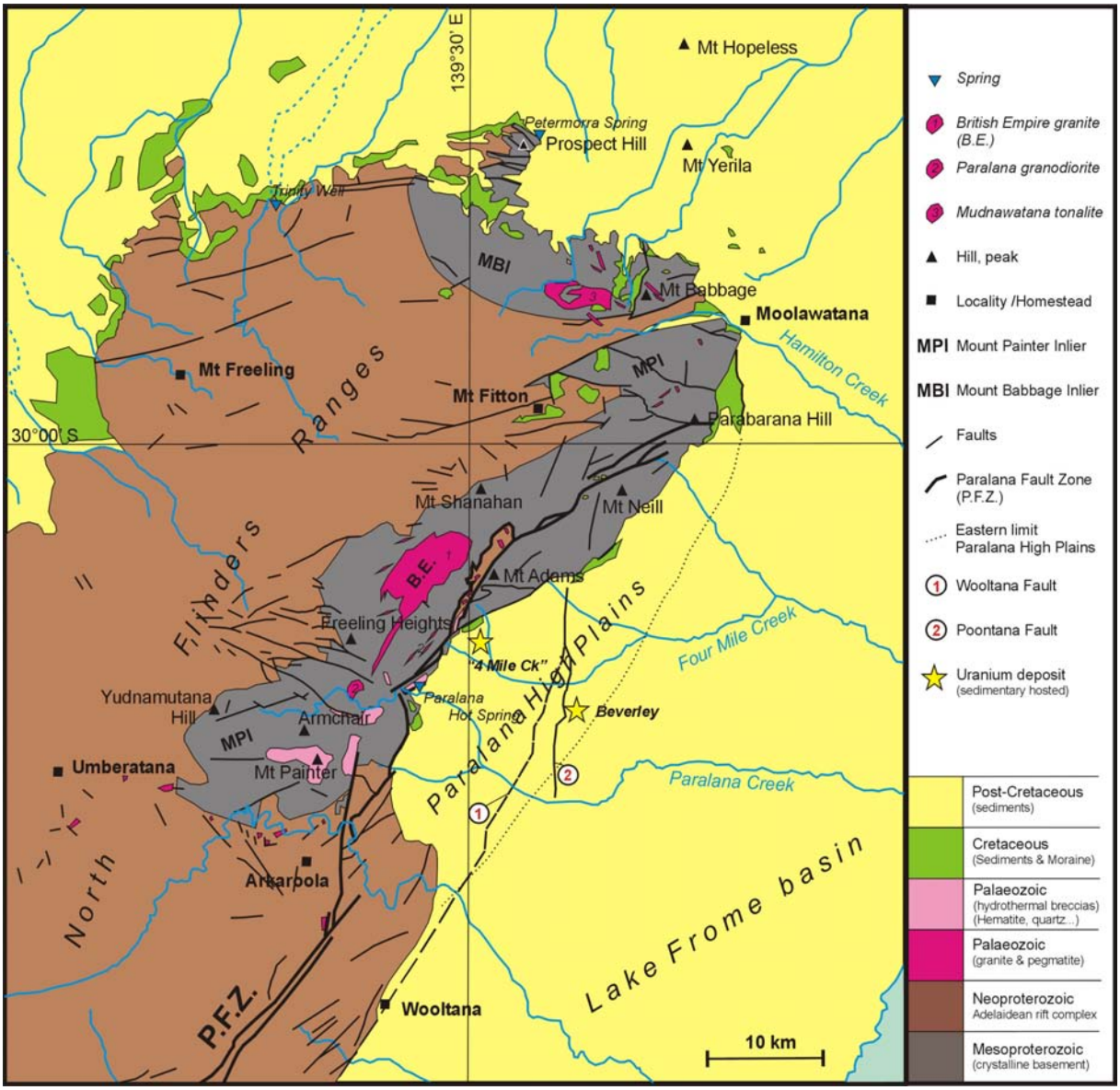

Fig. 4: Regional geological map of the Mount Painter Domain (MPD) and Paralana High Plains.

The PFZ approximately draws the NW border of the Curnamona craton. The simplified geological map underlines the major discontinuities: Neoproterozoic (~830 Ma), Cambro-Ordovician (Delamerian Orogeny), Cretaceous glaciation & sedimentation. The Cretaceous formation is widespread on and around the inliers.

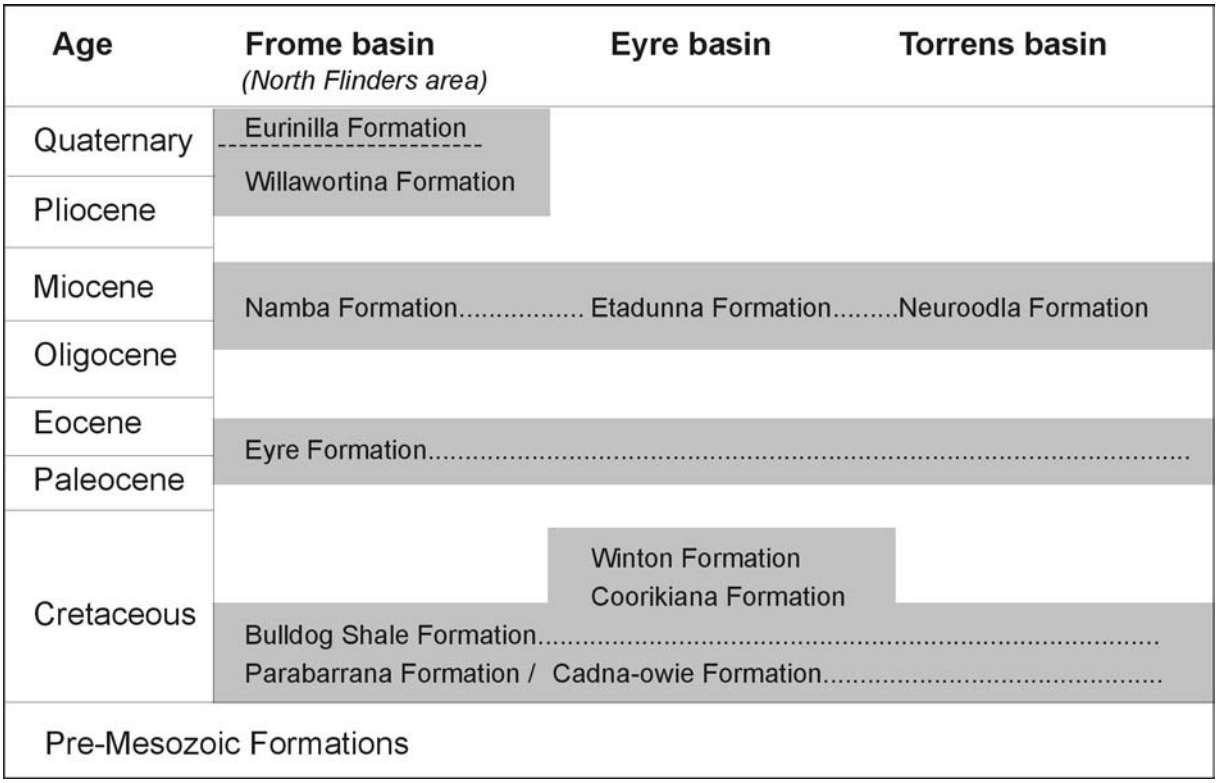

Fig. 5: Regional lithostratigraphy for the Mesozoic and Cainozoic Units

The age limits are drawn approximately and are discussed in the text.

2.1.4 Pliocene to Quaternary (Silcretes, ferricretes, Willawortina formation)

The Namba formation is locally capped by a silicic or ferruginous duricrust in the Lake Frome area. The age of this paleosurface is not exactly known. Kaolinite, alunite and gypsum are mentioned in the upper layers of Namba and have also been related to this weathering period (Benbow *et al.*, 1995, Callen and Tedford, 1976). The age of these layers is undetermined, but has been interpreted by these authors to be Late Pliocene.

During the Pliocene, the Curnamona craton is tectonically active and movements are recorded along its western margin. Displacement appears along normal faults and transcurrent (or transpressive) faults and the tectonic blocks along its western margin are uplifted of 100 to 200 meters and form the actual sharp piedmont of the North Flinders Ranges (Mt Neill and Mt Adams) as well as the Paralana High Plains. The Beverley deposit is located along the Eastern side of the Paralana High Plains, close to the Poontana and Wooltana fault zone (Fig. 4). This block is tilted as a half graben to the NW, exactly like the Mt Neill – Mt Adams block. Because of this, the deposition centre of the Lake Frome basin is shifted towards the East, locally exposing to the surface the lacustrine sediments. Recent seismic lines across the area also indicate the presence of a "horst-like" structure and the presence of more than 2 major faults (Burtt *et al.*, 2004).

Alluvial fans are building up a molassic foreland which progressively forms a large curved alluvial plain extending up to the shores of the present-day Lakes Frome, Callabonna and Blanche (Callen *et al.*, 1995b, Callen and Tedford, 1976). The Willawortina formation (Fig. 5) contains the coarser molasses but also fine clays and silts in the more distal lacustrine or plains environment facies. Simultaneously to the deposition of the Willawortina molasses, Lake Frome was progressively displaced to the East. Paleomagnetic data on the Willawortina sediments and paleosoils around the Lake Frome area indicate that much of the formation is older than 780'000 yr. (Callen *et al.*, 1995b). Correlatively, the same tectonic movements that were responsible for the North Flinders Ranges uplift have resulted in the regression of the sea off the Murray basin (150-250 kilometres south of the Lake Frome), and formation of the Lake Bungunnia over most of this basin. Paleomagnetic dating on the lacustrine clays (Blanchetown clay) indicates that the lacustrine sedimentation began around ~3.5 and 2.5 Ma ago, and finished at ~0.7 Ma (An *et al.*, 1986, Stephenson, 1986). The Murray basin is not reported on our maps.

The current period (from 0.7 Ma) is tectonically more calm and arid. However, the fault system (PFZ) is still active and light seismic activity can still be recorded (Sprigg, 1984).

The depositional environment around Beverley is concentrated in some fluvial channels of intermittent activity. The Paralana High Plains are subject to erosion and ferruginous soils are developing. The surface 3-4 meters at Beverley are part of the Eurinilla Formation (Fig. 5), a clay-rich ferruginous resedimented conglomeratic soil formation, forming residual quartz concentration at the surface (Callen *et al.*, 1995b).

2.2 Background information on the mineralisation and previous work

2.2.1 Geometry, relationship to formations and regional faults

The best-documented sources of information about the Beverley deposit geometry to-date are from the current mining operator Heathgate Resources Pty Ltd. We give here the current state of knowledge from publicly available literature and released mining information.

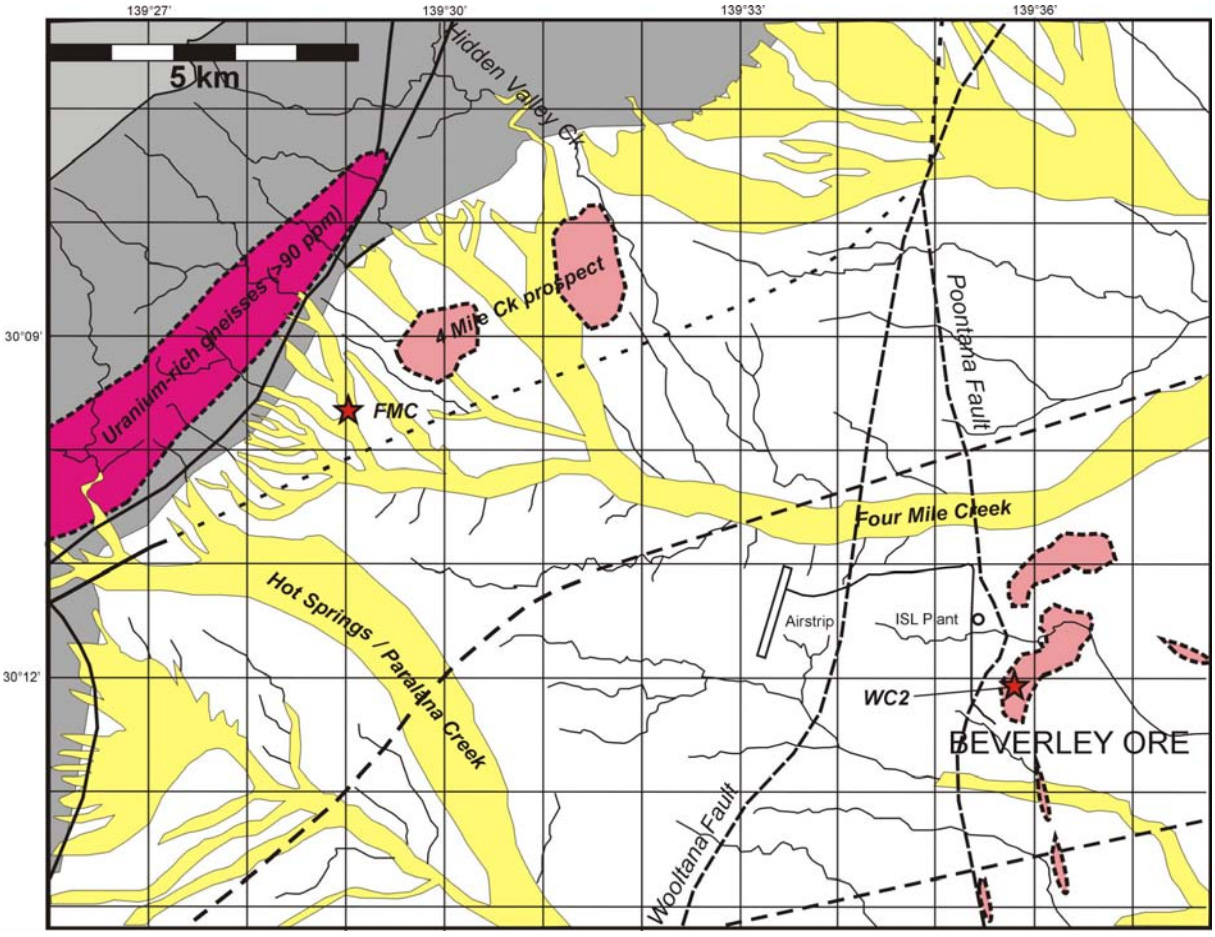

Fig. 6: Location map around the Beverley mine in the Paralana High Plains.

The Beverley uranium ore is displayed in pink as well as the approximate outline of the 4 Mile Ck Prospect. Two surficial radiometric anomalies are shown in light pink. Red stars: FMC sample, used for heavy mineral study and uranium speciation; WC2 drill-hole location, in the southern Beverley ore. The uranium-rich gneisses are indicated in bright purple-red, immediately to the West of the Paralana Fault System. Additional regional faults are also reported (Poontana, Wooltana faults)

The initially published geometrical models of Beverley all described a channel-type mineralisation with a NNE-SSW orientation (Haynes, 1975). A possible tectonic control was proposed later on, based on the presence of local faults defining a NE trending graben block (Curtis *et al.*, 1990). A genetic link between the deposition of the Miocene sediments and this structural feature was envisaged by Curtis *et al.* (1990). All authors interpret the sand formations hosting the mineralisation to represent a paleodrainage channel in the underlying lacustrine alpha-mudstone bedrock. Curtis *et al.* (1990) mention an oxidation interface with anomalous uranium traceable in the Namba formation along the same axis for 25 by 15 km. However, faults were never envisaged to have been the path for a basinal reduced fluid mixing with the lacustrine oxidised brine.

Heathgate Resources define a north and a central-south ore zones with both NE-SW trends, located immediately west of the Poontana fault in Miocene sands and in lower faulted compartment. Faulting is interpreted to have acted during Quaternary and extend through the upper Willawortina formation (Heathgate Resources Pty Ltd, 1998). The prolongation of the Wooltana fault (SW) is also interpreted to be extending West of Beverley and the Poontana fault

(Fig. 4 & 6). Additional ore trends were recently discovered to the south and the east of the main mineralisation. Based on paleosurfaces reconstitutions using drillings and airborne electromagnetic surveys, uranium mineralisations seem spatially linked to the edges of relief and depressions in the underlying mudstone (Marsland-Smith, 2005, McConachy *et al.*, 2006). The mineralisation is not conformed to the classical "roll-front" geometry but is of tabular shape. Origin of this disposition is interpreted to be either structural (faulting) or/and combining structural and paleoenvironment (Marsland-Smith, 2005, McConachy et al., 2006).

2.2.2 Mineralogy and geochemistry

Previous descriptions of the ore have shown little mineral diversity, with only fine-grained uraninite mentioned originally (Haynes, 1975) and later the recognition of coffinite, uraninite and pyrite (Brunt, 1978, Curtis *et al.*, 1990). The more recent data released by Heathgate Resources confirms the predominance of coffinite as uranium-host. Geochemically, uranium is associated with organic matter, Co and S, showing the U-Bi-Pb-Co-Ni-Cu-Cd and minor Zn, *L*REE, Y association (Marsland-Smith, 2005). The geochemistry of the ISL acid solutions also provides qualitative information on the leached mineralogy by comparing the solutions before and after reaction, taking into account mixing with the local groundwater (Heathgate Resources Pty Ltd, 1998): a relative increase of 10^2-10^3 is measured for the concentrations of V, U, Ni, Se, Cd and Al; 10^1-10^2 for Co, Fe, As and Cr as well as minor (>3) relative increase in F and Pb.

2.2.3 Genesis

The genetic model retained by authors is a roll-front type deposit, paleochannel hosted. However, concerning whether or not the Beverley ore sits in "paleochannel" structure, Haynes (1975) states the question is not yet resolved; the Beverley Sands could after him be either (1) stream channels, scour channels, or outwash plains but also (2) sand dunes.

The mentioned uranium sources for the deposit are the MPD basement (1), the Miocene formations themselves (2) or the alluvial fans of the Willawortina formation (3) (Callen, 1975, Haynes, 1975, Hochman and Ypma, 1987). None of the authors give a clear choice, but all mention the MPD basement to be the more likely source. Secondary uranium mineral dating in some of the MPD basement deposits demonstrate the current active mobility of uranium (Elburg *et al.*, 2003), whereas groundwaters contain uranium concentrations between a few ppb and 1 ppm (Brugger *et al.*, 2005). A study of the quartz thermoluminescence in the Beverley Sand Unit and the upper and lover Units was conducted to solve the question weather the uranium migrated as a roll-front (Hochman and Ypma, 1987); it reveals that the Beverley Sands were exposed or still are in contact with a radioactive source up to 4 km toward the West from the uranium mineralisation. The under- and overlying sandy formations are devoid of these glowing thermoluminescence characters as well as the sands to the East of the deposit. The question of the roll-front remains unsolved. The recently produced paleosurface map of the underlying alpha-mudstone around the Beverley ore (McConachy *et al.*, 2006) reinforces the sand dunes hypotheses of Haynes (1975) or an old shore line.

3 Methodology and information on WC2

The main part of this study has been conducted on the WC2 drilling core. Some additional sediment samples collected in the Paralana High Plains and on the neighbouring crystalline basement complete the dataset.

The position of the drilling is 0364'916 / 6658'366 (MGA zone 54) or 30° 11' 55.3"S / 139° 35' 48"E, altitude: 80 metres. The attained depth is 146.6 meters, ending in the alpha-mudstone layers of the Namba Formation. The available cored length extends from the surface down to 136 meters with a few meters missing. Two series of samples were collected on the 8.5 cm diameter cores (Samples No 628-234 to 628-278 and 966-964 to 966-978). The WC2 core was used as a type section to describe the Willawortina Formation (Callen and Tedford, 1976); for this reason, sedimentology and major minerals mineralogy have already been partly documented. We re-logged the core (Fig. 7) and used the samples with different analytical or separation techniques to define the origin of the sediments. The XRD clay analysis, granulometry determination and texture or sedimentary facies documented in the original works on WC2 have also been partly validated through our results and generally fit with our observations made on the core. The recovery rate of the entire core is low (50 %), especially in the Willawortina formation; this however didn't impact the results of this study based on samples from selected intervals.

The choice of using the old WC2 reference core was also justified because of its collection prior to any leaching process that could have affected the mineral assemblage. The core is available for inspection and stored in good conditions and will certainly remain accessible in the future, because of the status of the PIRSA core library, which is a museum-like facility.

Sample N°	Level [m] Below surface	Clay, Silt [%]	Total HM [%]	NM [%]	SM [%]	MM [%]	Carnotite	Coffinite	Copper	Barite	Sphalerite	Marcasite	Pyrite	Chalcopyrite	Rutile	Leucoxene	Zircon	Corundum	Anatase	"rutile index"
							Detailed mineralogy of the NM fraction (% by grain counting)													
34	1.5	18	0.164	0.006	0.011	0.147														
35	8.6	63	0.594	0.038	0.110	0.446									61		30	9		2.0
36	12.0	63	0.475	0.039	0.106	0.330									77		17	6		4.5
37	12.6	57	0.570	0.043	0.102	0.425							2		45		50	3		0.9
38	20.1	33	0.716	0.057	0.091	0.568									45		40	14	1	1.1
39	25.5	31	1.029	0.055	0.111	0.863			<1					<1	50		36	13		1.4
40	41.6	51	0.867	0.042	0.172	0.653														
41	48.1	51	0.299	0.036	0.044	0.218									52		40	7	1	1.3
42	51.7	19	0.169	0.052	0.014	0.104														
43	61.0	42	0.837	0.153	0.162	0.522									65		28	6	1	2.3
44	75.1	49	0.550	0.061	0.099	0.390									66	<1	30	3		2.2
45	77.0	57	0.381	0.054	0.069	0.258														
46	82.8	25	0.168	0.028	0.028	0.112							1		30		35	30		0.9
47	84.2	29	0.466	0.073	0.083	0.310									55	1	33	10		1.7
48	91.0	40	0.429	0.078	0.119	0.231														
49	95.3	56	0.245	0.060	0.040	0.145									74		16	10		4.6
50	97.1	41	0.021	0.006	0.007	0.007			3						80		6	6		13.3
51	100.1	69	0.075	0.053	0.012	0.010			5						88	<1	3	3	1	29.3
52	102.8	89	0.027	0.013	0.002	0.011			10	1					60	2	10	12		6.2
53	104.9	73	0.027	0.009	0.002	0.015			<1	30					60		5	5		12.0
54	105.5	97	0.001	0.000	0.000	0.001	1			<1					72	15	10	2		8.7
55	110.1	94	0.006	0.001	0.001	0.004	<1								95	3	2	<1		49.0
56	112.5	97	0.049	0.001	0.004	0.044	<1		<1						65	2	30	1	1	2.2
57	115.6	92	0.003	0.001	0.001	0.002			1				<1		15	10	70	<1	3	0.4
58	118.2	86	0.053	0.028	0.011	0.014									11	5	79	<1	4	0.2
59	119.2	91	0.038	0.019	0.014	0.005									14	6	80		<1	0.3
60	120.2	49	0.108	0.012	0.009	0.087	<1	<1	4				<1		8	8	75	<1	3	0.2
61	121.2	65	0.106	0.046	0.042	0.018	<1		<1						5	8	85	<1	1	0.2
62	122.9	55	0.083	0.048	0.035	0.000	<1								7	3	88	<1	1	0.1
63	123.4	39	0.415	0.174	0.054	0.187				<1	<1				6	3	90		2	0.1
64	125.6	77	0.023	0.001	0.002	0.020	2		<1	3	<1				40	<1	55	<1		0.7
65	126.5	55	0.053	0.013	0.004	0.035	<1								20	4	75	1	<1	0.3
66	127.4	80	0.054	0.028	0.025	0.002			<1			<1	<1		5	4	90	<1	1	0.1
67	127.9	70	0.143	0.053	0.021	0.069	2		3	40	2	<1	1	<1	35	5	10	<1		4.0
68	128.3	74	0.236	0.177	0.012	0.047	<1		<1	<1		6	35		5	4	48	<1	2	0.2
69	128.6	66	0.318	0.231	0.035	0.052			<1			6	35	<1	5	4	48	<1	2	0.2
70	130.0	86	0.294	0.250	0.023	0.021	<1		<1		<1	54	20	<1	2	1	12	<1		0.3
71	131.1	93	0.026	0.011	0.003	0.011	3	8	2	3	2	5	25	1	20	2	30	<1		0.7
72	131.2	89	0.197	0.182	0.004	0.011	3	8	2	3	2	5	25	1	20	2	30	<1		0.7
73	132.0	97	0.791	0.771	0.003	0.016		92			3	2	3		<1		<1			
74	132.4	98	0.010	0.009	0.000	0.001	5	15	<1	<1	<1	15	45	1	5	1	10			0.6
75	132.6	93	0.115	0.101	0.005	0.009	5	15		5		15	45	1	5	1	10			0.6
76	133.2	96	0.012	0.005	0.001	0.005	2	29		2	1	6	18		30	2	8	1		4.0
77	135.0	99	0.003	0.001	0.001	0.001	1	30	23	<1	2	7	8		15	1	12	1		1.3

Table 2: Heavy minerals assemblage in the WC2 drill core

The heavy minerals have been listed in the column with the authigenic species first followed by the detrital ones. The reported % is evaluated under microscope by grain counting in the sole NM (non-magnetic) fraction. The % of clay, silt corresponds to the washout from the panning, after drying and weighting of the remaining fractions. A total of 37.21g of HM has been recovered from WC2. Abbreviations: NM (non-magnetic), SM (semi-magnetic) and MM (ferro-magnetic), typically magnetite.

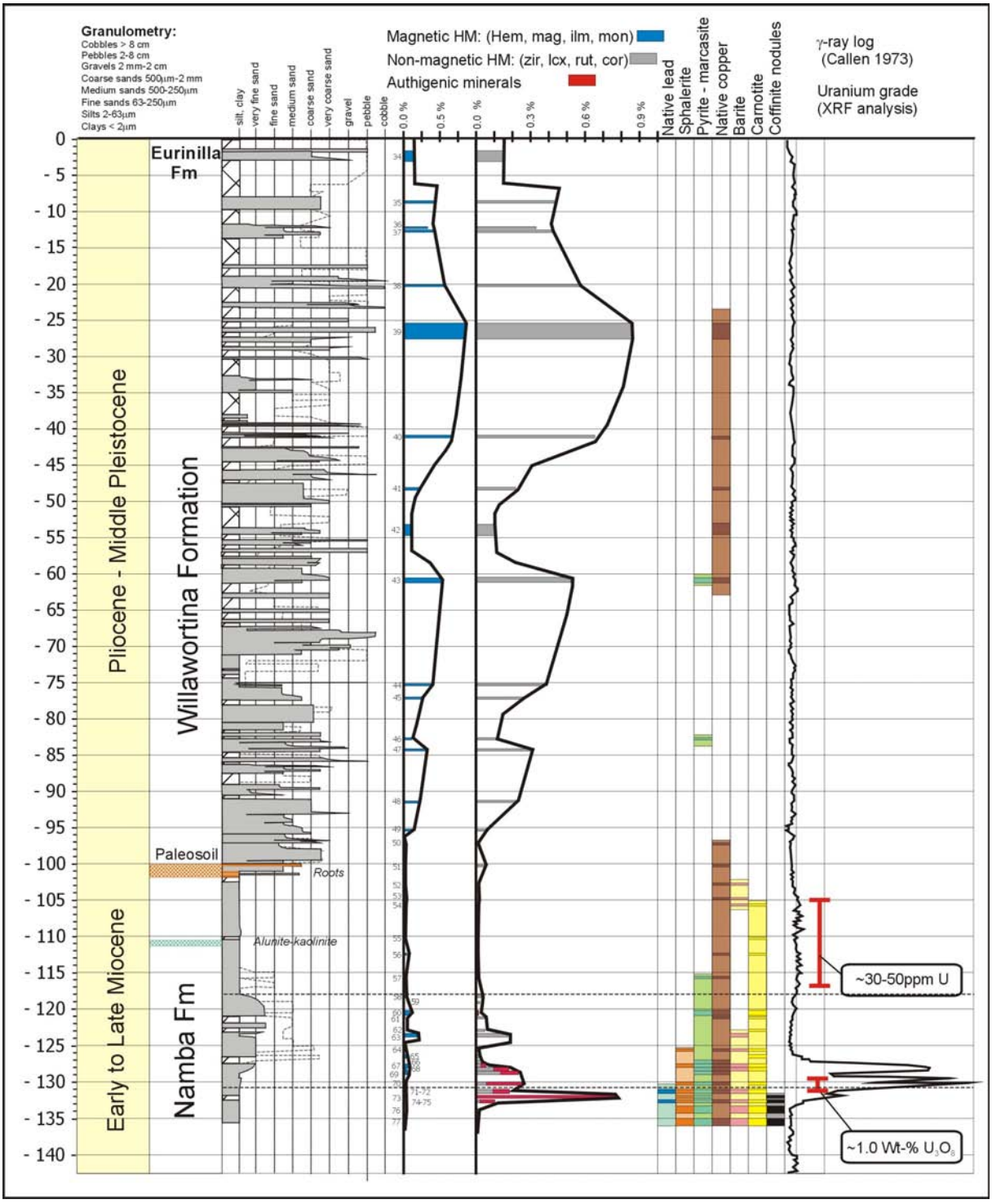

Fig.7: WC2 log with gamma, uranium grades and heavy minerals assemblage

The heavy minerals have been represented on two logs: non-magnetic (NM) and magnetic (MM). The authigenic minerals in WC2 appear to be non-magnetic and have been distinguished by a red colour on the log. A paleosoil with roots and oxidised cracks occurs between -100 and -102 meters; it defines the unconformity between the Namba Formation and the beginning of the Willawortina Formation sedimentation, essentially debris flows. Only ~50% of the core was recovered, with lost intervals hatched on the granulometric log. The Namba Formation is formed of three units: the Beverley clays, the Beverley Sands and the alpha-mudstone at the end of the hole.

4 The heavy mineral assemblages

The relative concentrations of the different HM fractions are reported in Table 2 and represented on the (Fig. 7) with the sedimentary log and the gamma-ray log. A special attention has been given to the separation of the authigenic minerals from the detrital assemblages. The two sampled formations (Willawortina & Namba) can be distinguished upon their HM assemblages and in general, the detrital content of the Namba sediments does not exceed 0.4 %, whereas the Willawortina Formation sediments nearly always carry more than 0.5%. Additionally to the small-sized samples from the WC2 core, a large representative sample has been taken from the Four Mile Creek bed four kilometres upstream the uranium mine, see FMC symbol on Figure 6. This sample provides a large quantity of HM's and accurate information on the Four Mile Creek watershed, which was the source area for the Willawortina Formation.

4.1 Detrital minerals populations

Alluvium from the Four Mile Creek bed bears high contents of HM (1-2%). The HM extracted contain some U-, Th-, REE-rich phases. Zircon, rutile, xenotime, monazite, polycrase-(Y), fergusonite, allanite, thorite, huttonite and apatite are abundant in these sediments. Detailed mineralogical content is given in Table 3.

The detrital minerals of the Willawortina Formation are rich in black magnetic minerals (MM): magnetite, ilmenite, hematite, and also bear SM minerals: epidote, hornblende, garnet, xenotime, columbite and monazite. The NM assemblage is dominated by zircon, titanite, followed by rutile and corundum, anatase, sillimanite, tourmaline, fluorite, apatite and topaz. Detrital sulphides (pyrite, chalcopyrite, galena and molybdenite) are also present. Quite often, pyrite is completely pseudomorphosed by hematite or goethite. Zircon is typically large and of brown, reddish or black colour. This assemblage is identical to the one recovered from the Four Mile Creek. The U-Th-REE phases have not been studied as extensively than in WC2 because of the small size of the samples (a few mg).

FMC: Sediment fractions and weights

> 5mm	1.5 – 5 mm	<1.5 mm	washout	
30%	10%	43%	17%	
4.57 kg	*1.54 kg*	*6.58 kg*	*2.60 kg*	
Total HM recovered:		321.43 g (2.1%)		
Separated fraction	Density [g/cm³]	Magnetism [Ampere*]	Weight [g]	Cps (Count /s)
Magnetite	> 4.0	0 -0.2 A	100.09	+60
Ilmenite-hematite	> 4.0	0.2 -0.3 A	185.50	+60
Garnet – Hematite	> 3.3	0.3 -0.5 A	12.31	+60
Monazite – Xenotime	> 3.3	0.5 -0.75 A	6.28	
Monazite (2)	> 3.3	0.75 -0.95 A	3.47	+900 cps
Titanite – Staurolite	> 3.3	0.95 -1.1 A	1.42	
Rutile, zircon, corundum	> 3.3	>1.1 A	9.50	
Apatite, tourmaline	2.9 – 3.3	>1.1 A	2.86	+230 cps
All observed HM species:	*Magnetite*	*Thorite*	*Samarskite*	*Rutile*
	Pyrrhotite	*Xenotime-(Y)*	*Euxenite*	*Columbite*
	Ilmenite	*Polycrase-(Y)*	*Zircon*	*Tantalite*
	Hematite	*Fluorite*	*Apatite*	*Scheelite*
	Andradite	*Titanite*	*Tourmaline*	*Corundum*
	Fe hydroxide	*Allanite-(Ce)*	*Epidote*	*"Sapphire"*
	Spessartite	*Cerite-(Ce)*	*Amphibole*	*Barite*
	Monazite-(Ce)	*Fergusonite-(Y)*	*Molybdenite*	*Pyrite*
			Malachite	*Chalcopyrite*
			Anatase	*Sillimanite*

Table 3: Heavy minerals assemblage in the FMC sample

The heavy minerals have been separated into fractions using the Frantz Isodynamic separator. Magnetic intensity is reported as current intensity in Ampere. Radioactivity has been measured with a SAPHYRO SPP2 scintillometer. The NaI crystal was placed next to a 3cm diameter disc filled with composite or single fractions of HM weighted to 10g each. The monazite-xenotime-fergusonite fraction is almost accounting for the total HM radioactivity.*

The Namba Formation displays a clear change in HM populations: the upper unit, the Beverley Clays unit, which is poor in HM, is dominated by rutile, with minor zircon, leucoxene and corundum. Minerals from the MM and SM fractions are rarer and may have been weathered out. Monazite is present in very small amounts. The following unit (Beverley Sands) contains mainly zircon, then rutile, anatase and minor corundum. The HM content is clearly higher than in the upper part. Zircon concentrates look different in colour and morphology from the Willawortina population and consists of mainly transparent colourless crystals. A detailed examination of them is following. A detrital chalcopyrite grain of 30-50 μm has been observed in the alpha-mudstone below the mineralised levels. The abundance of magnetic heavy minerals (MM) is extremely low compared to the Willawortina formation.

We evaluated the ratio rutile (*ru*) and zircon (*zr*) in the different samples by grain counting (Table 2). The *ru / (ru+ zr)* ratio varies around 1 - 3 in the Willawortina Formation and sharply increases (6 to 50) in the clays at the top of the Namba Formation and the Alpha-mudstone. Further down, the NM fraction of Beverley Sands is dominated by zircon with ratios between 0.1 and 0.7. This observation indicates these sands have a different origin to the hosting formation. The Beverley Sands cannot be the result of clay washings and the resulting HM concentration, because this mechanism would not change the *ru / (ru+ zr)* ratio as strongly. It implies another sedimentary source provenance or a mixing.

The detrital minerals in the Beverley Sands are composed of angular grains with multiple indices of volcanic or volcaniclastics origin; this is especially visible on the textures of some zircons which show extremely fresh fractures which cannot be the result of alluvial wearing.

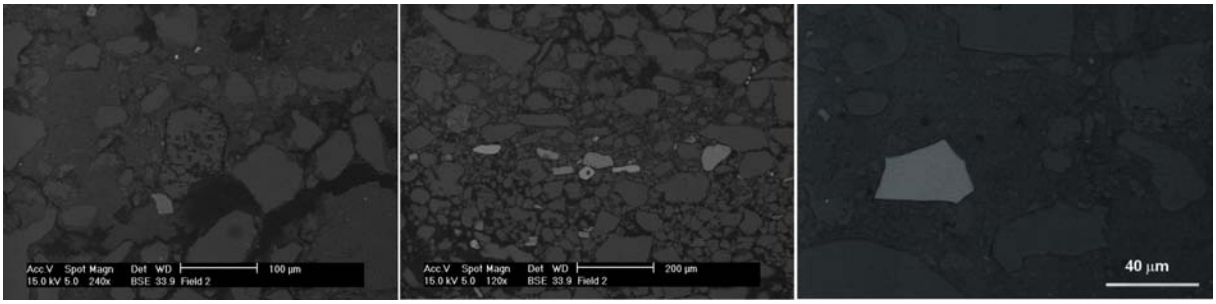

Fig. 8: Sedimentary textures in Beverley Sands

Left: fragment of zircon (light) next to a weathered albite euhedral crystal; centre: heavy mineral bedding in very angular quartzose sandstone (Beverley Sands). Zircons (white) & ilmenite (light grey); right: extremely fragmented fresh zircon of interpreted ignimbritic origin in a mudstone matrix

Another mineral is also interestingly distributed in WC2: corundum; this mineral, which is resistant to mechanical abrasion due to its hardness, is almost inexistent in Namba and begins to be common at the level [-106 m]. The mineral is colourless, blue, less frequently black and frequently bicolour. The mineral occurs widely in basement gneisses and metapelites of the MPI (Radium Creek Metamorphics). Corundum appears to mark accurately the beginning of sedimentation issued from the local MPD basement.

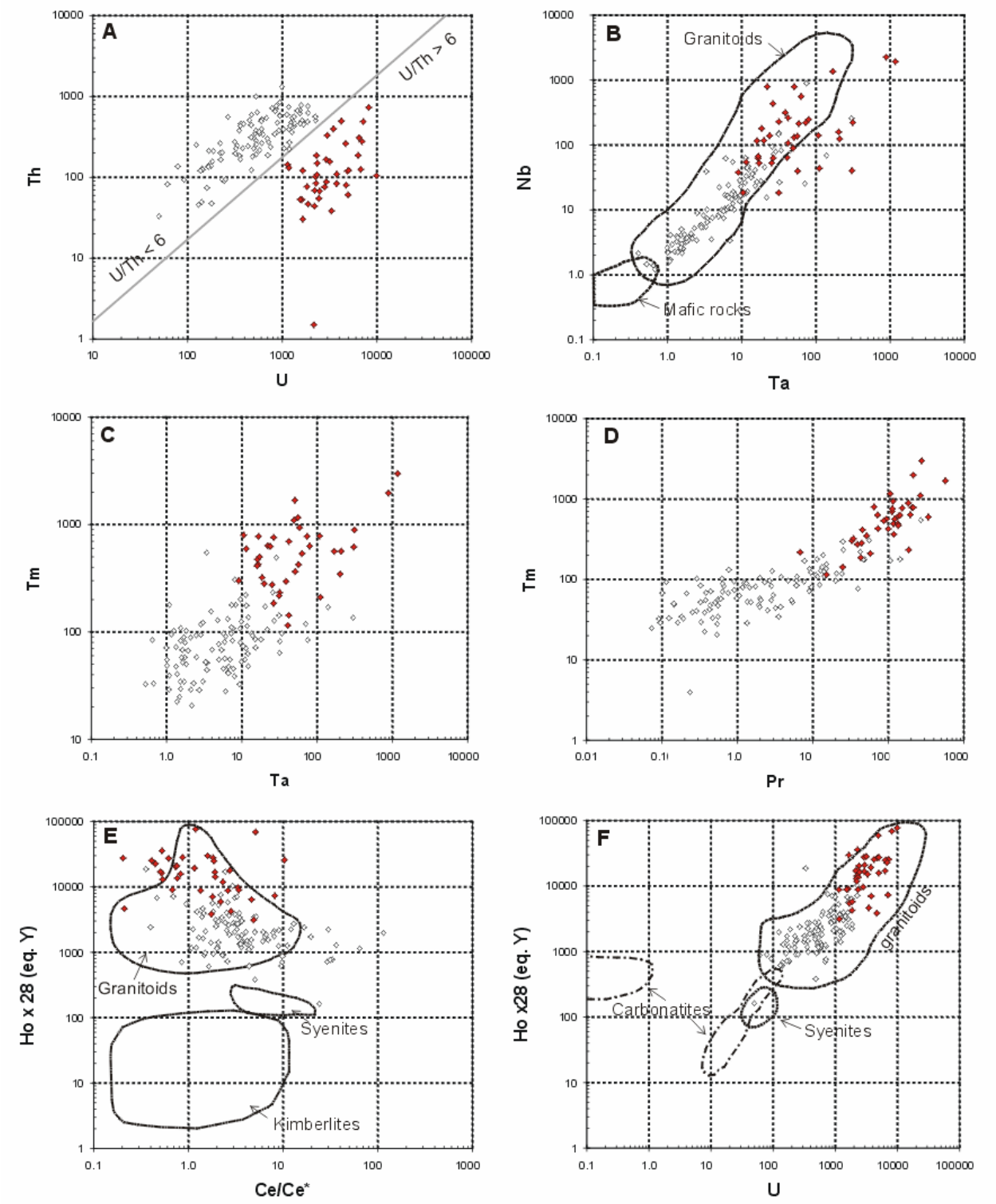

Fig. 9: Diagrams of trace elements in the zircons (ICPMS)

The circles fields reported are from Belousova et al. (2002), referring to the composition of igneous zircon. The zircons have been divided into two categories using U/Th ratio = 6.0. The red diamonds represent zircons with U/Th>6.

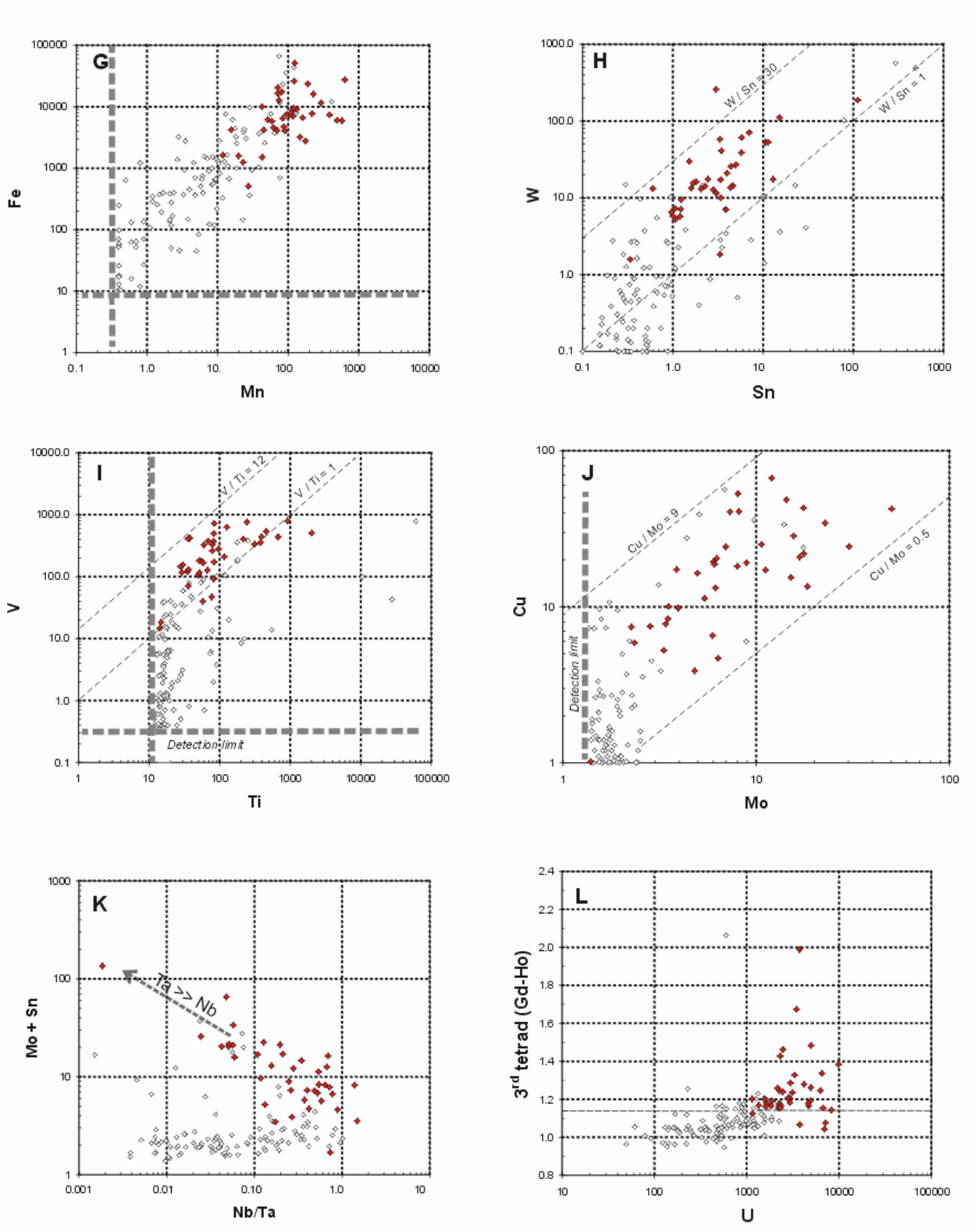

Fig. 9 (suite): Diagrams of trace elements in the zircons (ICPMS)

Tetrad effect is characteristic of hydrothermal (fluid-rock) or (mineral-fluid) interaction.

4.2 Trace element chemistry of zircon

Zircons were picked from the heavy minerals concentrates on different levels from Namba to Willawortina in WC2 and a hundred of them analysed randomly for their trace element chemical composition. Results are reported in the Appendix I. The aim was to measure the uranium content of the zircons in order to check whether the zircons themselves could have been the source for a sedimentary uranium deposit. Additionally, the vertical distribution of the zircon in WC2 was expected to show differences between formations. A large suite of elements was collected to enable the determination of the rock source by comparison with a database of zircons from the MPD. The trace element pattern of igneous zircon also changes upon the composition of the source rock. This permits to discriminate the magmatic zircons by source rock chemistry (Belousova *et al.*, 2002).

Zircon is a resistant refractory mineral with the following formula: $ZrSiO_4$. It incorporates many elements in its structure (P, Sc, Nb, Hf, Ti, U, Th, REE's, etc.) Zircon also forms isostructural series with xenotime-(Y) (YPO_4) and all other xenotime-(*h*REE) members (Bea, 1996), coffinite ($USiO_4$) and hafnon ($HfSiO_4$), leading to incorporation of these elements up to a few percents. Zircon geochemistry is dependent of its type of genesis: igneous zircon versus hydrothermal zircon. Most of the zircons form in igneous context and their geochemistry depend on the ionic radius & charge of the substituting elements. Partitioning coefficients between the mineral and the melt (mineral/melt) are high for Hf, U, Th, Nb, Ta, heavy REE's, Sc and Y. Zircons that have been fluid-altered or formed under hydrothermal conditions can contain hundreds of ppm of other elements that are incompatible during the igneous partitioning: *L*REE's, Sr, Ba, Ca, F, Fe, Mn, Cu, and many other incompatible elements (Rubin *et al.*, 1989). U- and Th-rich zircons become metamict with time and the resulting swelling of the crystal structure with associated opening of cracks facilitates trace elements incorporation and/or leaching. This type of zircon will be the best type of zircon to react with hydrothermal fluids and fix normally incompatible elements (Geisler *et al.*, 2003). The application of the La-ICP-MS technique to the zircons chemistry is complicated if the zircon hosts a few cracks that can be filled or coated.

We decided to distinguish two populations of zircons on the basis of their chemistry (Fig. 9). The high level of U, *h*REE and transition elements in some zircons shows the presence of an unusual population of zircons. The Th/U ratio makes a clear distinction between zircons from "classic granitoids" and other U-rich source rocks or hydrothermally altered zircons. In a strict igneous context, U and Th partitioning between the developing zircon and its surrounding melt have been determined experimentally. $D_U^{(zircon/melt)}/D_{Th}^{(zircon/melt)} \approx 6$, with D_U varying from 97 to 130 (Blundy and Wood, 2003). Very limited experimental data give a $D_U/D_{Th}^{(zircon/melt)} \approx 3.5\text{-}4.1$ for granitic compositions at 20 kbar and 800-850 °C (Rubatto and Hermann, 2007). Granitoids generally display Th/U between 5 and 2 but rarely less than 1. Zircon partitioning with $D_U/D_{Th} \approx 6$ results in Th/U ratio in zircons between 1 and 2. We have setup a limit at U/Th = 6 to plot 2 empirical populations (Fig. 9). Vertically in the different samples from the drilling, the distribution of U/Th values shows strong variations, evidencing mixing of different provenances (Fig. 10). The upper formation (Willawortina) hosts a much higher proportion of zircons with U/Th>6.

The diagrams represented in (Fig. 9) illustrate the distribution of different trace elements within the two (U/Th>6, U/Th<6) populations. Yttrium values have not been used because of calibration problems. The spectrometer frequently saturated on Y, P, Yb, and in a few cases with Er. For this reason, we could not use systematically Y in diagrams. We then used an approximation of Y (Y=28Ho) to plot some of the diagrams given in Belousova *et al.* 2002. The Y/Ho ratio is generally close to the chondritic value for magmatic zircon; it only deviates for high-silica magmas enriched in volatiles (leucogranite & granite pegmatites) where the ratio decrease down to ~20. This can also be observed for hydrothermal zircons (Pettke *et al.*, 2005).

High U/Th zircons (high U) are also Nb, Ta, hREE, LREE-rich. W, Sn, Mo, V, Cu and Ti also follow this general trend. The diagram Fig.8k (Mo+Sn) versus (Nb/Ta) tends to show a relative increase of Mo, or Sn with higher Ta values. U-rich zircons display (Fig.8h), high W values, which are also followed by high Sn. The high-U zircons also display irregular Chondrite-normalised curves with a positive tetrad effect (Monecke *et al.* 2002), especially marked on the 3rd tetrad (Gd-Ho). This is the signature of hydrothermally altered zircons. This later information is useful when looking back to the high-U zircons on the Y/U diagram (Fig.9) with the field of granitoids: these zircons should plot a lower for Y values (here 28 x Ho) close to the limit of the field (leucogranites, aplites and pegmatites field). This probably means that the Y/Ho ratio for these U-rich zircons is <15. Low Y/Ho ratios are characteristic from highly evolved magmatic systems and granite-pegmatite suites.

The $^{208}Pb/^{232}Th$ age has been calculated for each crystal. For many zircons, the $^{208}Pb/^{232}Th$ ratio displays a correlation between "extremely high apparent ages" (with a lot of common Pb) and high values of Nb, U, Sr, Ba, and rare earth elements. The presence of large incompatible elements like Sr and Ba clearly evidences the metamict state and the fluid-altered nature of this population of zircons, for which U-Pb dating is inapplicable. Apart from this problem, more than 50% of zircons ages can precisely be determined from Cretaceous (youngest at 85 ±7 Ma) to Cambrian) (Fig.11). The geochronology aspect is further documented in the next section with complementary U-Pb dating for zircons from the Beverley Sands.

Finally, the analysed zircons have been plotted into the CART trees and diagrams of the classification of igneous zircons developed by (Belousova *et al.*, 2002). The composition of a low-U zircon (Zircon 55-4), located in the Beverley Sands, 50 ppm U, 33 ppm Th with an age of 467 ±100 Ma (1σ) fits within the field of the syenites (or carbonatites). Another zircon (55-3) from the same level, 61 ppm U, 82 ppm Th, with an apparent age of 1023 ±190 Ma (1σ), plots in the dolerite field. All other zircons fit into the granitoids categories or are "atypical" because of their hydrothermal patterns. The CART trees only apply to magmatic compositions.

The trace elements data and age obtained from WC2 (all formations mixed) clearly evidence a sedimentary origin different from the local basement (MPD). This hypothesis is further investigated in the next sections.

Level		U/Th in zircon			
[m]	#	< 0.75	0.75 -1.49	1.50 – 5.9	>6.0
-2	34		3	4	3
-9	35			5	5
-13	37		1	1	8
-20	38		1	5	2
-25	39		1	7	2
-42	40		5	2	3
-48	41	1		3	6
-75	44			9	1
-83	46		2	5	3
-84	47		5	5	
-97	50	2	6	1	1
-110	55		8	2	
-121	61		3	4	3
-126	64			8	2
-130	70	1	3	3	3
Th/U rock*		> 8	8 - 4	4 - 1	< 1

*for igneous zircon, implying $D\mathrm{U}/D\mathrm{Th}_{\mathrm{zircon/melt}} \approx 6$

Fig. 10: Distribution of zircons in WC2 according to their level and U/Th value

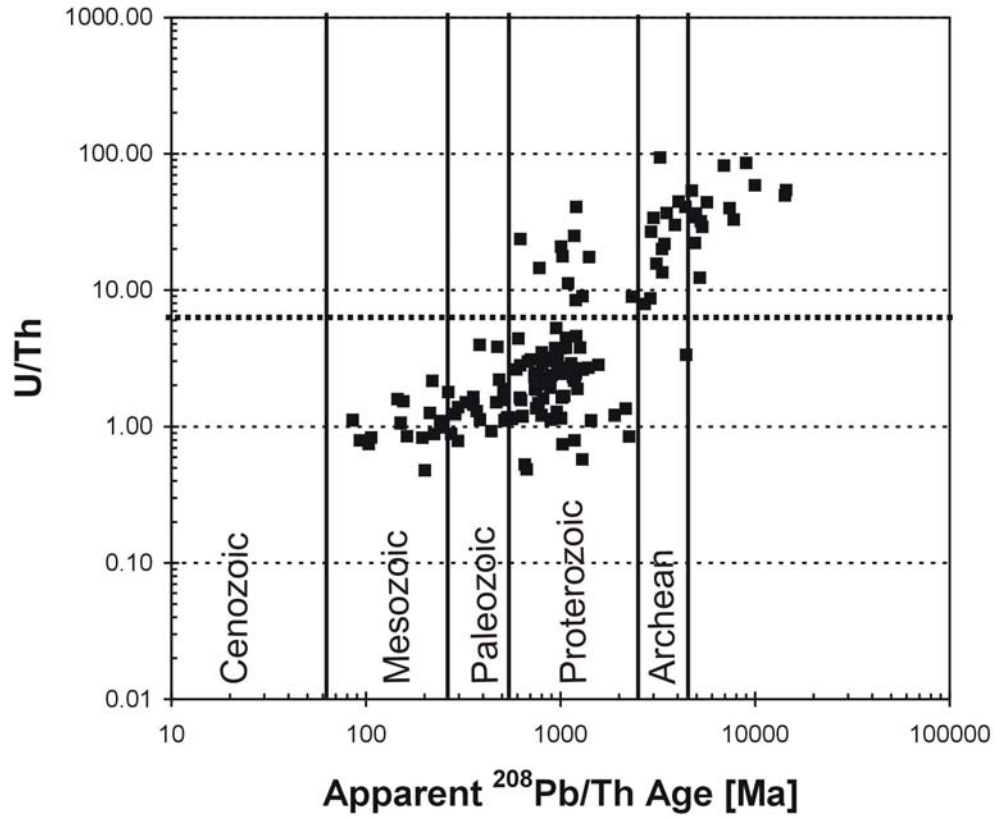

Fig. 11: Relationship U/Th ratio and apparent ^{208}Pb-^{232}Th ages in Beverley zircons

The reported apparent ages are highly variable due to different analytical errors and the absence of common lead correction. Nonetheless, it is possible to see a significant average increase of the U/Th ratio from the Mesozoic-Palaeozoic age group to the Proterozoic zircons.

4.3 Zircon typology and regional correlations

Zircon typology has been applied to determine the sources of the sediments at the Beverley Mine and its neighbourhood. To obtain a dataset of different origins and quantify some mixing in the sediments, additional sites have been chosen for a zircon typology study. Zircons were picked by morphology (colour, roundness, elongation) from HM's fractions, and examined for typology determination when possible.

The zircons used for the typology study come from 3 different locations: (1) ***WC2-63***, in the Beverley sands at [-123.4m], (2) ***FMC***: Four Mile Creek stream sediments 6 km upstream the mine (Fig. 4), (3) **SB**, a creek in the Babbage Inlier draining Mesoproterozoic granites only. The geological information about additional samples is:

- ***FMC,*** was selected because of its vicinity to the WC2 location and also because it samples a well-defined watershed of 12 km² containing: Palaeozoic leucogranites & pegmatites (10%), Mesoproterozoic granites and orthogneisses (30%) and Mesoproterozoic quartzite & paragneisses (70%). The Four Mile Creek watershed is probably accounting for 80% of the Willawortina formation in the Paralana High Plains around Beverley.

- ***SB*** comes from a sample of sediments on the MPD representing the Mesoproterozoic granites (Yerila and Terrapinna granites).

4.3.1 "SB" zircon typology

The zircons from SB are exclusively coming from the Mesoproterozoic granitoids. They display the same typological characters: an exclusive alkaline typology with "stocky", large prisms showing a dominance of (100) faces and combination of (101) and (301) pyramids. The presence of (301) pyramids is restricted to alkaline K-rich granites of high temperature (~900°C) (Pupin, 1980). K and T subtypes occur on the typology grids with the D and P types. This correlation is consistent to the overall MPI granitoids chemistry, which host K-rich granitoids (Stewart *et al.* 2001). These zircons bear plenty of fine cracks and are stained in black, brown or orange (Fig. 12). The observations made in SB can largely be extended to the whole MPD in which Mesoproterozoic granites abound. We base this argument upon additional observations made in HM separates from tens of crushed granites in the MPD. Zircons types are clustered around the D to P1 trend, generally centred on D or P5 (Fig. 13).

4.3.2 "FMC" zircon typology

Establishing zircons typology from the Four Mile Creek (FMC) sediments was extremely time-consuming because of the large number of zircons observed: 3000! The FMC watershed hosts Zr-rich (500-800 ppm) Mesoproterozoic granitoids (30%). The other intrusive rocks of Palaeozoic age are Zr-poor (<80 ppm) and account only for 10% of the source rocks. As a result of this contrast, we expected to find only 2 % of Palaeozoic zircons in the sample. The Palaeozoic zircons of the MPD are morphologically more complex and show colourless or milky crystals formed of inherited cores and magmatic overgrowths (Neumann, 1996). We expected the zircon typologies to be of S-type and decided to obtain U-Pb ages on all zircons differing from the D-P3 cluster. A total of 9 Paleozoic zircons were found, with S typologies but also P1-P2 types. The relationship between age and typology is represented on the (Fig. 14). The Mesoproterozoic zircons reported in the Figure 13 include "undated" grains of P3-D typologies.

4.3.3 "WC2-63" zircon typology

Sample 63 in WC2 is located in the Beverley Sands Unit and consists of fine sands and silts. An unusual population of clear zircons exempt of any wearing traces was recognised. The grid reported in the Figure 13 clearly shows the presence of "S type" zircons population mixed with a minor D-P type population of local origin (see FMC). The S-types zircons present in the population are clearly igneous and derived from calk-alkaline or peraluminous granitoids. This is especially evidenced by the presence of numerous L-types, which only occur in peraluminous granites. By comparing the percentages of the types in the MPD (SB, FMC) with WC2-63, only a maximum of 10-12% of WC2-63 can really originate from them. This implies the Beverley Sands have are mainly issued from a distal sedimentary source. To strengthen this observation, 48 zircons from these "distal" typologies with absence of alluvial wearing were dated using LA-ICP-MS U-Pb measurements. Some of the zircons also display melt and dark minerals inclusions; this character is frequently met in the zircons displaying fresh cracks; this suggests a volcanic origin.

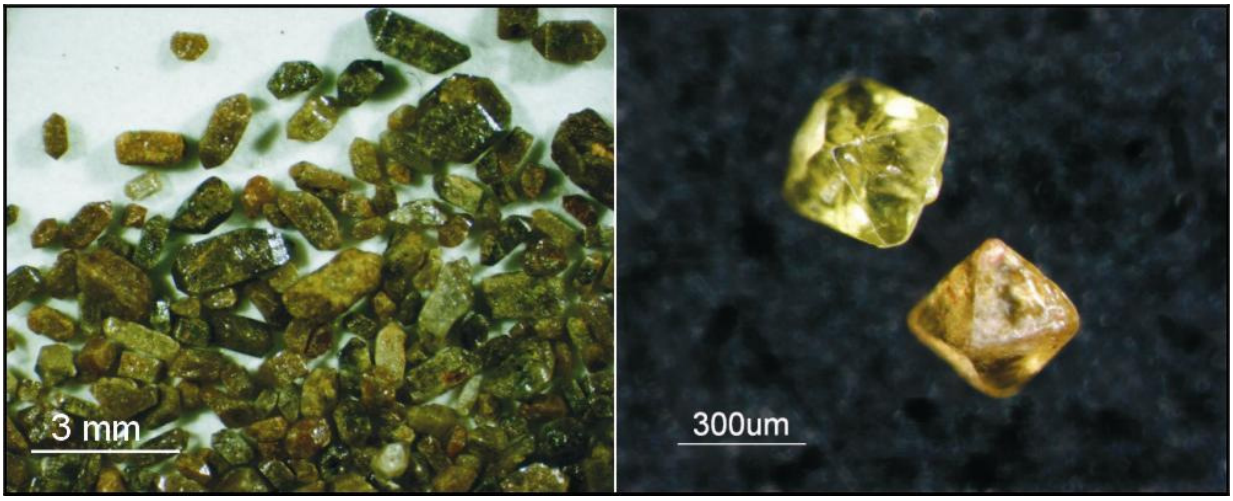

Fig. 12: Typical "D" zircons from K-rich granitoids (left) and xenotime crystals from FMC (right)

The absence of prism in zircon leads to an "A-type" morphology, exactly like the xenotime on the right. Xenotime is isostructural with zircon and forms a solid solution with it. Picking the A-type in samples generally produce a very nice fraction of xenotime. However, the mineral can be distinguished quite easily by its colour and refractive index.

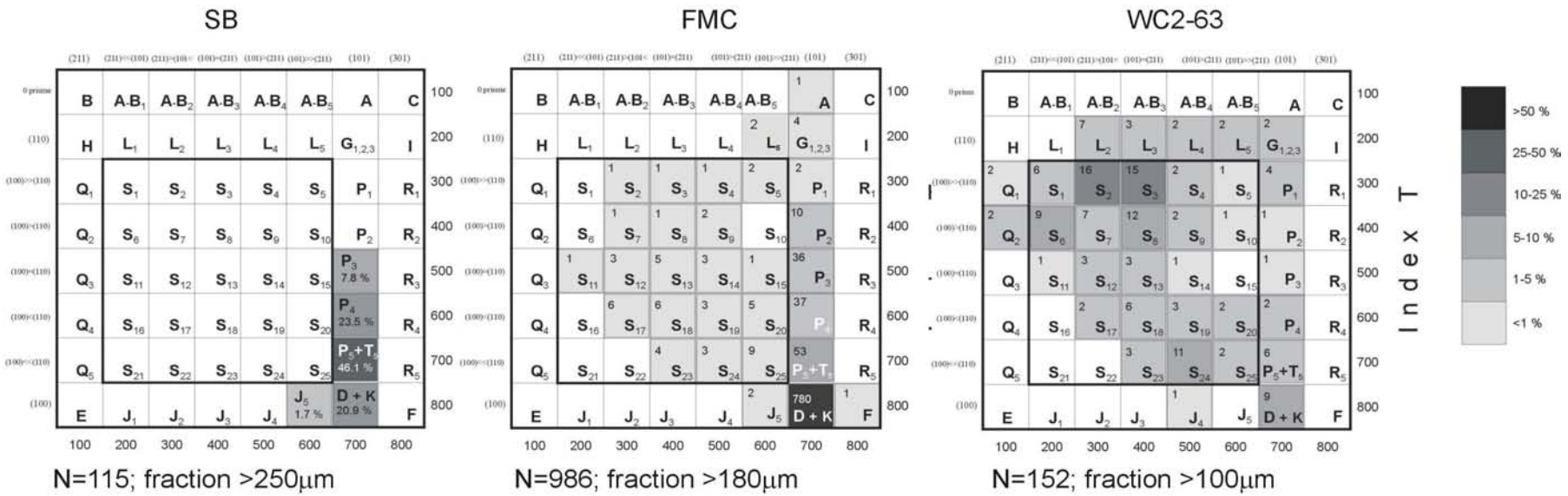

Studied fraction:	N=400	N=3000	N=360
Typology determined:	N=115	N=986	N=152
U-Pb dated:	N=35	N=80	N=48
Types dated:	All J5, P3, P4 30% of P5 / D	All S -types, J, A, G, F, P1, P2 30% of P3 / P4, 10% of P5, D	Selection of: "Zircons with fresh edges"
Location: (WGS84-UTM/UPS)	0361271 6691808	0354105 6662273	0364916 6658366

Fig. 13: Typology of zircons in WC2-63, FMC and SB

The typology grids report the frequency of apparition of the different morphological sub-types. N indicates the number of crystal measured and present on the grid. Undetermined zircons are not part of this number. We give more details about the picking, selection process and the U-Pb dating conducted ulteriorly. The composition of the WC2-63 sample allows a maximum of 10-12% mixing component with the SB-FMC samples from the local MPD. It implies the sedimentary source for the Beverley Sands is not to be found in the MPD but elsewhere. The S-types but also the L-types indicate peraluminous granites in the source.

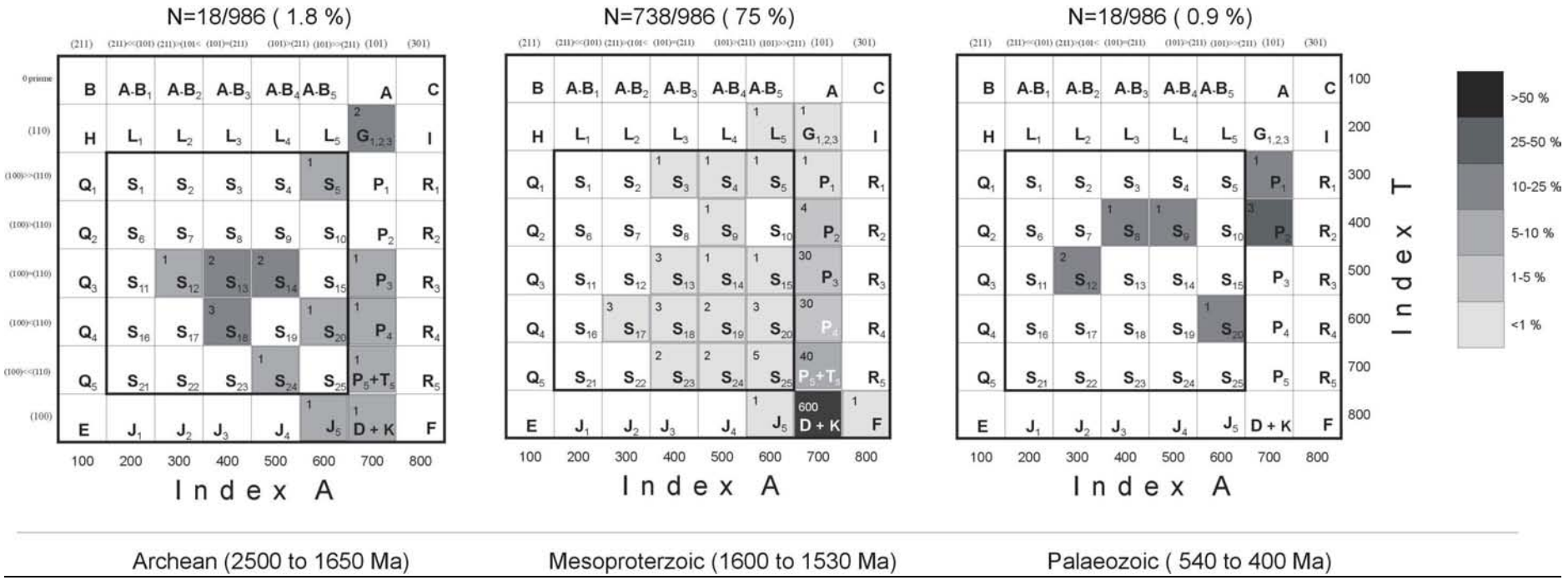

Fig. 14: Typology of zircons in FMC divided by age groups (from U-Pb data)

The typology grid from the precedent figure has been divided into 3 diagrams. As a result, minor populations are underlined. The group I: Archaean-Proterozoic present a mix of alkaline and calc-alkaline zircons; it certainly relates to the zircons coming from the metasedimentary basement unit (Freeling Heights Quartzite). The group II: Mesoproterozoic is identical to the alkaline zircons from MPD (SB). The group III: Palaeozoic displays a minor population of calc-alkaline zircons corresponding to the Palaeozoic local intrusives.

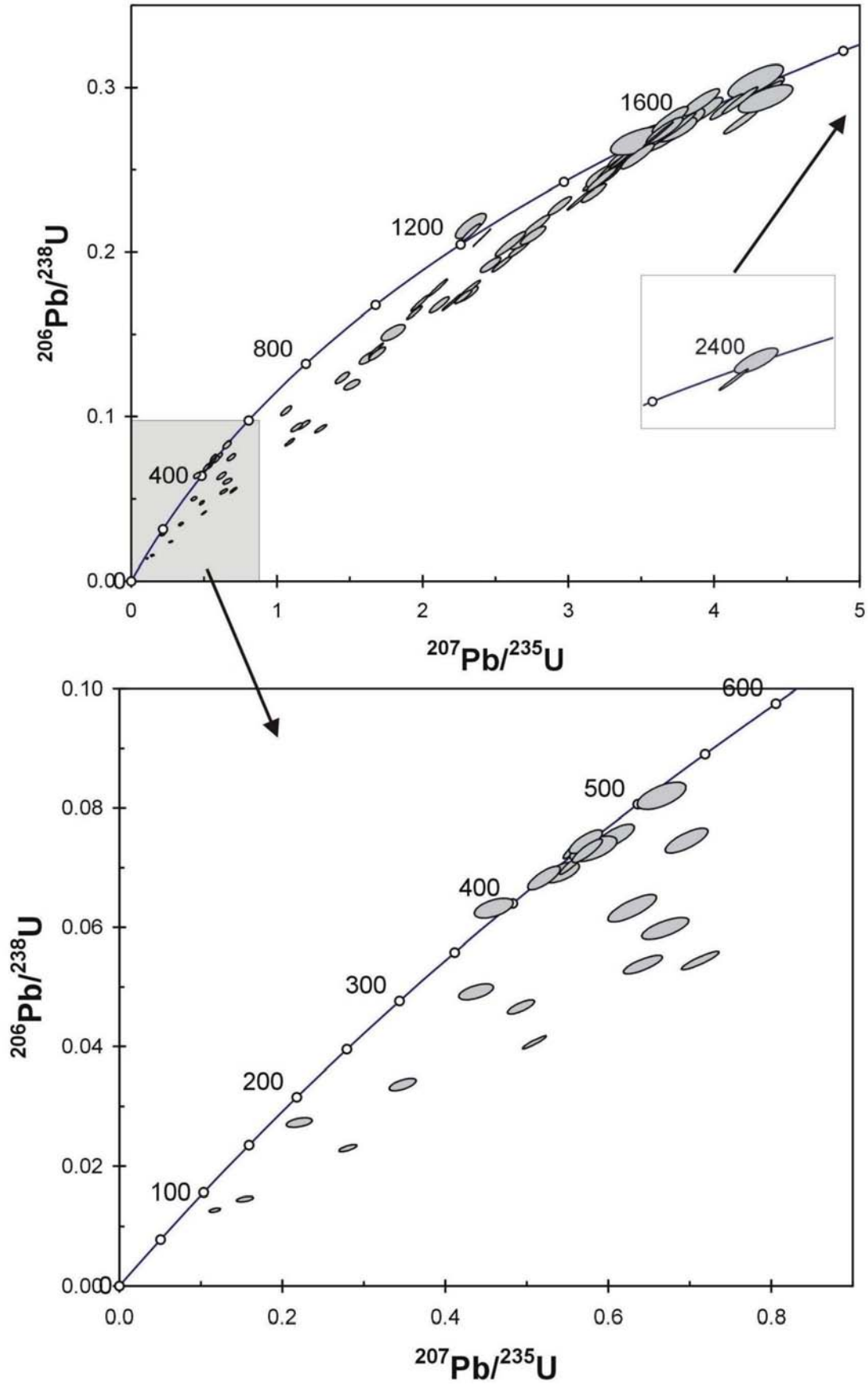

Fig. 15: U-Pb Concordia diagram of Four Mile Creek zircons (FMC) with 2σ ellipses

4.4 U-Pb zircon data

4.4.1 U-Pb ages of "FMC" zircons

U-Pb data were obtained by LA-ICP-MS on a representative subset of zircons with P3 to D morphology and on all zircons with other typologies picked from a bulk 3000 zircons sample. The original typology grid from (Fig.13) has been divided into 3 new diagrams of age group populations: Archaean to Mesoproterozoic (2500-1650Ma), Mesoproterozoic (1600-1530Ma), and Palaeozoic (540-400 Ma) (Fig.14); this representation helps to illustrate how a small proportion of zircons with different ages can be hidden in a typology grid, when mixed to a major component. A population of S-type zircons, centred on S13 (Fig.13) and dated around 1640-1730 Ma can be interpreted to be of calk-alkaline granite origin. The zircons are plotted on a U-Pb concordia diagram (Fig.15).

Finally, the selective typology dating proves to be an excellent technique to study minor age populations. A classic SHRIMP "shot-gun" approach on 100 zircons selected at random would have statistically produced only Mesoproterozoic and discordant zircons and no Palaeozoic ages. Even with such a bias, most dated zircons are Mesoproterozoic (~1560 Ma) and fit on a Discordia line toward 100-250 Ma. However, there is a total absence of zircons <400 Ma. The isotopic data are reported in Appendix V.

4.4.2 U-Pb ages of Beverley Sands zircons (WC2-63)

Zircons from the Beverley sands are especially abundant in some layers and maximum content was observed at the -124 metres level. The exotic populations observed during the morphology and typology study (Fig.9) were hand-picked from this level for U-Pb dating. The results are reported in Table 4. Special attention was given for the zircons with crystalline faces and free of mechanical wearing. As a result of the selective picking, 70% of analysed crystals were showing concordant U-Pb ratios. Data are plotted on the concordia diagram (Fig. 16) and the pictures of dated zircons reported in Fig.17.

Three major groups of ages are present: (1) Cretaceous-Jurassic zircons (24%) and (2) Permo-carboniferous zircons (56%), as well as a Lower Palaeozoic component from Ordovician to Devonian (20%). The selective picking of clear unworn zircons successfully correlates with the youngest zircons. The youngest zircons is 130±2.5Ma, giving a "maximum age" for the Beverley Sands. With a larger sample of selected zircons, this age could possibly be lowered to the Cainozoic; the search for younger zircons would be difficult owing to the quasi-absence of Cainozoic felsic igneous rocks in Australia. Palynology data on the Namba Formation remains therefore the best approach for dating the sedimentation interval from ~24 Ma to ~6-4 Ma (Martin, 1990).

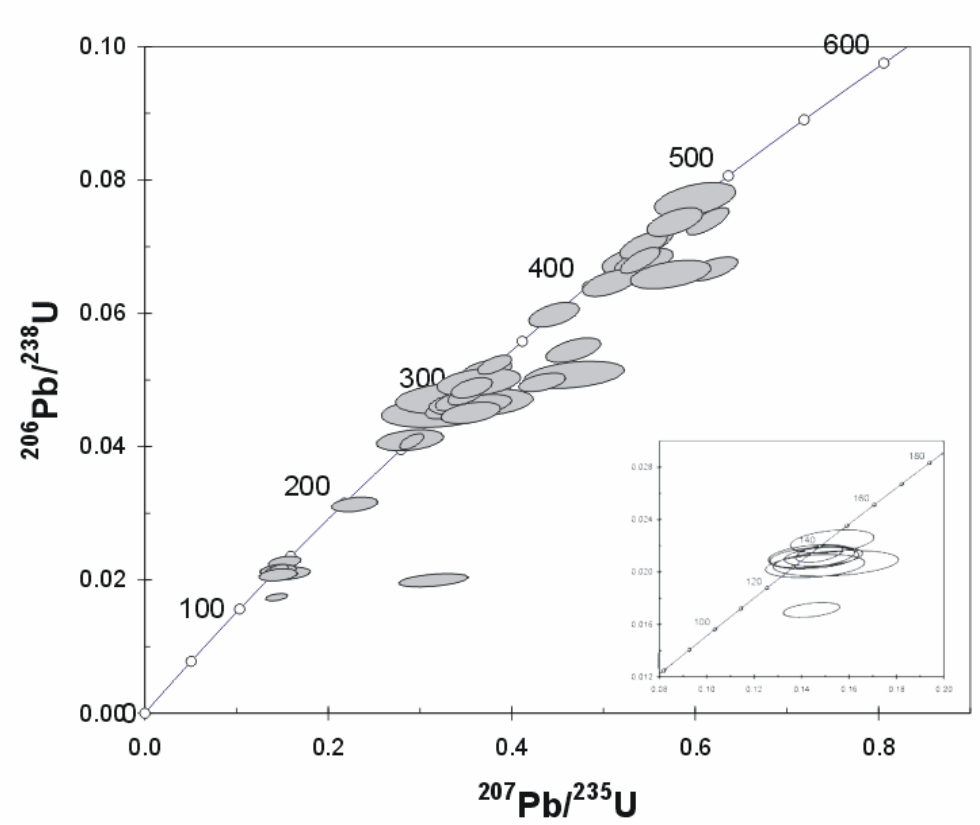

Fig. 16: U-Pb Concordia diagram of Beverley sands zircons (WC2-63) with 2σ ellipse

The major age cluster is Permo-Carboniferous and indicates a sedimentary provenance from Eastern Australia. The youngest zircon found at 130 Ma constraints the Beverley Sands to a maximum age. This could however be lowered by using a larger population of zircons.

					Concordant ages (Ma)	
Name	**Typology** (subtypes)	**Th** (ppm)	**U**	**U/Th**	**Age** ± 2σ	**Stratigraphic period**
BE03z01	S24	115	99	0.860	130 ± 2.5	Cretaceous
BE01z03	P4 (vo)	60	58	0.963	130 ± 4	Cretaceous
BE02z24	S20	101	81	0.800	134 ±4	Cretaceous
BE02z07	P1 (vo)	303	280	0.924	135 ± 5	Cretaceous
BE01z14	S4 -S5 (vo)	120	111	0.926	135 ± 5	Cretaceous
BE02z26	S?	317	277	0.874	136 -3/+4	Cretaceous
BE02z06	S14	188	182	0.970	142 -5/+6	Cretaceous
BE01z07	D (vo)	87	104	1.193	196 -4/+5	Jurassic
BE02z04	P3	217	289	1.334	255 -5/+8	Permian
BE01z02	S23 -S24	39	60	1.545	257 ± 10	Permian
BE01z05	S12 -S13	51	79	1.527	284 ± 15	Permian
BE01z18	S24	145	185	1.274	286 ± 10	Permian
BE02z05	–	70	87	1.239	290± 9	Permian
BE01z08	–	255	346	1.358	293 ± 8	Permian
BE02z14	–	182	173	0.953	294 ± 9	Permian
BE01z17	–	68	51	0.744	296 ± 15	Permian
BE01z09	P1	215	200	0.930	297 ± 8	Permian
BE01z20	–	185	141	0.763	297 ± 8	Permian
BE02z27	S23	244	306	1.252	300 ± 8	Carboniferous
BE02z23	–	250	231	0.924	304 ± 8	Carboniferous
BE02z03	S20 -P4	219	161	0.732	304 ± 11	Carboniferous
BE03z02	–	230	168	0.732	306 ± 10	Carboniferous
BE02z10	J4	145	122	0.844	312 ± 14	Carboniferous
BE01z04	S23	478	490	1.025	313 ± 8	Carboniferous
BE01z15	–	208	239	1.149	315 ± 20	Carboniferous
BE01z06	–	155	145	0.939	323 ± 10	Carboniferous
BE02z19	–	305	302	0.991	327 ± 8	Carboniferous
BE01z01	P?	197	182	0.923	373 ± 11	Devonian
BE02z08	–	279	290	1.040	404 -8/+15	Devonian
BE01z12	–	174	164	0.940	424 ± 11	Silurian
BE02z09	S19 -S24	139	153	1.101	437 ± 12	Silurian
BE02z01	S12?	178	598	3.370	441 ± 11	Silurian
BE02z22	–	239	196	0.820	459 ± 11	Ordovician
BE02z02	S24?	104	128	1.235	478 ± 17	Ordovician

Table 4: Ages of Concordant zircons from WC2-63 (Beverley Sands) and their typology

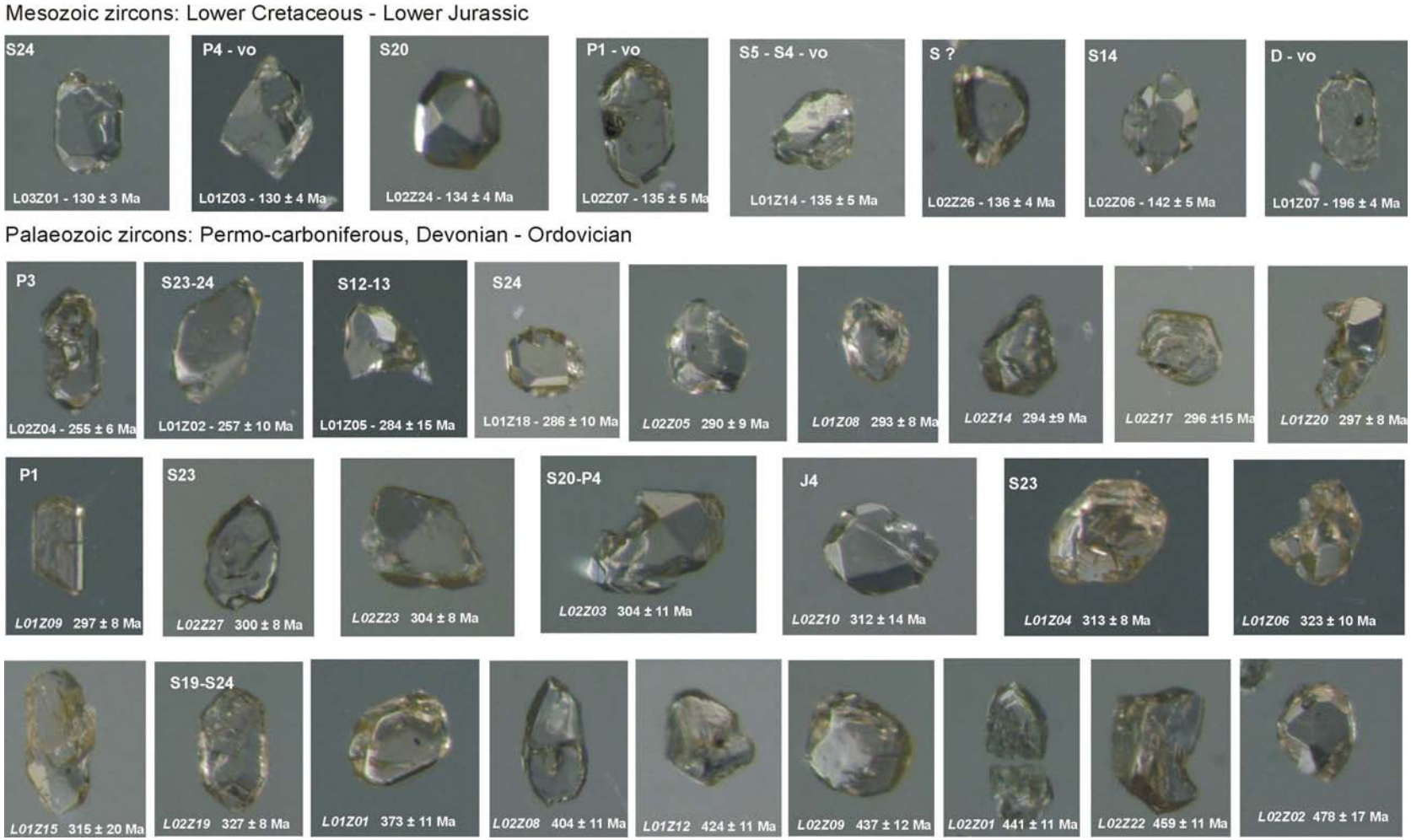

Fig. 17: Pictures of dated zircons from the Beverley Sands (level -124m) with the typology data & U-Pb ages

The typology subtypes are annotated with the "vo" mention, when melt inclusions or ignimbritic textures favour a volcanic origin.

5 Authigenic mineralogy

5.1 Native metals

5.1.1 Native copper and copper-zinc alloys

Authigenic native copper is present throughout the drilled length of the Namba Formation but also appears in minor amounts in the Willawortina debris-flows (possible contamination from down-hole during trays storage). Most of the grains of native copper appear bright red, with a metallic lustre. Some of these metallic grains are dendritic or spongy and authigenic origin is evident. SEM examinations of the natural grain surfaces reveal some sulphur, locally oxygen and frequent remnant of kaolinite. The oxidised rims are either dark red, corresponding to cuprite (Cu_2O) or black for tenorite (CuO) (Fig.19). The nature of sulphide-rich rims is more uncertain because of the thin irregular surfaces. Pb is also detected by EDS on some of the grain rims.

Electron microprobe analyses on polished surfaces gives excellent analytical totals. Native copper grains contain variable proportion of Zn, with most of the grains having Zn < 2 wt-%. All analyses fit linearly on the Cu-Zn system. More rarely, some grains of gold colour have Zn-rich compositions corresponding to Cu_2Zn (Fig.18). This latter composition is identical to a probable new mineral species described in (Jambor and Roberts, 2000, Novgorodova *et al.*, 1980). The chemical formula determined by electron microprobe is $Cu_{1.97}Zn_{1.03}$. Occurrences of this mineral composition were found in the upper enrichments of gold-bearing quartz-carbonate veins in Transcaucasia and Southern Urals (Russia) (Novgorodova *et al.*, 1980), in silicified zones in a porphyry copper deposit (Yulong ore district, Tibet) and brecciated zone of the Ruerogai gold deposit (Sichuan Province, China) (Jambor and Roberts, 2000). Compositions with less Zn are more common and were found in a wider range of environments: lunar regolith, kimberlites, basic and ultrabasic rocks, hydrothermal ores, volcano-sedimentary sequences and pelagic sediments (Dekov *et al.*, 1999).The origin of the mineral is interpreted to be hydrothermal, resulting from wall-rock interaction and reduction by graphite. The lustre of the Zn-rich grains rims is dull and a detrital origin is thought to be the more plausible. A contamination by a man-made alloy is unlikely because of the association with a extensive Cu-Zn composition range (Fig.18).

At a regional scale, native copper has been found at the basis of the Tertiary sediments on the Benagerie Ridge at the Kalkaroo Prospect and in some hard-rock copper prospects and old mines of the Mt Painter Domain (Noble *et al.*, 1983). Native copper is also certainly widespread on the basement-sediments interface of the Eastern side of the Frome Lake (Burtt *et al.*, 2004).

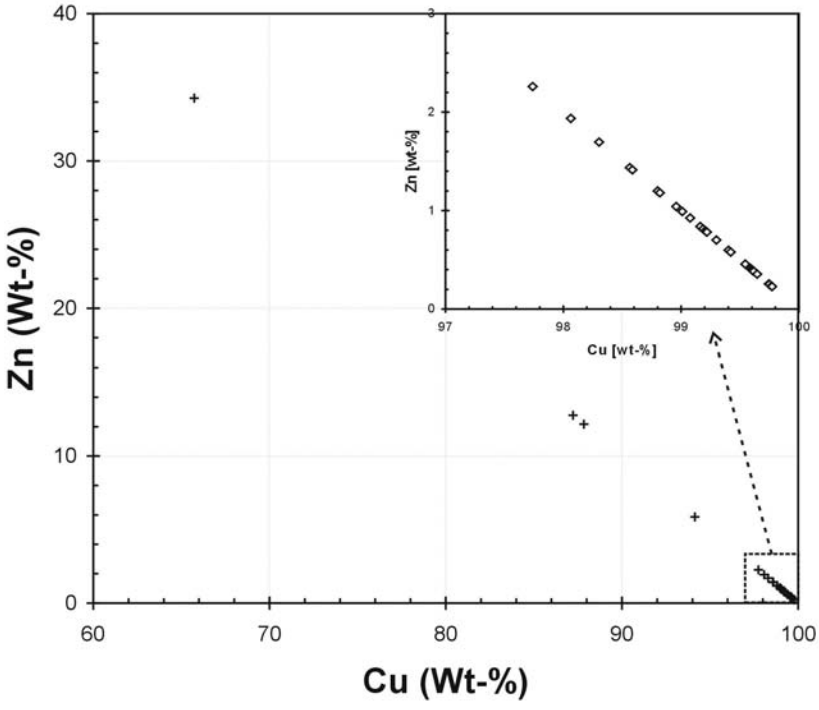

Fig. 18: EMPA analysis of native copper & Cu-Zn alloys from the Beverley Sands (WC2)

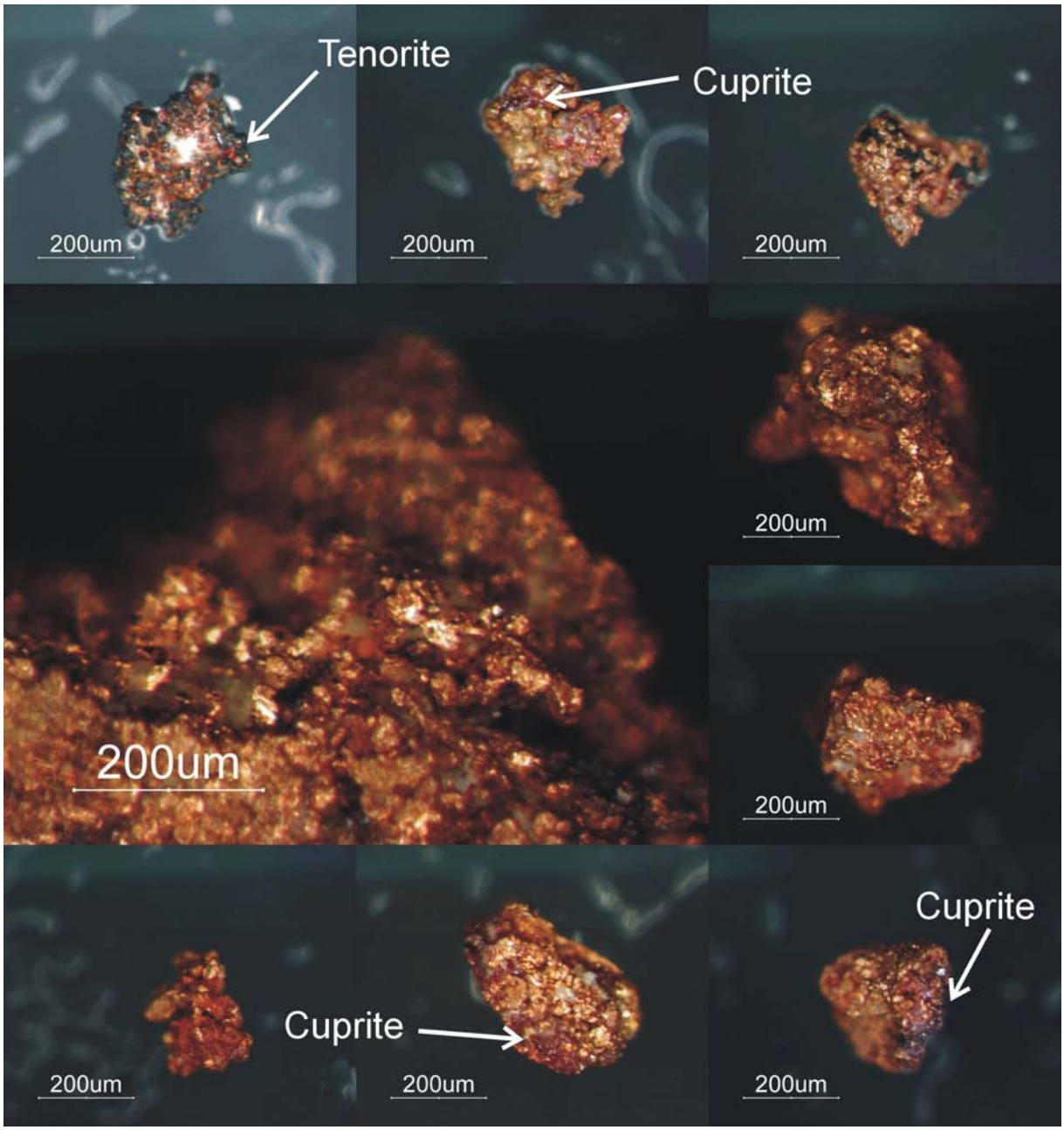

Fig. 19: Native copper grains from the Beverley Sands (WC2)

The bright metallic lustre is present on most of the grains, local coatings or rims of tenorite and cuprite are sometimes present.

5.1.2 Native lead (Pb)

Some native lead particles (up to 0.7 mm) have been found in the more reduced clay layers of the coffinite mineralisation (Fig. 20). The composition of the grains was determined using electron microprobe. Compositions vary from pure Pb to more complex compositions with Cu and As (Table 5). Beverley native lead is sometimes spongy and despite the careful polishing, some surfaces were inadequate for quantitative electron-microprobe analysis. Contents of sulphur are <0.1 wt-%. Surfaces were examined by electron microscope and EDS data acquired to check the absence of oxygen. Bluish and spongy-like zones are impure and are rimmed by PbS / PbO. High Cu (5.2%) and As (2.1%) enrichments are present in one grain. The permeability of the lead-bearing clay of Beverley is low and the recovered grains from the panning concentrates were bright metallic looking, bluish on some rims. The grains were clearly preserved of air oxidation in their matrix for the 31 years of storage.

The occurrence of native lead has been documented in a few tens of localities worldwide and its rarity is also biased because the mineral has frequently been disregarded as a contamination or an artefact. Most of the native lead occurrences are of hydrothermal origin, together with native metals (copper, tin, silver and gold) or sulphide minerals. Low-temperature formation, authigenic native lead is rare and was observed in the Polish Kupferschiefer

(Sawlowicz, 1990), present in microenvironments reduction spots in association with covellite, digenite and pyrite. Native lead contains few percents of Cu, Zn, Sb and lower amounts of Bi, Ni and Ag. Native lead is also mentioned in the well pipes and tanks of the oilfield brines in the Cheleken region in Turkmenistan, where it co-precipitates with sphalerite, galena and pyrite (Warren, 2000).

	Pb02	*Pb03*	*Pb04*	*Pb05a*	*Pb05b*	*Pb06*
Pb	95.00	91.55	100.26	99.92	90.95	91.20
Cu	<0.19	<0.19	<0.19	<0.19	5.20	<0.19
As	<0.21	<0.21	<0.21	<0.21	2.05	0.61
S	<0.10	<0.10	<0.10	<0.10	<0.10	<0.10
Fe	<0.06	<0.06	<0.06	<0.06	<0.06	<0.06
SiO_2	0.26	<0.20	<0.20	<0.20	<0.20	0.34
K_2O	<0.50	0.81	<0.50	<0.50	<0.50	1.93
P_2O_5	<0.18	<0.18	<0.18	<0.18	<0.18	<0.18
Total	95.26	92.36	100.26	99.92	98.20	94.08

Table 5: EMPA analyses of native lead particles

All values in Weight-%. Due to the porous texture of some grains, the sums are sometimes lower than 100%. Undetected: Se <0.16, Co < 0.10, Zn < 0.21, Ca < 0.14, V < 0.16, Pd < 0.16, Mo < 0.19, Ba< 0.32 wt-%

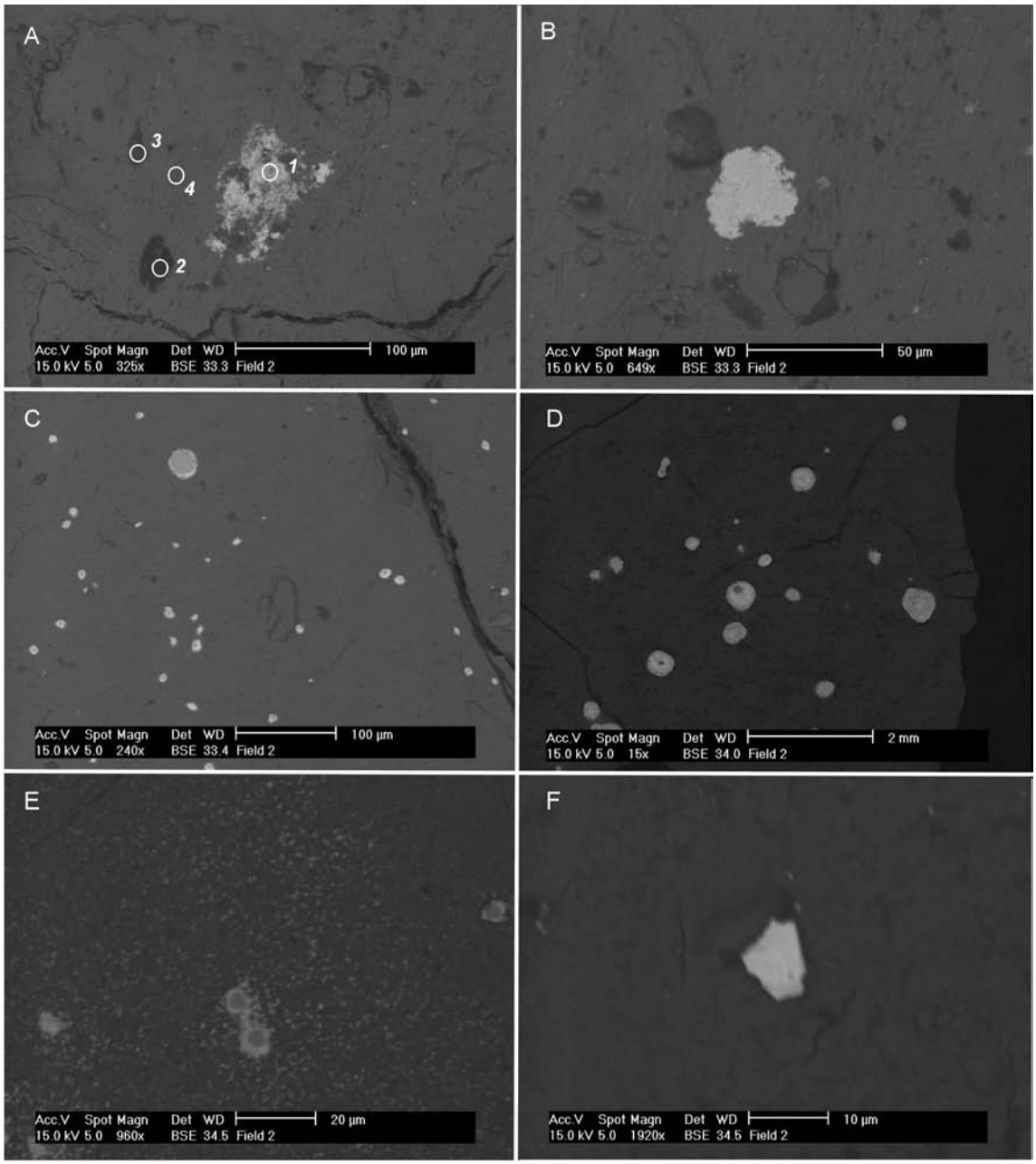

Fig. 20: Authigenic mineral inclusion in the Beverley sediments: barite, coffinite, native lead.

A) *978-1: Barite in alpha mudstone. EDS spots are: 1: barite, 2: organic matter (C, Cl, Si, Al, and Na), 3: detrital silicate (Mg, Fe, Al, Si, O, and H), 4: Clay matrix with Si, Al, Mg, K, Fe, Ca, Na, O, and H). Approximate elements ratio is* $Na_{0.9}K_{0.6}Ca_{0.4}Mg_{2.2}Fe_{1.1}Al_{10.0}Si_{24.9}O_{60.}$B) *978-2: Sr-rich barite.* C) *976: Coffinite - sulphides nodules (5-30 mm) in the mudstone matrix. Some sulphide cores show a losange shape that could be marcasite.* D) *976: Large coffinite nodules (up to 1mm) on the same sample.* E) *976: Coffinite cluster as individual particles (<2 mm) and pyrite-coffinite nodules (~5-10 mm).* F) *976: Authigenic native lead particle (first observed in heavy mineral concentrates).*

5.2 The "uraniferous nodules"

5.2.1 Introduction

Black nodules of coffinite-uraninite and framboids of carnotite are the only uranium minerals found in the authigenic assemblage. Quantitatively, the black nodules account for the major part of the uranium content. Several grams of them were separated from a mudstone containing 1 wt-% UO_2. Carnotite was found in association in all the nodules-bearing samples, disseminated in the mudstone-clay matrix. Carnotite appears as the exclusive uranium mineral in most of the sands-silts samples and kaolinite is frequently associated to it. Carnotite contains U^{6+} mineral and does not require reducing conditions to form.

5.2.2 Background data on coffinite

The coffinite composition is variable and its formula was first written as $(U[SiO_4]_{4-x}[OH]_{4x})$ by (Stieff *et al.*, 1956). Because of the inhomogeneous nature of coffinite and its water or hydroxyl content, electron microprobe data gives analytical totals that are frequently under 90%. The black masses frequently host fine mineral inclusions, and are characterised by high porosity and substitution of numerous elements such as Y, REE, Ca and P. Uraninite also forms mixtures with coffinite, complicating the knowledge of the exact composition of the mineral. This mineral mixture is quite common for coffinite (Ludwig and Grauch, 1980). U^{6+} has been measured in some coffinite by X-ray photoelectron spectroscopy (Goldhaber, 1977). Goldhaber (1977) suggested that hydroxyl groups are not present in the coffinite structure; this assumption was confirmed by the IR spectroscopic study by (Janeczek, 1991), which shows the presence of absorbed molecular water and but no structural (OH) binding. Janeczek proposed the new formula $USiO_4.nH_2O$, in simplification of the O = 4.00 normalised measured (U, Ca, Y, REE) / (Si, P) = 0.93-0.98. The low (U, Ca, Y, REE)/(Si,P) ratio may reflect an intimate mixture with uraninite. The formation of coffinite is described as a combined adsorption and reduction process by (Goldhaber *et al.*, 1987). They found that high dissolved silica concentration favours coffinite versus uraninite; concerning the reduction mechanism of the UO_2^{2+}, for example (Goldhaber *et al.* 1987) show experimentally that uranyl adsorbed on kaolinite surfaces is quantitatively reduced by dissolved H_2S (pH=7, 35°C, pH_2S = 0.081 atm.).

5.2.3 Chemical composition and morphology of the uraniferous nodules

Black uraniferous nodules abound in the mineralised basal silts and sands of the Beverley deposit. Nodules show a black resinous lustre on fresh fractures. Their sizes vary from a few tens of μm up to 6 mm (Fig. 20 & 21), but are more commonly between 0.4 and 1.0 mm. They frequently contain a Co-rich pyrite core. The pyrite cores are always spherical and frambroidal. The Co-contents of pyrite cores are homogeneous in a single nodule but vary a lot from one nodule to another. EMPA data are reported in Table 6. Small (2 μm) inclusions of clausthalite (PbSe) have been detected by EDS in coffinite compact zones. Microscopically, the texture of the coffinite nodules appears as a matrix of small elongates (oval) particles averaging a diameter of 1-2 microns. The pattern of the coffinite crystals is evocating of a bacterial origin (Fig. 22). Similarly, the smallest coffinite grains from the mudstone matrix are also in the 1-3 μm range, close to the bacteria-like ovals (Fig.20).

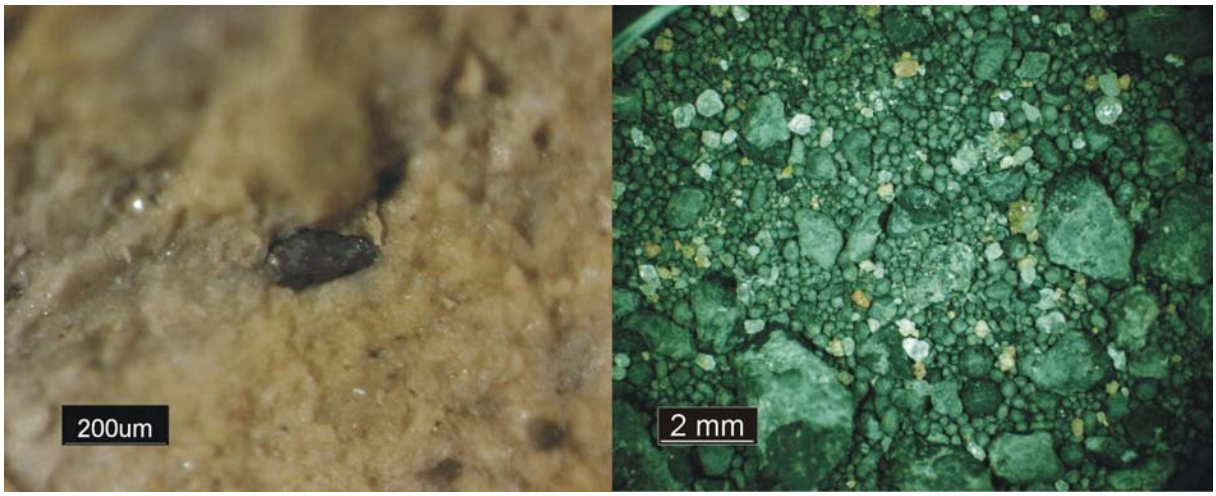

Fig. 21: Coffinite nodules in silt matrix (left) and HM concentrates from the Beverley Sands (right)

The nodules or aggregates of coffinite vary in size and shape but frequently display a spherical or ovoid morphology.

	1	*2*	*3*	*4*	*5*	*6*	*7*	*8*	*9*	*10*	*11*	*12*	*13*	*14*	*15*	*16*	*17*	*18*	*19*	*20*	*21*
S	53.55	53.68	51.09	54.17	51.80	53.32	53.39	52.77	52.95	53.53	53.66	52.20	53.65	51.73	52.41	50.05	44.11	45.46	53.32	53.46	54.31
Fe	38.08	45.44	41.62	46.06	46.58	40.88	40.38	39.83	39.50	39.81	47.39	34.32	41.38	35.25	37.54	41.44	39.16	44.25	41.71	44.84	46.04
Co	3.48	0.64	1.39	0.46	0.14	2.13	2.19	2.53	2.62	2.51	0.12	4.68	2.09	4.10	3.13	1.22	1.04	<0.10	1.04	0.32	0.16
As	<0.21	<0.21	0.51	<0.21	0.28	<0.21	<0.21	<0.21	<0.21	<0.21	<0.21	<0.21	<0.21	<0.21	<0.21	0.18	0.41	0.27	<0.21	0.23	0.25
Se	<0.16	<0.16	<0.16	<0.16	<0.16	<0.16	<0.16	<0.16	<0.16	<0.16	<0.16	<0.16	<0.16	<0.16	<0.16	<0.16	0.20	<0.16	<0.16	<0.16	<0.16
Sum	95.11	99.77	94.61	100.69	98.80	96.32	95.96	95.13	95.08	95.85	101.17	91.20	97.12	91.08	93.07	92.89	84.91	89.98	96.07	98.86	100.77

Table 6: EMPA analyses of Co-rich pyrite cores

All values are reported in weight-percents.

The electron microprobe analyses conducted on the nodules are semi-quantitative and the presence of Al is a good indicator of the presence of clay minerals in the excited volume. The coffinite composition is changing but invariably contains some P and Ca. Sulphur was frequently found in the nodules, nearly at the background level, but certainly because of small sulphides particles in the coffinite matrix. All nodules analyses range from 65 to 92% UO_2, and single nodules show large variations in chemical composition as represented of the cross-sections (Fig. 23). The varying U content is most likely related to the presence of varying amounts of uraninite admixture: a coffinite of stoichiometry $USiO_4 \cdot H_2O$ would contain ~78% UO_2. The values represent a minimum, in view of the systematic porosity, evaluated to be between 2 and 10 % from the SEM images (Fig. 22). The *(U+Ca)/(Si+P)* ratio of the theoretical coffinite should be between 1.00 and 1.20. Two different mixtures processes are evidenced: coffinite + uraninite and coffinite + SiO_2 (am) – water. The average water content of coffinite can be evaluated using the variation diagrams on Figure 24. The coffinite formula is certainly hydrated in the range of $USiO_4 \cdot nH_2O$, with $1.0 < n < 2.5$.

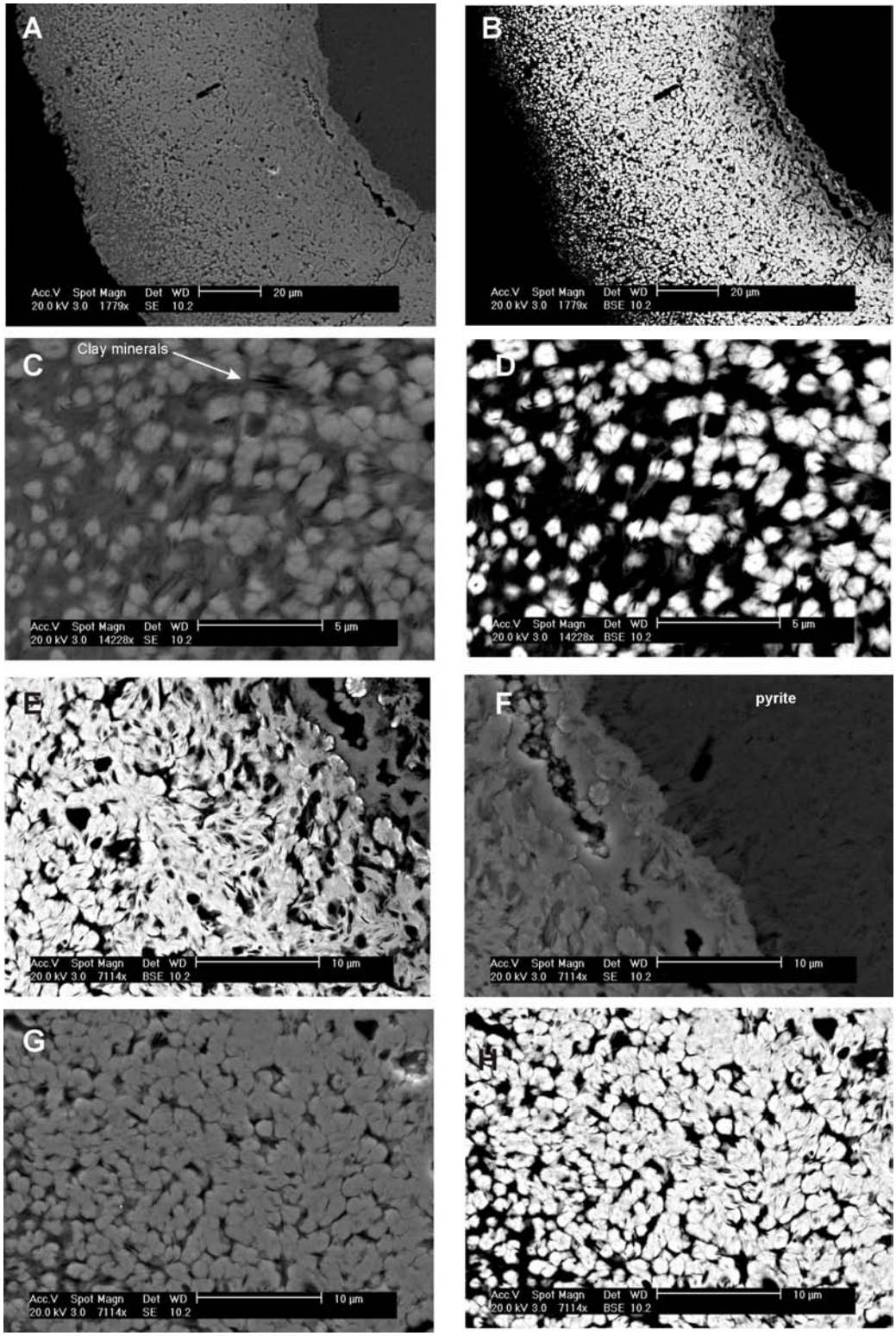

Fig. 22: Coffinite textures revealed by SEM images.

Coffinite nodule No. 157 - [-132 m], cobaltian pyrite & coffinite bacteria-like particles. Smectite flakes are also intermixed (black).Each view has also been photographed by BSE to enlighten the heavy elements (here U); a) and b) show the general view on the nodule and its core; c) and d) a zoom in the outer rim; e) and f) a zoom on the pyrite core and coffinite contact; g) and h) the denser coffinite zone.

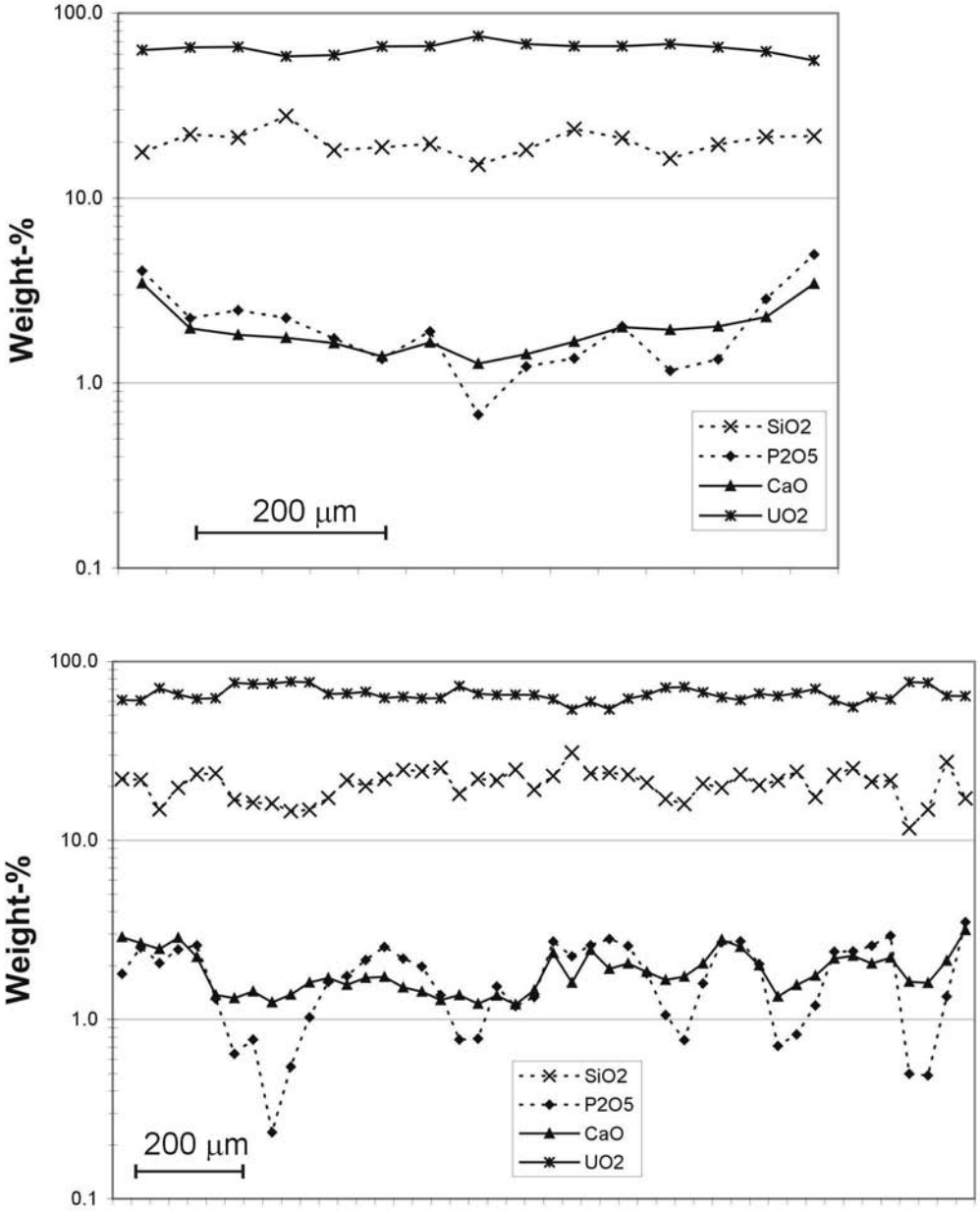

Fig. 23: EMPA cross-sections of two coffinite nodules.

Coffinite composition is extremely variable and displays chaotic patterns due to porosity and admixtures of, uraninite and amorphous silica. P is present in the coffinite structure and minimum peak spots are related to high uraninite mixing.

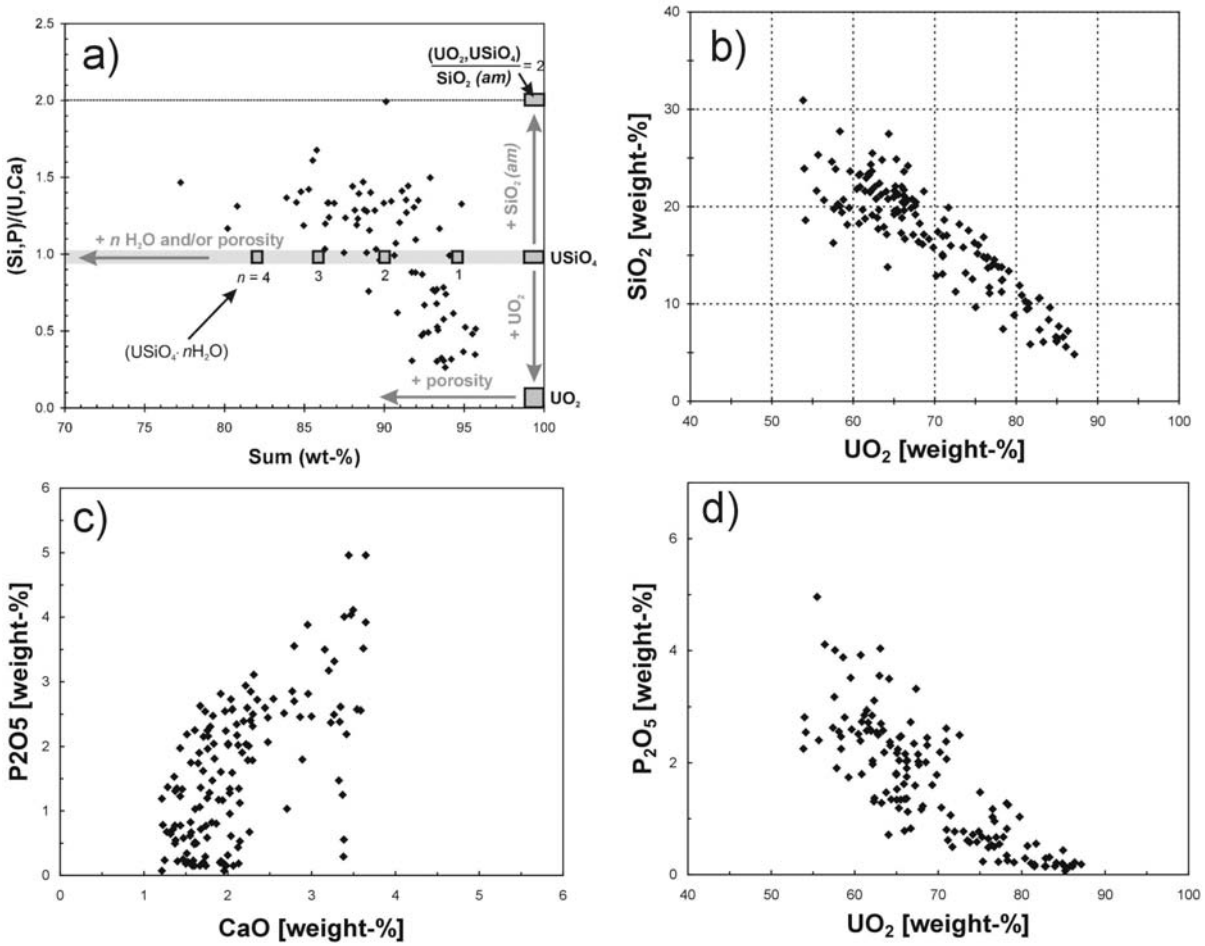

Fig.24: Chemical composition of coffinite based on EMPA

a) Chemical representation of coffinite nodules by (Si,P)/(U,Ca) ratio and analytical sum. The mixing processes with amorphous silica, porosity, water in the coffinite structure, and uraninite are represented on the diagram. Dark grey compositions represented are $USiO_4 \cdot nH_2O$, from n=0 to n=4, UO_2 and a mixture of anhydrous coffinite and silica 1/1. b) SiO_2/UO_2 diagram: compositions fit on a linear trend; c) P_2O_5/CaO; d) P_2O_5/UO_2.

A fraction of coffinite nodules (10 mg) was crushed and an X-ray powder diffraction dataset acquired. The diffractogram was processed using Rietveld refinement and the relative proportion of uraninite and coffinite determined. Peak processing gives minor uraninite (25%) and dominant coffinite (75%). However, the residual intensity on some of the coffinite peaks may represent anomalous peak intensities related to its poor crystallinity due to radiation damage (Fig. 25). Unit cell values for uraninite is a = 5.436(1) Å and for coffinite a = 6.971(2) and c = 6.255(2) Å.

In conclusion, the nature of the coffinite nodules can be considered to be a mixture of coffinite and uraninite mostly, with additional but variable proportions of amorphous silica, detrital quartz inclusions, Co-rich pyrite, clay minerals and porosity. This nature is somewhat problematic for the application of U-Pb dating techniques.

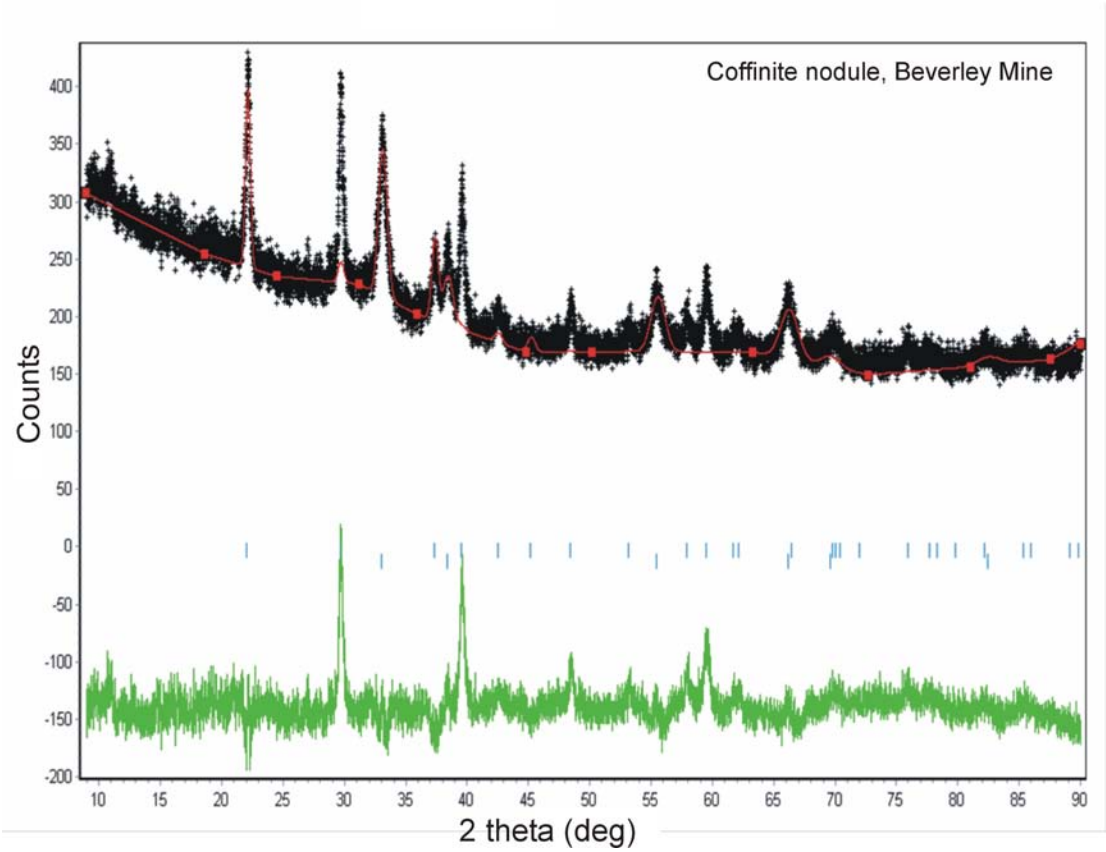

Fig. 25: Rietveld refinement of X-ray powder diffractogram with coffinite & uraninite.

5.2.4 U-Pb geochronology and geochemistry on coffinite / uraninite

U-Pb dating on coffinite has been successfully applied to some Wyoming sandstone-hosted uranium ores (Ludwig, 1979). Coffinite nodules from Beverley are of inhomogeneous nature and porous. Because of this, our La-ICPMS analyses systematically indicate the presence of high proportions of common lead (more than 50% of the total lead), while the measured isotopic ratio show that the nodules remained more or less open for Pb loss or gain since their formation. Isotopic data has been corrected for common lead and is reported in Appendix V.

Common lead corrections were applied using ^{208}Pb instead of ^{204}Pb, because of the precision required for the young age expected (<30 Ma) and the relatively low Th content compared to U. Error ellipse are drawn on a concordia diagram and several intersect the concordia curve, giving concordant to sub-concordant ages between 6.7 and 0.0 Ma, (2σ, decay-const. errs included) (Fig. 26).

The only hope to be able to get more precise ages on the Beverley black ores will be to find denser uraninite masses or to analyse the mineralised clays on different samples of dissolved sediment. The U-Pb system could act more closed at a centimetre scale rather than at the micron scale. A sample of U-rich mudstone sample was analysed by La-ICP-MS on a fused homogenised rock powder (80 grams) used for XRF. XRF data on the same powder gives $Pb^{tot}/U = 0.00639$ whereas ICP-MS measurements give $U^{tot}/Pb = 0.00475$ (based on ^{208}Pb measurement only). Deducing the common Pb out of the whole-rock (XRF-ICPMS difference, the remaining Pb (~7.4 ppm) is expected to be the radiogenic one. Calculated age for this values ($Pb^{rad}/U = 0.00097$) gives **~5.3 Ma**, with an unknown error.

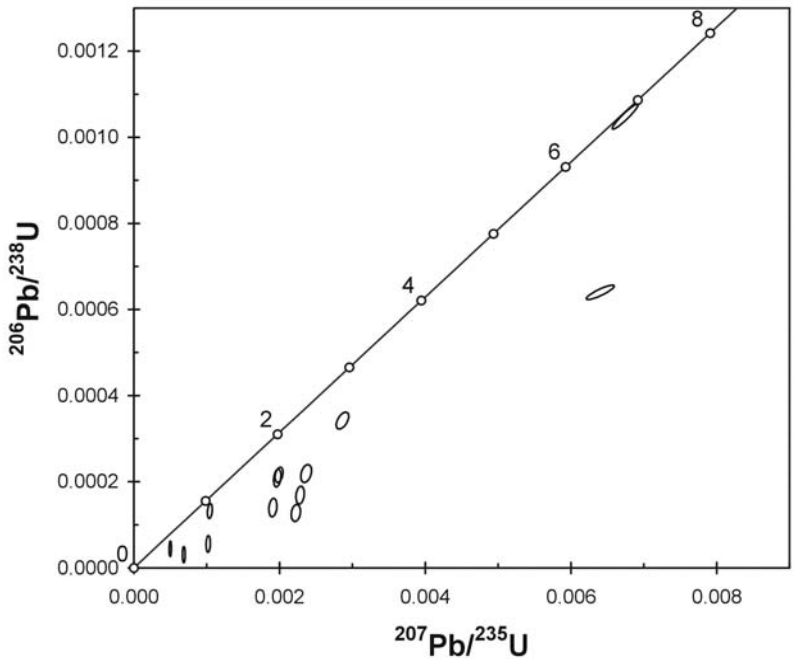

Fig. 26: Concordia plot of coffinite nodules (La-ICPMS)

Most values are discordant and spread from 0 to 7 Ma. This witnesses the difficulty to date porous coffinite.

5.3 Sulphides

5.3.1 Pyrite and marcasite

The two polymorphs of iron disulphides (FeS_2) have been observed: pyrite and marcasite. These minerals can be present as individual euhedral crystals, as framboids and as polycrystalline aggregates. They occur as "free sulphide" grains, in opposition to the already described coffinite nodules bearing Co-rich pyrite cores. The morphology of free pyrite crystals in Beverley sands can be octahedral, cubic, and cubo-octahedral; pyrite frequently forms clusters of 10-30 individuals. The largest recovered crystals reach 400 μm in diameter.

Marcasite occurs as single crystals, twinned crystals or develops aggregates of parallel individuals aligned on their long axis. Twins form perfect angles with an invariant 54° "fer-de-lance" summit. Marcasite forms crystals of similar dimensions to pyrite (Fig. 27).

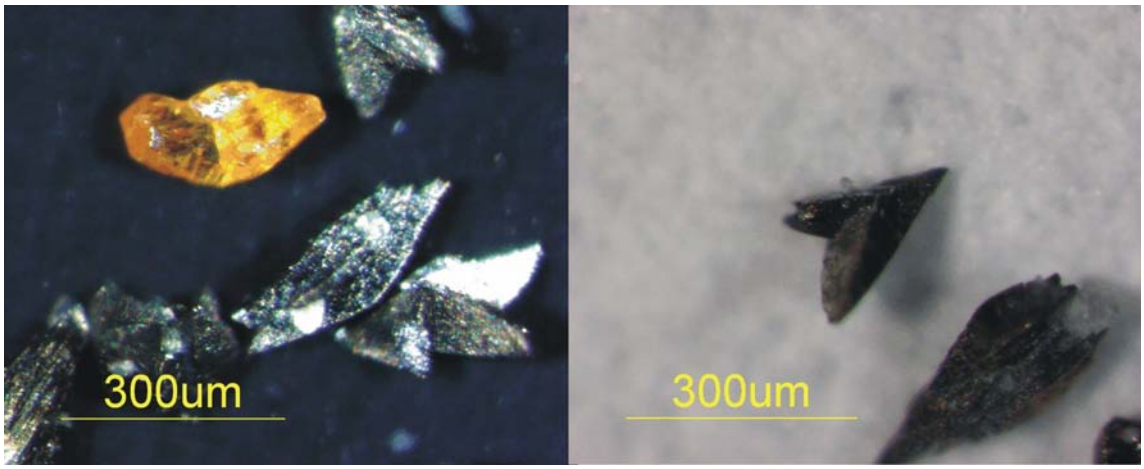

Fig. 27: Marcasite crystals and twinned "fer-de-lance" couples.

Rutile crystal (orange) on the left picture with marcasite twinned crystals

Iron disulphides framboids are of composite nature. They seem to be essentially formed of pyrite but with a minor component of marcasite. No quantification by X-rays diffraction refinement (Rietveld method) like on the coffinite-uraninite nodules was conducted. Instead of this, the limited amounts of clean sulphide fractions were used for the determination of sulphur isotopes (see section 5.3.4).

The chemical composition of the 'free' crystals of pyrite and marcasite is always Co-poor (always < 1 %), in contrast to that forming the cores of coffinite nodules.

5.3.2 Sphalerite

Sphalerite is present in the most reduced level of the coffinite-rich mineralisation (alpha-mudstone). It forms frambroidal grains up to 2 mm in diameter. Sphalerite is easily recognizable by its high refractive index and yellow-brown colour in the heavy non-magnetic concentrates. Framboids generally host numerous small octahedral pyrite crystals, amorphous silica and detrital quartz grains. The composition of sphalerite is invariably ZnS and Fe is barely detectable in EDS spectra.

5.3.3 Chalcopyrite

Chalcopyrite has been observed in the sulphide concentrates in minor amounts. However, the mineral is almost exclusively restricted to a depth of -131 to -133m, in the coffinite-rich layers (Fig.7). Chalcopyrite grains are very small (<100 μm) and difficult to recognise in the sulphides-rich concentrates. The mineral has been identified by EDS.

5.3.4 Sulphur isotopes

Co-rich pyrite cores in coffinite nodules show a $\delta^{34}S$ of +1.0 ± 0.3 $^0/_{00}$. This contrasts with 'free' euhedral crystals of pyrite, marcasite, pyrite and sphalerite framboids which give an average $\delta^{34}S$ values ranging from – 26.2 to -35.5 $^0/_{00}$. Both types of sulphides are authigenic and derived from sulphate reduction, probably from sulphates of similar isotopic composition. Very different conditions of sulphate reduction can explain such isotopic differences (Rollinson, 1993). The sulphate isotopic composition of the groundwater can be estimated from the diagenetic gypsum isotopic composition from soil layers in the Four Mile Creek catchment: $\delta^{34}S$ of +14.0 $^0/_{00}$. This value is

quite similar to other gypsum compositions reported in soils and lakes in north South Australia (Bird *et al.*, 1989, De Caritat and Kirste, 2005).

The strongly negative values found in the sulphides indicate they formed at low temperature by bacterial reduction (Rollinson, 1993); Fractionation process due to the reduction of sulphate from waters (e.g. +14 $^{0}/_{00}$) will produce sulphides with lighter sulphur composition (- 26 ± 10 $^{0}/_{00}$). Waters of the Callabonna Sub-basin display sulphur isotopic compositions ranging from $\delta^{34}S$ +11.5 to 17.0 (De Caritat and Kirste, 2005). As a comparison, sulphides from Eocene organic-rich sandstones from the Eyre Peninsula and the Eromanga Basin sediments (Cretaceous) give negative values between $\delta^{34}S$ -6.1 $^{0}/_{00}$ to -18.4 $^{0}/_{00}$ (Bird *et al.*, 1989). Two explanations can be proposed to explain the isotopic composition of the Co-rich pyrite nodules: (1) Co-rich pyrites were formed by inorganic reduction at temperature >75°C in presence of hydrocarbons, or a similar reaction involving sulphur from organic compounds (Trudinger *et al.*, 1985) ; (2) an authigenic freshwater mud-sulphide precipitation (Rollinson, 1993). This later hypothesis is favoured since we haven't found any indices of higher temperature fluid circulations. The presence of organic matter in the mineralised coffinite mudstones favours a genesis in freshwater lacustrine environment at the time of sedimentation.

High $\delta^{34}S$ sulphide values could also have been explained whether the system would have operated closed, but the absence of intermediate values permit to reject this possibility, the obtained values corresponding to a mixed sample of more than 300 nodules.

In conclusion, the isotopic signature of sulphides associated with the mineralisation of uranium (nodules) indicate they probably formed by inorganic reduction during the mudstone sedimentation. The second category of sulphides (light isotopic composition) certainly formed by bacterial reduction. The coffinite mineralisation which overgrowths the sulphide cores probably formed between these two sulphides generations.

5.4 Sulphates: gypsum, barite, alunite

5.4.1 Repartition of sulphates

Large diagenetic crystals of gypsum (up to 4 cm) disrupting lamination of Quaternary sandstones can be found in the Four Mile Creek alluvial plain. Such gypsum occurrences around the Lake Frome basin have been interpreted to be of evaporitic origin (Draper, 1974). More rarely, gypsum appears as crusts (0.2-0.4 mm crystals) on clay fissures of the Namba Formation. It also clearly originates from evaporitic conditions, which have lead to the saturation of gypsum in desiccation fissures.

Alunite, $KAl_3(SO_4)_2(OH)_6$, was found by Callen and Tedford (1976) in the WC2 drillcore. The presence of this mineral was confirmed by XRD at depth between -105.8 and -116 m. During our SEM observations, we also identified this mineral in the upper layers of the Namba formation, especially associated with kaolinite and highly oxidised sediments. It is noticeable to correlate the absence of sulphides in the -105.8 to -116 m alunite interval. The size of the observed alunite crystals is <2 µm. The denser alunite samples probably contain 10-50% alunite. Alunite is formed in acidic (pH < 4.5) and oxidising conditions and has been found in acid lakes from Eastern Australia (Bird *et al.*, 1989, Long *et al.*, 1992). A tectonic uplift of sulphide-rich sediments can also lead to exposure and oxidation of sulphides and then produce acid water at the surface (Arancibia *et al.*, 2006). Alunite generally forms in arid or semi-arid conditions. Alunite is a potassium-rich mineral whose crystal structure can efficiently retain the argon produced by the ^{40}K radioactive decay; therefore, the formation of the mineral can be dated by the K-Ar or $^{40}Ar/^{39}Ar$ methods (Arancibia *et al.*, 2006, Bird *et al.*, 1990, Itaya *et al.*, 1996). We unfortunately have not found samples pure enough for dating. We interpret alunite of Beverley to have formed under acidic conditions in a lacustrine-marsh system with surficial sulphide oxidation. The presence of a paleosoil at -100 to -102 m with roots remnants and the absence of sulphides from -100 to -116 m favour this interpretation.

Barite is present in the fine mineralised sediments of WC2 as small transparent flat transparent crystals or as spots in the mudstone matrix (Fig.20 & 28). The higher concentration of barite, as observed in the HM concentrates is located in the carnotite mineralisation zone, associated to alunite. Barite is also accompanying the coffinite and sulphide zones. In an attempt to purify alunite fraction, we digested an alunite-rich sample in hydrofluoric acid; the residue of leaching was containing very small barite crystals (<30 µm), unrecoverable using the panning techniques. The chemical composition was only investigated by EDS and is generally pure $BaSO_4$. However, Sr has been detected in one crystal.

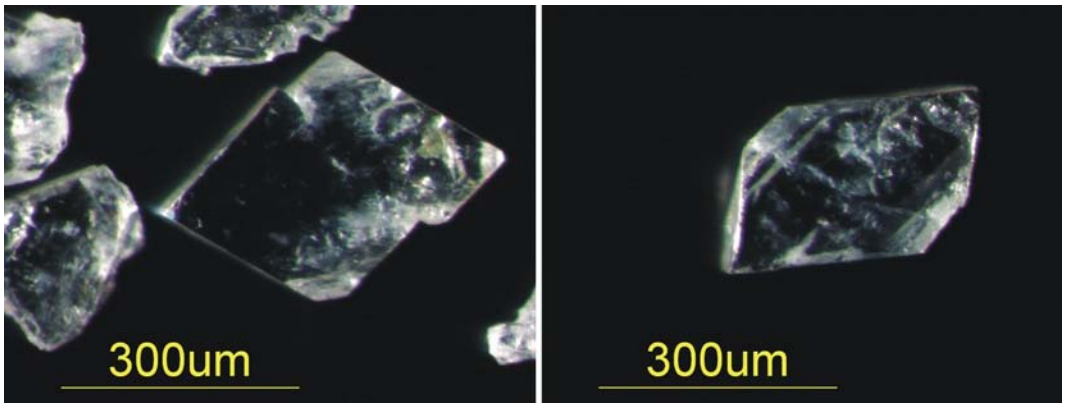

Fig. 28: Barite crystals in HM concentrate from WC2

5.4.2 Sulphur isotopes

Gypsum from Four Mile Creek area gives an average value of $\delta^{34}S$ at + 14.0 $^{0}/_{00}$. A selection of sulphides (pyrite, chalcopyrite, molybdenite and arsenopyrite) from the nearby basement rocks were analysed and found to be lower: +1.8 to +10.1 $^{0}/_{00}$. In the Beverley sands of the Namba formation (WC2), $\delta^{34}S$ in barites ranges between +14.9 and +16.7 $^{0}/_{00}$, (average 15.7 $^{0}/_{00}$).

The high values measured in gypsum and barites suggest sulphates to be the product crystallisation (evaporitic conditions, gypsum saturation) rather than sulphide oxidation from the basement rocks. However, a mixed origin cannot be excluded. Crystallisation of sulphates in evaporitic conditions produces a $\delta^{34}S$ enrichment of around +1.65 ± 0.12 $^{0}/_{00}$ in the crystal phase relative of aqueous sulphate (Thode and Monster, 1965). This is in total agreement with the sulphur isotopic composition measured further east in the Callabonna Sub-basin and the Yarramba Eocene paleochannel, to the South of the Lake Frome (De Caritat *et al.* 2005).

We lack of $\delta^{34}S$ data for alunite in Beverley because of its impure and micro-crystalline nature. For comparison, sulphur isotopes on alunite have been analysed elsewhere in Australia, in the Lake Agar (Eyre Peninsula) and Lake Tyrell (NSW); the $\delta^{34}S$ values are generally between +9.0 and +20.0 $^{0}/_{00}$ (Bird *et al.*, 1989), suggesting a sulphur sources in the sulphates from waters with minor if no contributions from oxidised diagenetic sulphides (more negative $\delta^{34}S$ values) (Alpers *et al.*, 1992).

5.5 Vanadates: Carnotite, $K_2(UO_2)_2(V_2O_8).1\text{-}3H_2O$

Carnotite, $K_2(UO_2)_2(V_2O_8)\cdot 1\text{-}3H_2O$ is part of a mineral group called the uranyl-micas, because of the sheet-like structure (Burns, 1999). K^+ can be replaced by other monovalent ions such Na^+, Rb^+, Cs^+, Tl^+ and Ag^+. Divalent ions can also be substituted giving the $M(UO_2)_2(V_2O_8)\cdot 3\text{-}8H_2O$ where M can be Pb, Mn, Ba or Ca (francevillite, fritzscheite, tyuyamunite, metatyuyamunite and curienite). Owing to the numerous possible substitutions and the interstitial nature of the ions (K, Pb, and Ba), an important amount of common Pb is expected to be present in natural carnotite. However, the sheet-like structure and the ability of the mineral to keep Pb, or even larger ions like Cs is an excellent factor for avoiding any radiogenic lead loss out of the crystals.

Carnotite is an important uranium mineral species, frequent in many sandstone-hosted uranium deposits, especially in the Colorado Plateau-type U-V deposits, where oxidation of the reduced uranium ores leads to the formation of carnotite (Weeks *et al.*, 1959). Carnotite can also precipitate directly from uranyl-bearing groundwater in calcretes in some arid environments and playas lakes shores. In Colorado deposits, when some reduced musdstone of the sulphide-rich ores are oxidised, it leads to the development of kaolinite, alunite, jarosite and gibbsite layers; as a result from this oxidation, allophane and uraniferous opal have been observed in joint surfaces (Weeks *et al.*, 1959).

Carnotite is of economic importance and can form deposits where U is solely represented by it. For example, carnotite is the only uranium mineral at the Yeelirrie deposit (Western Australia) (52000 t U_3O_8)(Cameron, 1990). In the latter deposit, the carnotite mineralisation was described as "valley calcrete" or "groundwater calcrete" to refer to the drainage origin. Uranium is concentrated in the playa lakes margins and along the surface drainage channels. Uranium deposition at Yeelirrie is thought to be of Late Tertiary-Quaternary age but is still ongoing. Minerals associated with carnotite at Yeelirrie include gypsum, calcite, dolomite, clays (smectite, kaolinite) and celestite (Mann and Deutscher, 1978a, Mann and Deutscher, 1978b).

5.5.1 Chemistry and mode of occurrence

Carnotite is the only U^{6+} and vanadium phase identified in the mineralisation at Beverley. The mineral was easily recovered and identified from the zircon concentrates because of its bright yellow colour. It appears in small isolated monocrystals of 10-20 µm or as frambroidal aggregates ranging up to a millimetre in diameter. The mineral is generally disseminated in the silts and sands of the Namba formation. Carnotite forms the upper uranium mineralisation, overlying the coffinite-sulphides ore basal level. Its presence at Beverley also explains the high increase in vanadium in the ISL extraction solutions. The mineral is observed in the kaolinite-rich clay samples and kaolinitic sands; it fills some cracks associated with botryoidal allophane (Fig. 29). In addition to the kaolinite, carnotite-rich samples also contain some strong red-oxidised bands of hematite or limonite.

The EMPA analyses reveal that the composition of the Beverley carnotite is close to the theoretical formula $K_2(UO_2)_2(V_2O_8).3H_2O$. The following analysed elements (given in weight-%) were below detection limits: Ba <0.28, Pb <0.11, Cs <0.16, Pd <0.18, As <0.22, S <0.06, P <0.10, Si <0.10. Mo varies between 0.15 and 0.25 wt-%, certainly as minor substitution of VO_4^{3-} as MoO_4^{2-}.

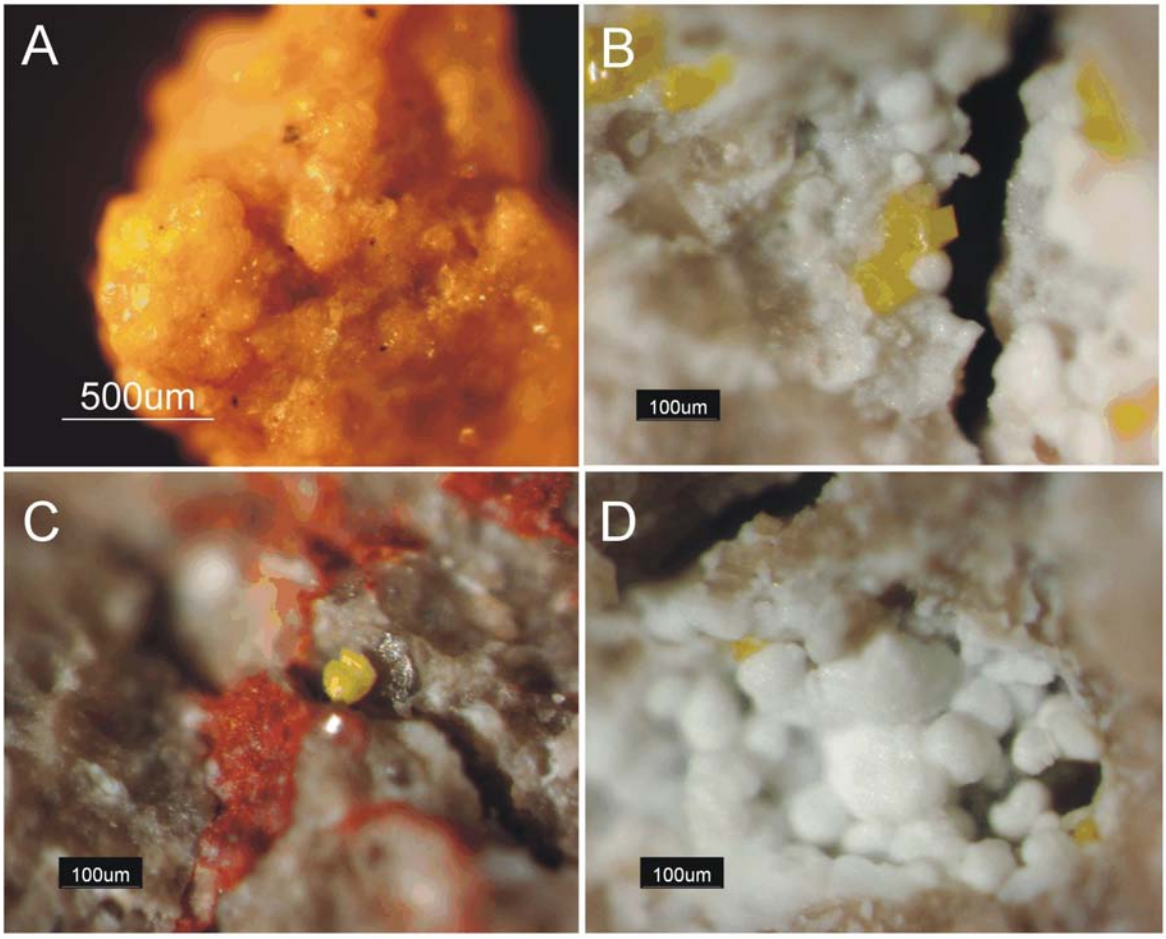

Fig. 29: Carnotite crystals from the Beverley Sands and clays

A) Large aggregate of carnotite (3 mm) from panned concentrate. B) Carnotite crystals with monoclinic habit on allophane (hydrated silica). C) Carnotite with hematite (red) on a smectite-alunite matrix. D) Crystals of carnotite in a small crack covered by allophane (hydrated silica).

5.5.2 U-Pb-Pa-Th geochronology

Dating of secondary uranium minerals is commonly made using the disequilibrium technique based on ^{238}U-^{234}U-^{230}Th and ^{235}U-^{231}Pa. This technique has been applied successfully to carnotite (Cheng *et al.*, 1998, Kaufman *et al.*, 1995) allowing checking the concordance state of the analysed minerals. The method is applicable for ages going up to 0.5 Ma. Our first measurements on carnotite crystals of Beverley were carried on a Multi-collector (MC)-La-ICPMS and showed equilibrium or near-equilibrium values taking the errors in account. We conclude the carnotite was older than ~0.4 Ma and investigated the ^{238}U-^{206}Pb / ^{235}U-^{207}Pb system with ^{208}Pb and ^{204}Pb simultaneously measured for common lead correction. The U-Pb measurements are summarised in the Appendix V. The common

lead correction was applied using the ^{208}Pb values, very accurately because of the near-total absence of ^{232}Th in carnotite. The calculated ages are all concordant to sub-concordant and range from **3.4 to 5.5 Ma** (Fig. 30).

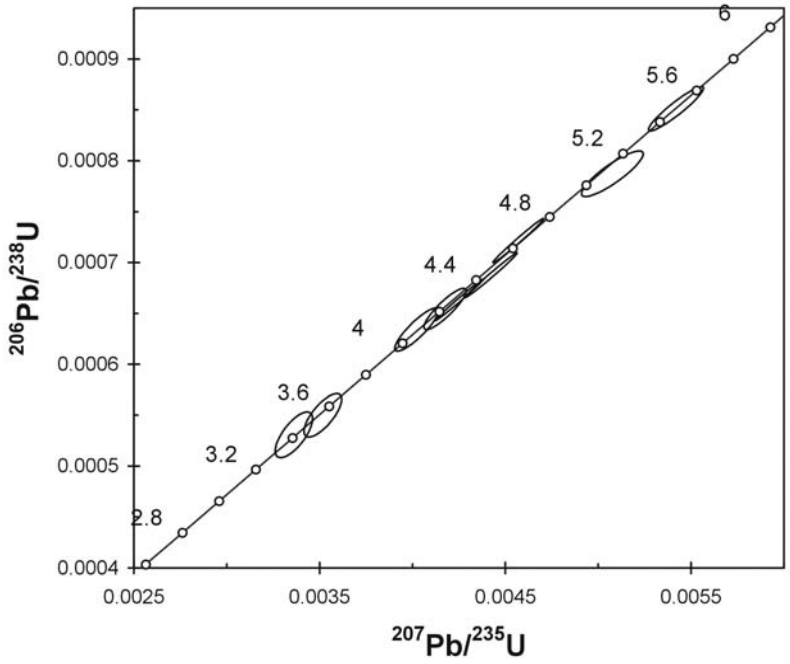

Fig. 30: Concordia plot of carnotite (La-ICPMS)

No zoning as a function of strata layer could be observed. All analysed carnotites come from the Beverley Sands and Clays.

5.5 Carbonates

Dolomitic nodules are present in the Namba clays, especially in the Alpha-mudstone, but also in the upper layers capping Namba. According to the predominance of dolomite and/or palygorskite in the sediments, the waters of the lake were of hydrogeno-carbonated type, with Ca ≤ Mg and HCO_3 ≥ (Ca+Mg). Dolomite remains a minor phase in the Beverley sediments.

6 Whole-rock geochemistry

6.1 Major elements and general mineralogy

The chemical composition of sediments is reported in the Table 7. In average, the sediments from the Willawortina are coarse and contain detritus from the crystalline MPD basement. Quartz, K-feldspar, plagioclases and micas are the dominant components and as a result, the K_2O content is higher than in the Namba Formation. Values for Al_2O_3, TiO_2, and LOI (H_2O) are also higher in Namba. The kaolinite-rich levels of the upper Namba display high content of S, which is hosted in sulphate minerals exclusively (alunite, gypsum, barite), and reported as SO_3 in the Table 7.

6.2 Trace elements and geochemistry of mineralisation

Trace elements patterns first show the sediment chemistry and mineralogy but also the geochemical overprint of the uranium mineralisation. The detailed mineralogy being identified, we can assign some trace and minor elements to specific observed minerals. High levels of Y, REE, Th, Nb and Ta, but also low Cr reflect the major Mesoproterozoic granitic component of the sediment in Willawortina. Cobalt levels are meaningless for geochemistry due to contamination in the crushing process by the tungsten carbide. The crushing time was approximately the same for each sample and high Co levels correspond to higher quartz content in the sediment.

Uranium mineralisation is observed in the upper strata of Namba, in the sulphate zone. In these sediments, only carnotite is observed, and this observation can be extended down the hole to the reduced basal Beverley siltstone-mudstone. U concentrations vary from 7 to 50 ppm and V from 65 to 125 ppm. Sulphate layers also show an increase in Sr (alunite, gypsum), a less marked Ba increase (barite), Pb and Cu (native metal particles), and Mo (carnotite). Oxidation conditions in the sulphate layers sediments were high with Fe^{2+}/Fe^{3+} ratio less than 0.05.

The basal sediments of Namba (clay, silts and fine sands) are more reduced and also contain the coffinite-uraninite and sulphide mineralisation. Uranium reaches 1.0 wt-% UO_2 in the richest sample analysed. The following elements show a positive anomaly related to the nodules: Ni, (Co), (Cu), Zn, Pb, V, As, Mo and REE* (see 6.3). The coffinite-rich sample (976) is reduced and Fe^{2+}/Fe^{3+} ratio is 0.31. Samples of mudstone 976 and 978 showed a black residue of organic matter at the end of the acid dissolution for iron oxidation state determination.

Fluorine is enriched in the acid lixiviation solutions of the Beverley in-situ leaching plant (Heathgate, 1998) and could originate from apatite dissolution. We however lack of data for PO_4^{3-} and Sr concentrations in the aquifer and the ISL fluid. Alunite-group minerals can accommodate large cations in the A-site (Ca, Sr and Ba) replacing K. At the same time, PO_4^{3-} can partly substitute SO_4^{2-} (Li *et al.*, 1992, Stoffregen and Alpers, 1987). The samples 968, 969 and 974 are all kaolinite-bearing and all present high Sr content (>1000), low Ca/Sr ratios (<5.0) together with P_2O_5 content between 0.14 and 0.23 wt-%. We attribute these patterns to the alunite group minerals intermixed with kaolinite. All three samples have minimum Fe^{2+}/Fe^{3+} ratios.

6.3 REE patterns

Values of REE are reported in the Table 7 and PAAS-normalised REE spectra in Figure 31 (Post-Archaean average Australian Sedimentary rocks) (McLennan, 1989). In general, Willawortina samples have higher REE concentrations, reflecting the contribution of the Mesoproterozoic granites. The sediments of the Namba formation yield much lower values (up to one order of magnitude difference). All samples show a negative Eu anomaly whereas Ce is never anomalous, when normalised to Chondrite C1 (Taylor and McLennan, 1985).

The coffinite mineralisation shows a REE pattern with values of light REE increasing to culminate on the Pr-Nd-Sm segment. Similarly, the underlying less mineralised alpha-mudstone shows a less marked, but similar effect. Quantitatively, the REE sums divided in light (*l*), intermediate (*m*) and heavy (*h*) groups present distinctive characters: (1) the Willawortina sediments contain ~87% *l*REE - ~8% *m*REE – 4% *h*REE, (2) Namba sediments with carnotite mineralisation have ~92% *l*REE, ~5% *m*REE, ~3% *h*REE, (3) the coffinite mineralisation have ~75% *l*REE, ~16% *m*REE, ~9% *h*REE.

This intermediate REE enrichment in the mineralisation zone is correlated with coffinite, which display high *m*REE centred on Sm. This contrasts with the coffinite/uraninite compositions reported in literature, which fractionate HREE and Y (Hansley and Fitzpatrick, 1989, Janeczek, 1991). The REE in the coffinite mineralisation are strongly fractionated and $La_N/Sm_N = 8$. The spectra are reported on the (Fig. 32). A very strong Eu* anomaly is also present.

The REE patterns in the alpha-mudstone underlying the coffinite mineralisation displays the highest heavy REE concentrations (Fig. 30) and this can be correlated with neither coffinite (U<<REE) nor detrital minerals. We explain this by the presence of an unidentified authigenic phase rich in *h*REE. The selective scavenging of intermediate REE from U- and REE-bearing fluids into coffinite mineralisation certainly produced a residual fluid with elevated *h*REE which then crystallised a Y-*h*REE phase (e.g. xenotime).

The carnotite-rich layer with kaolinite and alunite possess the lowest sum of REE: 80 ppm. Although uranium is present in carnotite, REE have not concentrated in the rock and the patterns indicate the REE are controlled here by minor concentrations of detrital minerals: monazite and zircon; this reflects the different nature of the mineralising fluid involved here.

Recent experiments of alunite-jarosite dissolution in acidic conditions at pH 3 and 4 have shown that *m*REE are preferably leached from the sediment (Welch *et al.*, 2007). An interaction between an oxidising fluid and REE-bearing minerals can produce a selective leaching of *m*REE into the fluid phase. In other words, this means *m*REE can be dissolved from their source and mobilised together with uranium. An acid leaching of U- and REE-bearing rocks or sediments could explain the signature of the Beverley ore.

Formation:	Willawortina ---------->			Namba ---------->						
Sample	964	966	967	968	969	971	972	974	976	978
level [m]	- 35 m	- 84 m	- 98 m	- 106 m	- 111 m	- 120 m	- 127 m	- 130 m	- 132 m	- 135 m
Major & minor elements (weight-%)							** = ICPMS data*		***Sulphur as SO_3*	
SiO_2	63.76	79.59	75.17	58.90	52.05	81.38	82.13	59.19	59.27	59.18
TiO_2	0.71	0.36	0.66	1.05	0.73	0.75	0.91	0.60	1.11	0.77
Al_2O_3	16.80	9.32	13.80	19.36	26.27	9.40	10.15	20.53	23.03	17.78
Fe_2O_3	4.62	2.48	1.21	5.30	3.99	2.31	0.88	5.92	2.55	7.98
FeO	0.40	0.50	0.40	0.20	0.10	0.40	0.20	0.10	0.70	0.30
MnO	0.02	0.03	0.01	0.01	0.00	0.01	0.01	0.01	0.01	0.02
MgO	2.56	0.74	0.61	1.35	0.54	0.35	0.27	1.18	0.79	2.47
CaO	0.54	0.25	0.20	0.72	0.35	0.18	0.15	0.70	0.43	0.81
Na_2O	1.49	0.99	0.70	0.69	0.42	0.34	0.33	0.60	0.39	0.66
K_2O	3.31	2.59	2.58	1.74	1.38	0.95	0.97	0.68	0.83	1.60
P_2O_5	0.05	0.05	0.05	0.23	0.19	0.07	0.08	0.14	0.06	0.06
UO_2	0.00	0.00	0.00	0.01	0.01	0.00	0.00	0.01	*0.99*	0.00
BaO	0.05	0.04	0.04	0.06	0.04	0.04	0.04	0.03	0.02	0.04
ZrO_2	0.04	0.03	0.05	0.03	0.02	0.04	0.05	0.02	0.03	0.02
Rb_2O	0.03	0.02	0.02	0.02	0.01	0.01	0.01	0.01	0.03	0.04
SrO	0.01	0.01	0.01	0.20	0.18	0.03	0.05	0.14	0.01	0.04
ZnO	0.01	0.00	0.00	0.01	0.00	0.00	0.00	0.00	0.01	0.03
Co_2O_3	0.01	0.03	0.03	0.00	0.00	0.02	0.02	0.00	0.00	0.00
V_2O_5	0.01	0.01	0.01	0.02	0.02	0.01	0.01	0.02	0.04	0.03
LOI	5.35	2.38	4.00	9.58	13.46	3.55	3.29	9.76	8.96	7.99
S	0.24	0.06	0.86	**1.28	**2.35	0.15	0.17	0.65	0.21	0.00
Sum	99.77	99.42	99.55	99.48	99.76	99.84	99.55	99.64	99.26	99.82
Trace elements (ppm)										
Ba	410	377	371	559	349	327	344	258	159	378
Rb	310	167	190	198	52	47	49	60	263	333
Sr	109	64	52	1655	1502	257	461	1167	110	180
* Y	61.7	63.4	57.9	19.5	8.0	14.6	16.7	7.4	120.5	144.2
Ni	12	7	6	8	4	7	6	6	28	*49
Cu	54	24	17	88	23	18	16	43	42	30
Zn	56	34	35	75	21	37	27	38	101	239
* Pb	15.9	20.3	18.0	80.8	19.1	9.9	10.8	28.1	41.6	15.0
Ga	25	15	21	31	19	12	12	12	26	<10
V	60	48	30	124	94	76	65	103	236	170
Sc	19	8	8	40	31	9	8	35	24	** 20*
Cr	35	23	23	57	111	50	48	76	109	** 74*
Co	75	187	185	16	16	136	139	30	23	* 37
* As	<1.9	4.1	<3.8	3.2	5.2	<2.4	<2.6	<1.5	2.7	6.6
* Mo	1.23	1.85	2.94	6.19	1.03	2.55	1.14	2.90	9.20	1.04
Zr	290	223	336	230	120	265	336	125	198	130
* Nb	30.69	19.58	33.59	34.51	10.05	10.11	9.38	9.11	14.31	9.89
*Hf	8.09	6.22	8.74	5.77	3.25	7.60	8.94	3.78	3.92	3.76
*Ta	3.64	4.25	5.13	3.11	0.85	2.51	1.89	1.02	0.85	0.93
Th	40	38	18	37	8	15	7	18	* 19	28
* U	10.1	7.2	11.4	49.3	29.2	28.2	6.9	50.9	8771	9.0
*La	103.23	104.62	92.50	60.71	25.00	39.88	112.69	33.28	44.47	67.32
*Ce	157.64	160.07	153.27	65.14	34.87	63.59	122.05	30.52	125.56	157.29
*Pr	18.13	18.70	15.44	5.90	3.22	5.35	8.54	2.07	21.01	18.62
*Nd	63.39	67.06	52.29	19.02	9.59	18.35	24.75	6.24	96.47	82.80
*Sm	9.76	9.74	8.72	3.81	1.53	3.51	3.44	1.17	26.04	15.77
*Eu	1.28	1.17	0.72	0.53	0.26	0.35	0.35	0.24	4.09	2.85
*Gd	9.64	11.38	7.07	3.61	1.54	2.46	3.17	0.88	20.98	20.08
*Tb	1.35	1.97	1.02	0.50	0.15	0.32	0.50	0.20	3.76	3.31
*Dy	10.00	11.33	11.52	3.28	1.42	2.28	4.00	1.03	22.19	22.41
*Ho	2.34	2.64	1.77	0.72	0.17	0.51	0.71	0.36	4.35	5.30
*Er	5.64	6.10	5.34	2.58	0.81	1.45	1.78	1.03	11.03	16.87
*Tm	0.93	1.05	1.19	0.27	<0.07	0.40	0.25	0.18	1.37	2.38
*Yb	5.54	5.90	7.69	2.94	0.79	1.31	2.46	1.05	10.52	16.14
*Lu	1.07	0.96	0.98	0.40	0.21	0.23	0.42	0.12	1.46	2.47
Σ REE	390	403	360	169	80	140	285	78	393	434
% *l*REE	87.8	87.0	87.2	89.0	91.4	90.8	94.0	92.0	73.1	75.2
% *m*REE	8.2	8.8	8.1	6.9	6.2	6.4	4.0	4.5	19.6	14.9
% *h*REE	4.0	4.1	4.7	4.1	2.5	2.8	2.0	3.5	7.3	10.0
Fe^{2+}/Fe^{3+}	0.10	0.22	0.37	0.04	0.03	0.19	0.25	0.02	0.31	0.04

Table 7: Chemical composition of the WC2 drilling sediments at the Beverley Uranium Mine

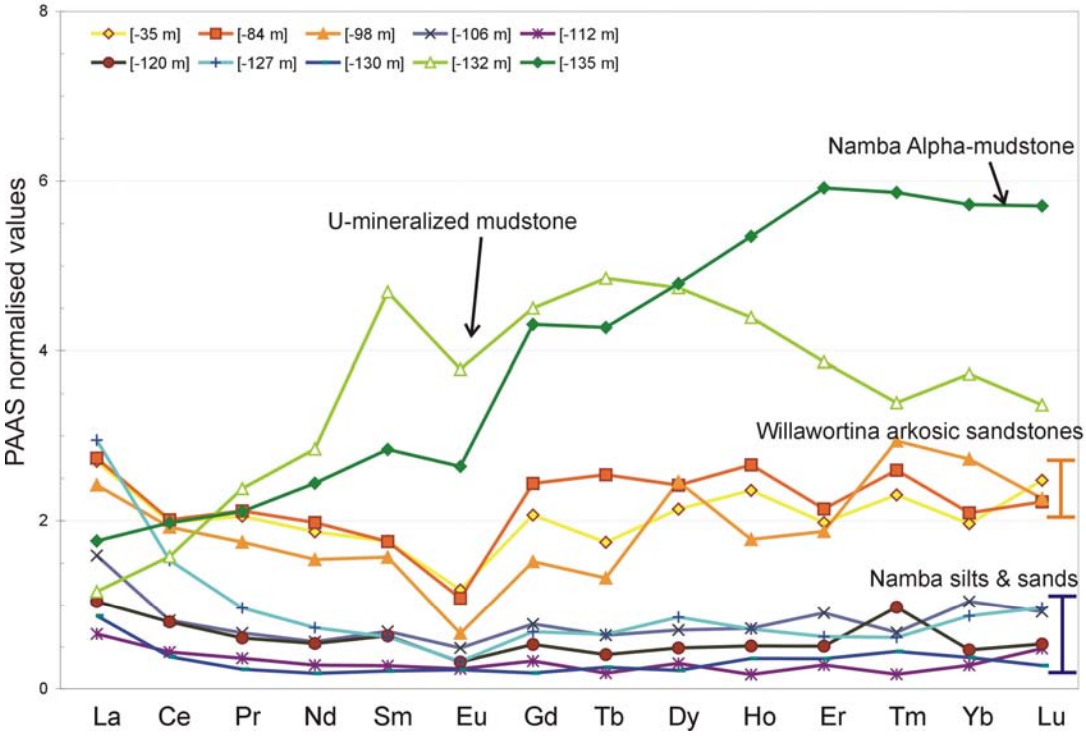

Fig. 31: PAAS-normalised REE spectra for Beverley sediments

PAAS: "Post-Archaean average Australian Sedimentary rocks" (McLennan, 1989). *The three units present different patterns and only overlap around the light REE area. Willawortina sediments display much high RE concentrations related to the high proportion of material sourced in the local Mesoproterozoic granites. The mineralised mudstone is showing a very high intermediate REE curve. The alpha-mudstone which immediately underlies the uranium mineralisation is also showing very high intermediate REE values and the highest heavy REE values; it probably indicates the presence of a Y-rich phase (e.g. xenotime). Layers -106 and -111 contain the alunite-jarosite minerals; it coincides with the lowest REE values (depletion).*

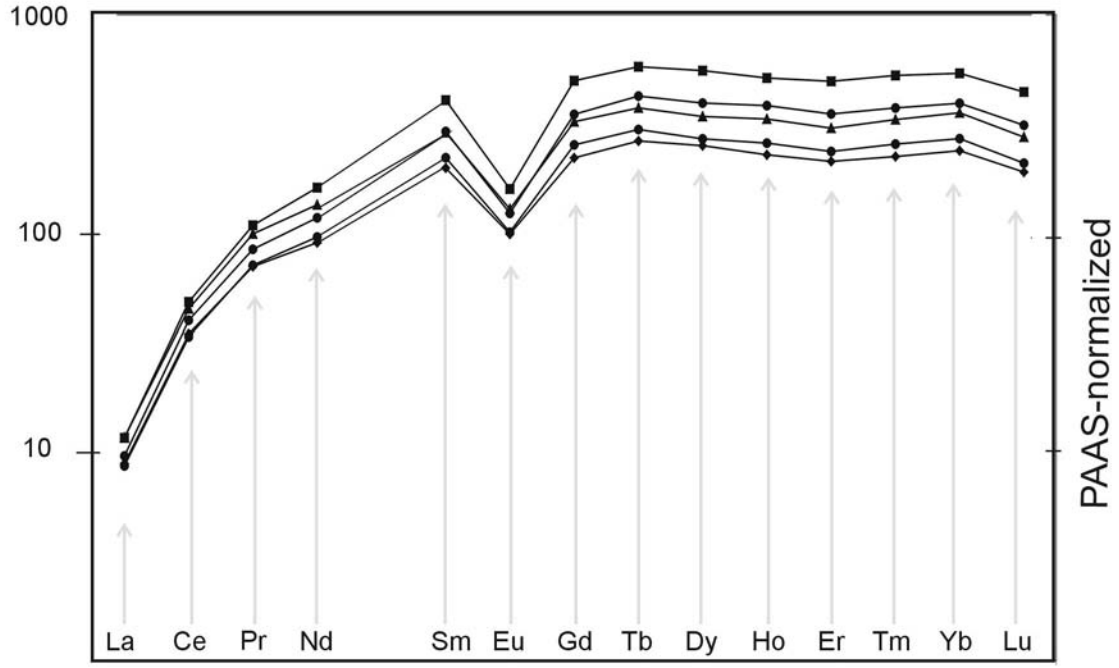

Fig. 32: PAAS-normalised REE spectra for Beverley coffinite nodules

The coffinite nodules show a strongly enriched intermediate to heavy REE signature which correlates with the whole-rock composition. The dominant REE after Y is quantitatively Nd, Ce, Dy, Gd and Sm. This character suggests the uranium source may be also be a REE-rich source. The U/Σ(REE) ratio varies between 21 and 41.

7 Interpretation of data

The multiple data, analyses and observations regrouped during this study are discussed in several categories: paleoenvironment and origin of the sediments (1), age of the mineralisations (2), physico-chemical conditions (3), and possible sources of uranium (4).

7.1 Paleoenvironment and origin of the Beverley sediments

7.1.1 Alpha mudstone unit

The Alpha-mudstone Unit, which hosts the lower level of the mineralisation of Beverley, is clay-rich (smectites) and poor in HM's issued from the local MPD basement. The sediment is characteristic of lacustrine environment and contains organic material; the composition is rich in FeO, MgO and Al_2O_3, reflecting the clay content and the presence of palygorskite or dolomite. The presence of these two minerals reflects Mg-Ca hydrogeno-carbonated water chemistry for the Lake Frome at the time of the dolomitic nodules deposition (Callen et al., 1995a; Cojan and Renard, 1997). The clays also contain zircon fragments with volcaniclastic morphology (Fig. 8). The proportion of MPD Mesoproterozoic zircons in the alpha-mudstone (D typology) is low, which is in accordance to the exotic origin of the sediments. Rutile is clearly dominant over zircon (Table 2), which also requires a source elsewhere the MPD, typically a source region with metamorphic rocks and/or more mafic rocks. Hence, we interpret the alpha mudstone to be mainly sourced from volcanic rocks, with a high proportion of volcaniclastics. The low energy environment and the interpreted water paleo-composition both indicate lacustrine conditions.

7.1.2 Beverley sands unit

The next unit, the Beverley Sands Unit, is coarser with silts and fine sands containing kaolinite. This latter mineral is thought to be issued from the outwash of the local kaolinised regolith, which also may be represented by sub-outcropping granite saprolith. Some kaolinised outcrops of sediments in the Paralana High Plains could correspond to a lateral equivalent. The dominant mineral species in the formation is represented by quartz, forming a medium to very fine sand; its morphology is very angular, excluding a long distance alluvial transportation. The feldspar proportion is very low and this excludes a fluviatile deltaic origin sourced in the MPD basement. The HM assemblages are poor in Fe-Ti oxides and this totally differs with the alpha mudstone or the mineralogy of the MPD; the later is containing a high proportion of hematite and magnetite. The combination of selective geochronologic and typologic approaches used for the study of the zircon population of these sands provides here an exceptional source of information about the sediments origin.

1) U-Pb zircon dating

Age populations show a dominant Permo-Carboniferous group, a Devono-Ordovician group and a Jurassic-Cretaceous group (Fig. 15). The only possible source for the Early Cretaceous to Jurassic zircons lies in the Eastern Australian Volcanic Province (Whitsunday Volcanic Province), a calc-alkaline volcanic arc extending along the Eastern margin of the former Gondwana (Bryan *et al.*, 2000). This Province is also referred as the Tasman Arc (Sircombe, 1999) and the only other region that could have supplied granitic or rhyolitic material of this age is in Antarctica (Fig. 33). The major Permian and Carboniferous zircon population certainly has its origin in Eastern Australia in the New England Fold Belt. The remaining population of Devonian to Ordovician zircons can also be originated in the Lachlan Fold Belt orogen granitoids. These granitoids extend from Northern Queensland to Southern Victoria. As discussed by Sircombe (1999), zircons of Cretaceous-Jurassic age are present in the Eromanga and Surat Basins (Fig. 33). The volcanic arc and the orogenic calc-alkaline granites are nowadays both located in the eastward watershed of the Great Dividing Ranges, but palaeocurrent directions must have been westwards during the Cretaceous, prior to the end of the subduction, and a further uplifting period.

2) Typology and morphology of zircons versus age groups

The morphological observations can be reported by age group: (1) Cretaceous (130-142 Ma) calc-alkaline typology (S24, P4), high temperature index, presence of fractured surfaces resulting from explosive volcanism with melt and dark inclusions (Fig. 17). Dark-pink gem quality zircon (S20) with magmatic smoothed edges originated from alkaline basalts (A.B.) but this should be confirmed by further geochemistry; (2) Jurassic (196 Ma) zircon of D typology, fragmented pyramids, presence of dark inclusions: probably from alkaline basalts; (3) Permian to Carboniferous zircons also display fractured surfaces that can be resulting from explosive volcanism. However the proportion of crystals with inclusions and volcanic patterns is smaller and most of them are of probable granitic origin.

The lack of rounding and mechanical wearing observed on the crystal surfaces of Mesozoic-Paleozoic zircons and also on quartz grains can be explained by a two processes differing from fluviatile river transportation:

- A volcanic dispersion: volcanic rocks of silicic types can be air-carried during major ignimbritic eruptions. The dacitic to rhyolitic compositions are producing extremely viscous magma and lead to violent eruptive events. The extension of pyroclastic flows can reach more than 1000 kilometres, and the distance to the Eastern Australian Volcanic Province varies between 1400 and 1600 km.

- A glacial dispersion: until recently, the last recognised glacial event in Australia was thought to be Permian. Recent discoveries have evidenced an Early Cretaceous glaciation (palynology ages from 144 to 131 Ma). This age range coincides with our youngest dated zircons (130 ± 3 Ma).

We think that volcanism has contributed partly to volcaniclastics dispersion but not sufficiently to explain the broad assemblage of Paleozoic-Mesozoic volcanic zircons in the sediment; this would especially not give any explanation to the angular morphology of the host sands. The combined data from zircons dating and typology/morphology provide a strong evidence for glacial transportation. A volcaniclastic origin cannot be excluded and should be retained as a minor possible contribution to the sedimentary assemblage.

The more probable sedimentary provenance using the age population groups, lies between Brisbane and Townsville on the Queensland shoreline where Cretaceous and Permo-Carboniferous granites and volcanics are abundant (Fig. 33). Devonian to Ordovician granites also occur inland and would have been partly incorporated into the glacial rock loading. The more recent paleogeographical reconstitutions give ~70°S for the paleolatitude of this source area at 150 Ma and it coincides with mountain chains of over 1000 metres altitude (Veevers, 2006). The ideal conditions for a glacial dispersion towards the West are met. From the paleorelief and the paleolatitudes it is likely that the path of the glaciers extended over the Eromanga basin towards an average SW direction.

This interpretation provides some additional support for the glaciation event described recently by Alley *et al.* (2003). The palynological data restrict this glacial period between 144 and 131 Ma. This would also explain the absence of younger Cretaceous zircons from the same volcanic province (up to 95 Ma) at Beverley and especially the simultaneous occurrences of fresh Permian-Carboniferous zircons and angular quartz grains in the sediments.

Since the Cretaceous moraines are generally composed of heterogeneous element with very coarse granulometry (tillite), we interpret the Beverley sands to contain reworked Early Cretaceous glacial and fluvioglacial/glacio-lacustrine materials. The fine granulometry of the sediments and the mixing with kaolinite can be explained by a low energy washout of the Cretaceous materials during the Miocene. The mineralogical maturity of the assemblage (quartz-rich, Fe-Ti-oxide disappearance) can be explained by the intense weathering of the Cretaceous formations during the Miocene- Oligocene. The paleoenvironment of deposition of the Beverley Sands Unit is therefore interpreted as the shoreline of the freshwater lake, where the Cretaceous sediments washout has been redeposited.

7.1.3 Beverley clay unit

The mineralogy of Beverley Clay Unit is dominated by kaolinite and quartz with locally alunite. The source of the sediment is interpreted to be partly similar to the Beverley Sands Unit and the mineralogical difference explained by the change of depositional environment. The non-magnetic HM reveal an abrupt change in relative proportion:

- The rutile index *[Ru /(Ru+Zr)]* increases from 0.1 – 0.7 in the Beverley Sands to reach 6 – 50 in the Beverley Clays; this could be related to a sedimentary change but also be the result of a selective mineral disappearance. Due to the overall immaturity of the sediment, a change in sedimentary source remains the most likely explanation.

- Corundum is quite rare in the Beverley Sands and suddenly begin to be abundant in the Beverley Clay Unit, after the level [-106 m]. The regional sources of corundum are widespread in the MPD and especially in the Radium Creek Metamorphics from the southern MPD and the Freeling Heights Quartzite in the Mt Adams area. This element gives further weight for a change in the sedimentary source.

This information clearly indicates that the MPD starts to be the dominant source of sediment since this time and underlines the onset of a tectonic uplift event or simply the change from lacustrine to emerged conditions. The appearance of the corundum also coincides with kaolinite in the upper part of Namba and records a change from lacustrine to littoral and finally emerged conditions. Sulphides are oxidised and acidic soils are developed, leading to the formation of alunite.

7.1.4 Willawortina Formation

The HM assemblages of the Willawortina Formation show a wide variety with several U-REE-Th-Y minerals reflecting the major component issued from the Mesoproterozoic - Palaeozoic basement rocks of the MPI. The zircon typology also indicates a dominant Mesoproterozoic granite-gneissic origin. The sedimentary sequence of the Willawortina Formation coincides with the period of uplift in the North Flinders Ranges and is a typical coarse molasse.

Fig. 33: Polar projection of the southern Gondwana area at ~150 Ma.

The relative position of Australia and East Antarctica remains identical until 80 Ma. Subduction under the eastern margin of Australia/East Antarctica is accompanied by silicic explosive volcanism and calc-alkaline magmatism. The volcanic arc and the Eastern Australian mountains range are both drained into the inland basin (Eromanga basin or GAB). Paleolatitude and relief also allow extensive glaciers spreading. Modified from (McLoughlin, 2001)

7.2 Age constraints and timing of the mineralisation

The uranium mineralisation at Beverley is hosted in the Miocene to Pliocene Namba Formation. Palynology indicates sedimentation from ~24 Ma to ~6-4 Ma (Martin, 1990). Our provenance studies on zircon did not reveal any Miocene detrital mineral which could have constrained these limits. The youngest zircon (130 Ma) only evidences an remote exotic component discussed before.

Our U-Pb dating obtained on the carnotite crystals and coffinite nodules defines a mineralizing event during the Pliocene epoch, between 6.7 to 3.4 Ma. We suspect the first coffinite mineralisation to have eventually occurred slightly before 5.5 Ma but only whole-rock sample U-Pb dating (at a scale where the system may have behaved closed) could provide such information. If bulk coffinite samples reveal identical ages to those of carnotite, the mineralising event will chronologically be constrained to the sedimentation hiatus that occurred prior to the major uplift which lead to the building-up of the thick Willawortina molasses. In term of genetic classes as commonly used in economic geology, the mineralisation is syndiagenetic, and also possibly syngenetic, if older coffinite ages could be measured (Hobday and Galloway, 1999).

7.3 Reconstitution of the physico-chemical conditions during mineralizing time

The local environment during the Miocene was lacustrine and changed to arid conditions at the Pliocene, with emerged conditions and soil development. Several syndiagenetic processes can be envisaged during this changing paleoenvironment: (1) a direct adsorption and reduction of uranium from oxidised groundwaters into the organic matter-rich lacustrine mudstones and quartzose sands from the lake shores; (2) a later paleosoil forming in a emerged environment with arid conditions; intense weathering of the outcropping outwash plain sediments and basement; (3) the mixing of reduced basement brines with shallow oxidised groundwaters along the syngenetic Poontana fault structure.

7.3.1 Chemistry of groundwaters

The nature of the waters prevailing during the deposition of the Namba lacustrine sediments is constrained by the presence of dolomitic nodules. These are present in the Namba clays, especially in the Alpha-mudstone, but also in the upper layers capping Namba. The combined presence of dolomite and palygorskite in the sediments implicates the waters of the lake to have been of hydrogeno-carbonated type, with Ca ≤ Mg and $HCO_3 \geq (Ca+Mg)$. The transportation of uranium in this type of waters is controlled by uranyl carbonate complexes such as $[UO_2(CO_3)_3]^{4-}$. Evocation of a possible syngenetic uranium mineralisation at this stage would be limited to the high-U concentration of black nodules in the alpha-mudstone. However, no direct evidence for this hypothesis can be advanced at the moment. The paleoenvironment changes from lacustrine to littoral conditions (Beverley Sands) and finally to emerged conditions. The present groundwaters compositions at Beverley and in the neighbouring bores is available in literature: the Namba aquifer (Beverley Sands) bears $1.6 \cdot 10^{-2}$ $[SO_4^{2-}]$, $5.6 \cdot 10^{-2}$ $[Cl^-]$ and ~$4 \cdot 10^{-3}$ $[HCO_3^-]$; $[HCO_3] << [Ca+Mg]$ and $[Ca] \approx [Mg]$ (Heathgate Resources Pty Ltd, 1998, Ker, 1966). The data from Heathgate (1998) also provide a wide range of trace elements. The measured pH is 7.6 and temperatures in the Beverley Sands aquifer is around 25°C. These data have been used for the building of the Log fO_2 – pH diagrams shown in Figure 34.

The present-day Lake Frome brines are (all values in M): Na=5.055, Mg=0.042, Ca=0.014, K=0.009, Cl=4.892, SO_4=0.146, HCO_3=0.002, Br=0.002 [M] (Draper, 1974). These brines were certainly less concentrated 4 Ma ago, when the climate was less arid, but it is probable the global chemical composition was not significantly different.

7.3.2 The reduced mineralisation

The reduced mineralisation at Beverley is characterised by coffinite (± uraninite) and pyrite dominantly. These three minerals represent >90% of the authigenic minerals. Smaller amounts of sphalerite, native copper, chalcopyrite, and barite are also present. Carnotite is present in small quantity relative to coffinite (<1%). Chalcopyrite and native lead and a copper-zinc alloy are extremely rare accessories.

The presence of native lead in the reduced ore zone is constraining the physico-chemical condition quite strongly. The mineral forms in environments were the activity of reduced sulphur species is extremely low (Fig.34f); Sawlowicz (1990) suggests that native lead forms in microenvironments where organic matter in decomposition is able to liberate organic bases or NH_3 into solution ($fCH_4(g) >> fCO_2(g)$). These conditions can be met in the mudstone, which contains organic matter clasts surrounded by impermeable matrix. The presence of native lead hence documents the possible extreme reducing conditions that prevailed locally during the ore genesis.

The presence of Zn^0 in the native copper particles does not require stronger reducing conditions of formation than pure Cu. Pure native Zn is not stable in presence of water (Fig.34e).

Physico-chemical changes are also observed on the rims of native copper particles, which often display a cuprite (Cu_2O) and minor tenorite/malachite rim. Chalcocite rims have not been properly identified, but S has been observed as a minor component of some spongy copper particles. The presence of sphalerite and minor chalcopyrite in parts of the coffinite mineralisation can be explained by stronger reducing conditions, independently of sulphur concentration (Fig. 34b & e). The role of micro-organisms in the development of these reduced micro-environments is supported by the strongly negative $\delta^{34}S$ values in both sphalerite and pyrite/marcasite, hinting to bacterial reduction of sulphates from groundwater.

Co-rich pyrite cores in coffinite nodules show a $\delta^{34}S$ of $+1.0 \pm 0.3$ $^0/_{00}$ value, which is interpreted as an authigenic syngenetic freshwater mud-sulphide precipitation and predates the mineralisation. We also think that part of coffinite nodules mineralisation may have occurred by reduction of the UO_2^{2+} by dissolved H_2S during an early stage of mineralisation. It is difficult to clearly assess this hypothesis with the limited amount of measurements on coffinite nodules (<1 g).

Overall, the mineralogical observations combined with isotopic data fit well in the Log fO_2 - pH diagrams, favouring a bacterial reduction for most of the mineralisation using the organic matter present in the sediments. The presence of microenvironment is evidenced by lead with the most extreme reduction conditions that can occur in the water stability field.

7.3.3 The oxidised mineralisation and alteration

Carnotite in Beverley is widespread in the silts and sands and is also commonly associated with coffinite. Geochemical diagrams (Fig. 34d) show that carnotite is very stable in relatively oxidised groundwaters and requires very little vanadium to form. This means that vanadium cannot be carried simultaneously with uranium and carnotite precipitation is likely to occur in V-rich environments (V-rich clays or accessory V-rich minerals) or at the mixing of groundwaters bearing separately V and U.

The samples containing the highest concentrations of carnotite occur at the top of the mineralisation (Beverley Clays) and are also kaolinite-rich and alunite-bearing. Additionally to these minerals, we observed some hematite or goethite bands, which suggest local oxidation and remobilisation of iron sulphides. This is confirmed by the absence of Fe^{2+} in whole-rock analysis. Alunite forms in acidic conditions (pH < 4.5) and its presence together with kaolinite and carnotite restricts the forming conditions of the mineral assemblage (Fig. 34a & d). We estimate the prevailing conditions to have been between pH 3.9-4.5 and with Log fO_2 from atmospheric to -30 (oxidising conditions). These conditions in the upper layers of Namba can be explained by the presence of an acid lake or marsh where the exposure of sufidic mudstone initiated acid formation. This phenomenon was mentioned by the early workers in Colorado carnotite ore (Weeks *et al.*, 1959), where an oxidation of exposed pyrite-rich uranium black ores (coffinite) leading to acidic conditions, uranium redissolution and finally carnotite precipitation.

As a comparison, it is important to understand the calcrete-hosted type of uranium deposits, which systematically host carnotite, although this is a different context. The Yeelirrie uranium deposit in Western Australia contains 52'500 tonnes U_3O_8 at a grade of 0.15% U_3O_8 and hosts carnotite as an exclusive U phase. This is also the case for numerous calcrete-hosted uranium occurrences in Western Australia. Detailed groundwaters study at Yeelirrie show pH between 7.5 and 8 and vanadium concentrations generally <5 ppb with a maximum of 37 ppb (Briot, 1983). Uranium is provided by surficial oxidised uranium-rich waters (up to 400 ppb U) sourced in local U-rich Archaean granites. Vanadium (V^{4+}) is dissolved by poorly oxidizing saline waters from nearby sedimentary pre-concentrations (V-rich clays, calcretes). The mineralisation is formed at a redox front by mixing between these two waters, provoking oxidation from V^{4+} to V^{5+} and a strong decrease in $p(CO_2)$ activity by dolomitisation of the limestone; this results in the decomplexation of uranyl carbonates and carnotite precipitation (Briot, 1983).

Carnotite at Beverley contains minor amounts of Mo, which enters the mineral structure as a substitution to the VO_4^{3-} as MoO_4^{2-}. The low level of Mo in the reduced ore (9 ppm) underlines this element plays only a minor role for the mineralisation.

Barite and gypsum display positive $\delta^{34}S$, indicating a groundwater origin for the sulphates. Calculations of saturation index for Beverley water (Fig. 35) show the minerals have SI between -1 and 1, suggesting that barite and gypsum still control the groundwater chemistry nowadays. Arsenic is present in the reduced native lead particles and as trace element in the sulphide minerals. Arsenic concentration in the ore and sediments is <7 ppm As. Simulations with local basement waters and organic matter bearing sandstones have predicted the formation of minor As bearing minerals for the Beverley deposit with final ore composition at 219 ppm As (Brugger *et al.*, 2005).

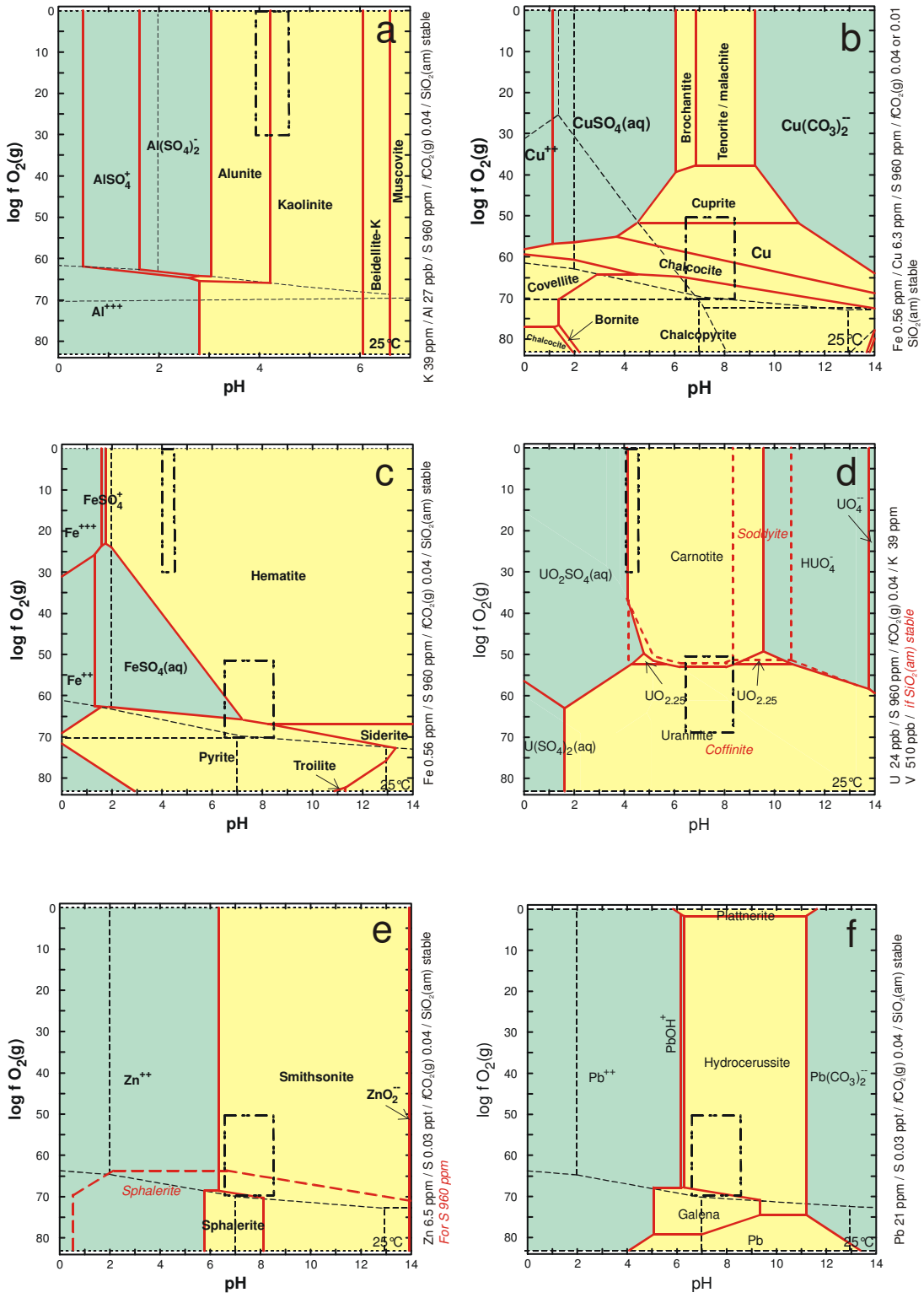

Fig. 34: Log fO_2 (g) vs. pH diagrams for U, Cu, Pb, Zn, Fe and Al

The diagrams are based on the water compositions measured in the Namba aquifer around the Beverley mineralisation. For discussion, the S concentration has been changed in diagrams e and f (960 ppm to 0.03 ppt S). Two fields are drawn to represent the conditions to form mineral assemblages observed in the mineralisations: oxidised mineralisation / reduced mineralisation. All calculations were done using the Geochemist's Workbench (v.6; Bethke 1996), with thermodynamic data taken from the Lawrence Livermore database (LLNL V8R6).

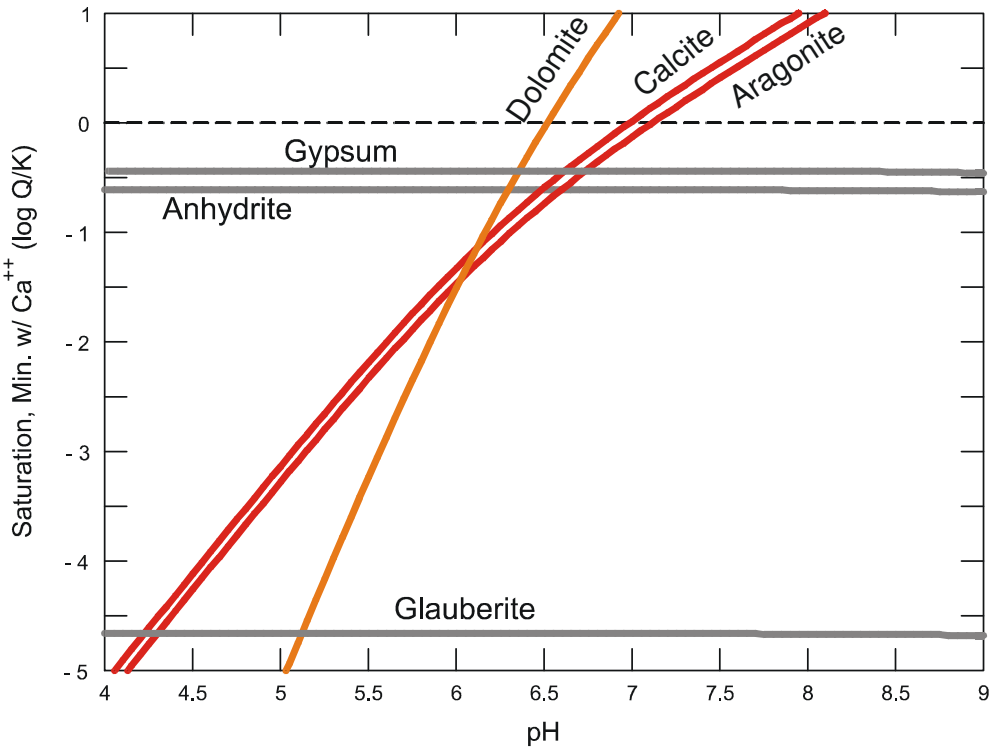

Fig. 35: Saturation index as a function of pH for the Beverley water

SI=log Q/K; SI=0 equilibrium, >0 supersaturation, <0 undersaturated; if SI <1 and >-1, one can suspect that the mineral may control the composition of the fluid. Dolomite and gypsum are both observed at Beverley. Dolomite is equilibrated with the water at pH ~6.5. Dolomite from ore is dissolved during the ISL mining operated between pH 1.5 and 2.5. Ca and sulphate concentrations are monitored to prevent gypsum formation, which could lead to porosity sealing in the sands and silts of the ore zone near the re-injection wells or in the wells themselves. These problems could have a disastrous economic impact on the mine life by lowering the uranium recovery rate.

7.3.4 REE geochemistry

The REE geochemistry of the ore is showing a distinctive enrichment in Pr, Nd and Sm (*m*REE) which is related to the coffinite-uraninite nodules composition (Fig. 31 & 32). Furthermore, the alpha-mudstone underlying the uranium-rich layer displays a composition highly enriched in *m*REE and *h*REE. The REE patterns of the Willawortina Formation are logically showing a high global REE repartition (~400 ppm REE) due to the presence of materials coming from the REE-rich granitoids of the MPD. In conclusion, REE geochemistry is fingerprinting the ultimate source of the uranium ore: the MPD Proterozoic basement. It also enhances either a water-interaction leaching process at the source-rock or a mineralogical control of coffinite in trapping mREE preferentially.

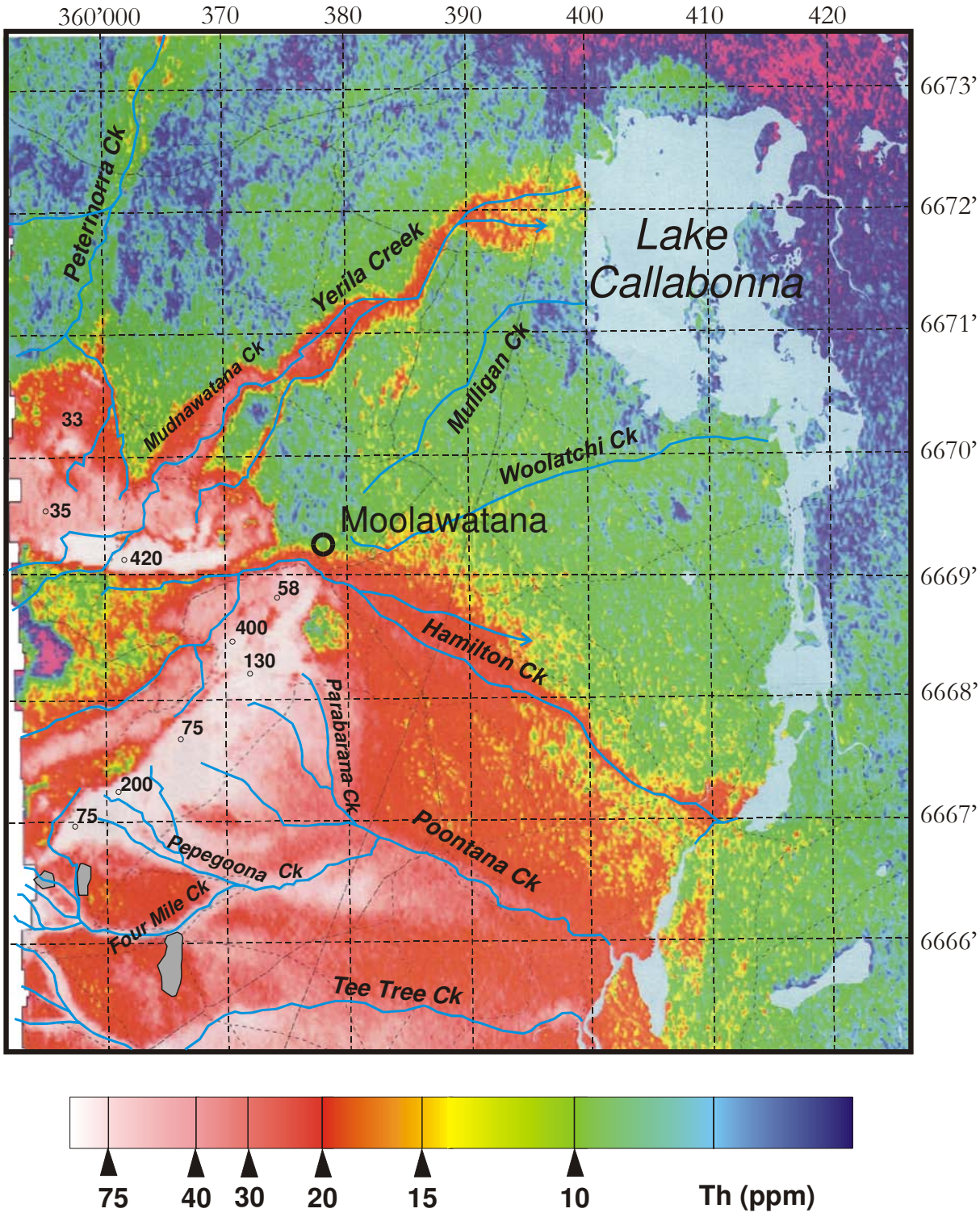

Fig. 36: Thorium map of the Lake Callabonna – Mount Painter Domain

Thorium has been chosen for its high contrast compared to uranium. Both maps show similar images. The values indicated on it are calibrated on ground values (local average).The Beverley and the Four Mile deposits are represented in grey on the bottom left corner of the map.

Uranium reservoir	Arguments for	Arguments against	Missing information
Namba Formation (sandy aquifers)	Presence of acid volcanic material (rhyolites, dacites) in the sediment.	Contains organic matter (U-trapped). Low U content compared to other reservoirs (<10 ppm U). The Beverley Sands are of limited extend and represent a littoral lacustrine formation.	
Namba Formation (kaolinite-alunite layers)	Leached under acidic and oxidative conditions. Presence of secondary U minerals Higher % of HM from MPD basement (corundum, U-rich zircons). *m*REE-enriched signature of the coffinite ore.	Kaolinite & alunite layers derive from the reworking from clayey pyrite-rich material. More likely to be a residual formation of mineralised alpha-mudstone and/or Four Mile ore type. Carnotite ages fit in the range 5.3 to 3.1 Ma, which is identical to the layer attributed age (pre 3.5 Ma).	Dating of alunite by K-Ar or Ar-Ar technique. Sulphur isotope on alunite.
Willawortina Formation	High U, REE & Th content (40 ppm U) with high proportion of metamict minerals.	Willawortina Fm mostly postdates the dated mineralizing event (5.3 – 3.1 Ma). Willawortina & Namba aquifers are not connected.	
Paralana High Plains crystalline basement	Presence of kaolinite in several level of Beverley (feldspar alteration directed from basement rocks). High U content. Proximity (present-day upstream). Location next to Poontana fault that may have be a conduit for fluids	Was essentially not outcropping and is partly capped by Cretaceous formation. Modern-day 'deep' groundwaters such as PHS is reduced (H_2S stable) and U-poor.	Lack of knowledge on the basement nature (granites, rhyolites, metasediments).
Four Mile Uranium deposit	Proximity (upstream) Uplift of the Paralana High Plains may have provided exposition of the ore to surface, developed acid sulphate soil.	Four Mile deposit could postdate the Beverley deposit. Similar grades of uranium could suggest similar genesis but not remobilisation downstream from Four Mile.	No information on possible weathered top soils horizons. No geochronology data. No geochemical or mineralogical information
Crystalline basement of the MPD	Presence of the Four Mile deposit even closer to the MPD. High U in the watershed (frequently >100 ppm U). Was sub- or outcropping before 3.5 Ma; Presence of Mesoproterozoic zircons (favours chemical over mechanical U transportation). Presence of angular sands in the Beverley Sands with Cretaceous zircons; this indicates low energy transportation from Cretaceous formations. Major Miocene uplift on Paralana fault (dated by fission tracks).	Was possibly covered by Cretaceous sediments (< 5 ppm U) over large parts.	Lack of information on the orientation of the watershed over the MPD during Pliocene and Miocene.

Table 8: Uranium reservoirs and their possible link to the Beverley Uranium deposit genesis

7.4 The source(s) of uranium

Where does the uranium source lies? The question aroused many answers by geologists and prospectors. R. W. Haynes writes about the origin of the uranium: "The geomorphology of the area and the proximity of the Beverley sedimentary uranium deposit to the relatively rich uranium source rocks of the Mt. Painter complex provide such an obvious association that it would be difficult to seriously consider any alternative origin for the uranium contained in Beverley" (Haynes, 1975). The same author also comments on the dispersion of radioactive sediments visible on airborne-radiometric data. It is effectively difficult to think differently when looking on the radiometric maps. The radiometric map (Fig. 36) which reveals the many uranium sources in the regional basement and the U/Th dispersion in the sediments towards the Lake Callabonna. The radioactive contrast given by the Mesoproterozoic granitoids is extreme and the dispersion can be followed up to 50 km downstream in the Yerila-Mudnawatana Creek to the North of the Mount Babbage Inlier. However, the current drainage do not necessarily reflect the paleo-environment during which mineralisation formed. For this reason, we need to consider all possibilities.

7.4.1 Potential uranium reservoirs identification

Here is an exhaustive list of the potential uranium reservoirs from which the uraniferous fluids could have originated and accounted for the Beverley ore genesis:

- The Namba Formation itself (Beverley Sands)
- The Alunite-sulphate soils over Namba Fm
- The Willawortina Formation
- The Crystalline basement under the Paralana High Plains
- An ancient exposed Four Mile uranium deposit type (Eyre Formation?)
- The Crystalline basement of the MPD in the watershed

The arguments for and against these possible reservoirs are listed in Table 8 without considering the quantities of uranium available in each of them.

Before discussing the possible sources of the uranium in Beverley, it is important to remember that the mineralisations are accompanied by a minor group of elements such as Fe, Cu, V, Co, Ni, MREE, As, Zn and Se. Some of them may have travelled with uranium from its source(s). The presence of MREE-enriched patterns in the uranium mineralisation is an element which strongly favours an origin where uranium is associated to REE-bearing rocks or sediments. More precisely, the source of REE's in the ore can originate from accessory minerals such as monazite or allanite to mention the most common ones in the region. These minerals are rare in the Namba sediments but abundant in the regional crystalline basement and the Willawortina formation sediments.

The presence of a minor population of Mesoproterozoic zircons in the Beverley Sands indicates the MPD was at least sub-cropping during the Miocene and this provides a potential argument for the direct derivation of uranium from the MPD as early as during the Miocene.

Acidic conditions (i.e. pH <4.5 necessary to form alunite) are able to efficiently leach out old metamict U-Th-bearing heavy minerals such as zircons but also allanite, thorite, monazite, polycrase, etc. Massive amounts of U and other traces can be liberated under acidic oxidising conditions (Bajo *et al.*, 1983a, Bajo *et al.*, 1983b). From the mineral analyses; we estimate the U and REE contribution from zircon to the Willawortina and Namba Sediments whole sediment: 10% of total U and 1.5% of total REE's. Our observations made in the Four Mile creek sediments closer to the ranges indicate the dominant hosts for U and Th are xenotime and monazite (~60% of total U). U-rich minerals like samarskite or polycrase are also present in the sediments and contribute to at least a few % of the bulk U. In conclusion, it is important to underline that Willawortina sediments and the MPD basement rocks have a higher availability of U for leaching than do the Namba sediments.

7.4.2 Mass balance calculation for uranium reservoirs

To complete the data on the potentiality of the identified sources of uranium, we estimated the quantities of uranium available from each, using the size of the different reservoirs and average values for U concentrations and estimating the U availability factor for release from the mineralogy: 1.00 for total availability to leaching (e.g. coffinite, uraninite), 0.2 to 0.1 for MPD basement rocks or Willawortina sediments (high metamict HM's content) and down to 0.05 in the case of uranium in the Namba sediments (U in crystalline HM's mostly). The details of the calculations are reported in Table 9.

Uranium reservoir	Evaluated sizes	Volume [km^3]	U [ppm]	U availability coefficient	Reservoir [x 10^6 tonne]	U reservoir [t U_3O_8]
Namba Formation (sandy aquifers)	15 x 5 km on 20 m	1.50	7	0.05	2700	1113
Namba Formation (kaolinite-alunite layers)	15 x 0.4 km on 2 m	0.012	15	0.80	21.6	305
Willawortina Formation (1) Willawortina Formation (2)	12 x 6 km on 50 m 6 x 2 km on 50 m	3.60 (0.60)	35	0.15	7920 (1320)	48993 (8165)
Paralana High Plains crystalline basement	5 x 5 km on 10 m (saprolith)	0.25	30	0.10	550	1944
Four Mile Uranium deposit type	1 x 0.3 km on 2.5 m	0.0008	5000	1.00	1.65	9721
Crystalline basement of the MPD	25 x 8 km on 10 m (saprolith)	10	25	0.10	22000	64805

Table 9: Mass balance calculation and evaluation of the potential uranium reservoirs for Beverley

Considering the tonnage of the Beverley mineralisation, including the sub-economic and unrecoverable resources, a global estimation sits around 30'000 t U_3O_8. The size of the mineralisation requires other sources than the Namba aquifers (~1000 t U_3O_8) or its weathered alunite-kaolinite capping (~300 t U_3O_8). In addition, because of their downstream location, these two reservoirs are not suitable for the genesis of the Four Mile deposit. The basement of the Paralana High Plains, which is outcropping in the vicinity of the Paralana Hot Springs, is also considered too small to have provided enough uranium for Beverley. The availability of this reservoir to uranium liberation is also subject to interpretation in the absence of an exact knowledge of its uranium content and whether it had some connection to the Namba aquifers.

Though the Four Mile deposit has not formally been included in this study, it is necessary to include it in the discussions and to consider the same reservoirs for its genesis. The entire tonnage of the deposit is not currently known and only 15'000 t U_3O_8 were indicated so far; however, there are indications that the deposit may reach 40'000 t of U_3O_8. Because of its location closer to the ranges and the MPD basement, the potential Willawortina reservoir becomes smaller and too small for providing enough uranium to the Four Mile deposit (Willawortina 2) on Table 9. The crystalline basement of the MPD remains the only possible reservoir that could have provided enough uranium for the Four Mile mineralisations.

Coming back to Beverley, the remaining reservoirs to consider are (a) the MPD basement, (b) some exposed Four Mile mineralisations upstream and also (c) the Willawortina formation.

The geochronological data indicates that most of the uranium mineralisation at Beverley predates the building-up of the Willawortina. This excludes this reservoir for the genesis of the deposit. For hydrogeologic reasons, the absence of interconnectivity between the Willawortina aquifers and the Beverley Sands aquifer also impedes this possibility. In conclusion, the remaining possible sources for Beverley are the MPD basement watershed, and the remobilisation to some extend of the Four Mile style-mineralisation upstream. This later source cannot be considered to be the unique source of uranium and does not rule out the direct origin in the MPD.

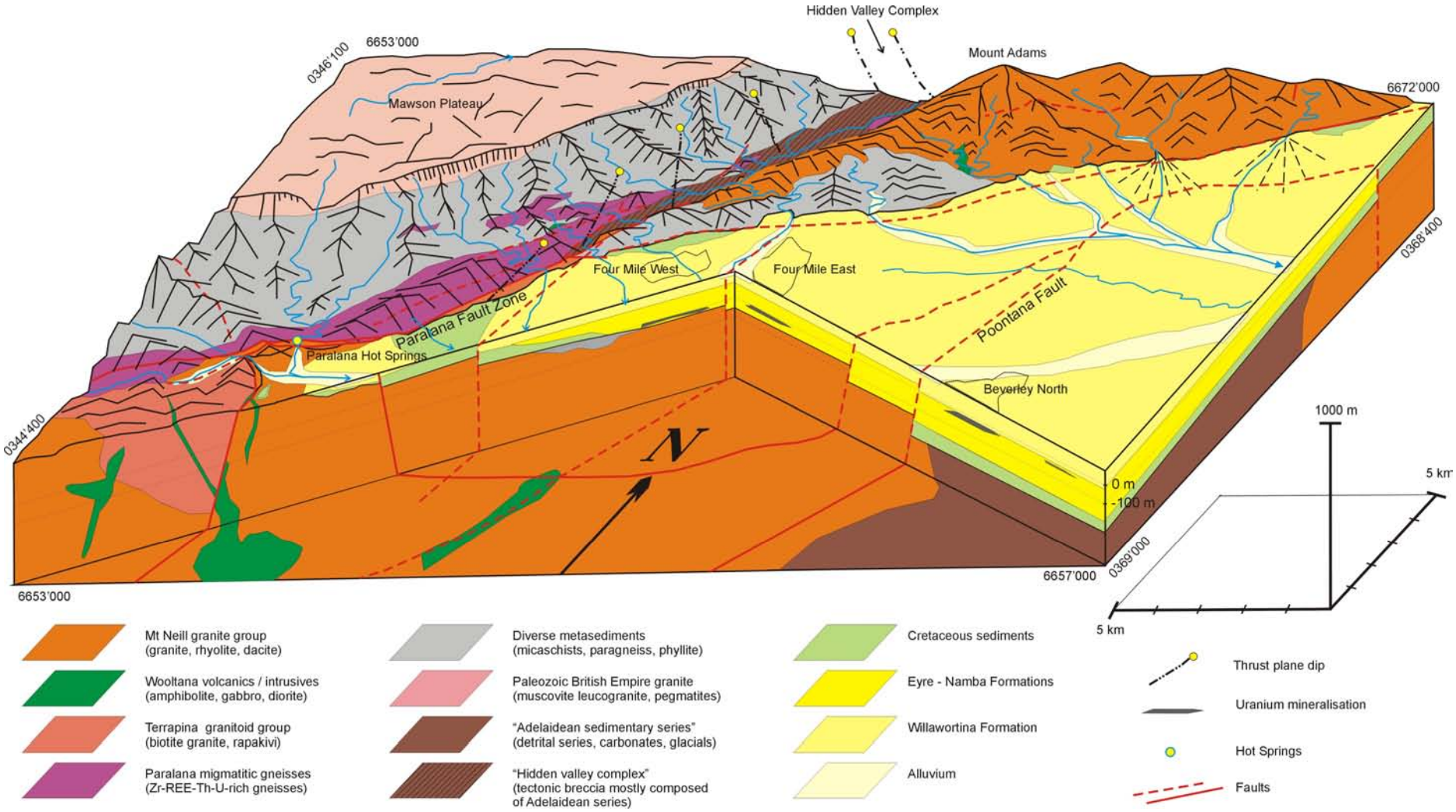

Fig. 37: Cross-section and perspective projection of the Paralana High Plains to the MPD

The geology reported on the figure is mostly inspired form the 1961 maps, with integration of new field information and the use of the radiometric (U) data to delimitates the migmatitic radioactive gneiss unit.

The figure has been drawn at scale with a vertical exaggeration. Faults reported in the basement window are partly from Heathgate Resources data and from personal interpretation.

7.5 The path of the mineralised fluids

To account for the sudden increase in Cretaceous sedimentary component in the Namba Formation, it is necessary to consider a Miocene-Pliocene uplift, which exposed the Cretaceous formations present on the crystalline basement or simply enhanced the relief, permitting their partial reworking into the lake watershed. The uplift considered here produced a flux inversion in the sedimentation at Beverley and a transition from lacustrine to littoral environment. This tectonic event produced some transpressive constraints towards the NW and a faulting along a network of NE-SW sub-parallel faults. The Paralana High Plains are the final result of several basement compartment uplifts on the Eastern side of the Paralana Fault Zone. The succession of uplifts along the faults under Paralana High Plains has lead to a progressive shoreline regression towards the East. The path of the fluids originating directly from the MPD was either perpendicular to the fault directions (maximum dip) or canalised along the fault overprint made to the surface (Fig. 38). This interpretation means that the uranium from Beverley could come from the West (through Four Mile) or alternatively from the NNE, following the Poontana fault lineament. The Paralana High Plains substratum can be schematised in a stairs-like group of blocks. Each of these blocks may have lead to the formation of shoreline structures in the Cenozoic formations.

The projection and cross-section on Fig. 38 also shows the altitudes of Four Mile (+ 20 m) and Beverley (-30 m). This underlines the possibility of gravity driven fluids crossing both deposits and precipitating their uranium in the appropriate environment. The thermoluminescence study of the quartz around Beverley complies with both possibilities, indicating the sediments to the West of the Poontana fault have been in contact with mineralisation (or mineralised fluids). The only data available to the NNE of Beverley also indicates an identical trend in this direction, indicating part of the uranium at least came from this direction. The data density is however low to the north of the deposit.

The period of time required to form the Beverley ore cannot be determined precisely. The geochronology data on carnotite and coffinite indicates at least 2-3 Ma.

8 Conclusions

The Beverley deposit is hosted in a detrital sandy local formation (Beverley Sands) of Miocene age. The angular quartz and the presence of coarse ferromagnesian minerals (hornblende) indicate a short transport of the sediments. The heavy minerals indicate that the mineral assemblage is unlikely to originate from the local inlier only (MPD); especially, the absence of corundum and the rarity of xenotime and monazite prove that the nearby outcropping crystalline basement was not the main sedimentary source. Both the typology (different from local rocks) and the U-Pb dating geochronology (different ages) of the zircons indicate that a different source is required. The presence of Cretaceous zircons (130 Ma) with volcanic textures and inclusions, calk-alkaline by typology, mixed with Permo-Carboniferous zircons of S-type granitoids origin can only be interpreted as coming from Eastern Australia (New England Orogen). The origin of these HM's is interpreted to be in the Cretaceous sediments (fluvioglacial and glacial origins) presents on the Paralana High Plains crystalline substratum and previously on the MPD.

The mineralisation of Beverley is mostly composed of coffinite with minor uraninite, copper, pyrite, marcasite, carnotite, sphalerite, lead, barite, chalcopyrite and kaolinite. The presence of reduced mineral species such as lead witnesses the occurrence of highly reducing microenvironments ($fCH_{4(g)} >> fCO_{2(g)}$). Using the groundwater composition and the observed mineralogy, the prevailing conditions during the mineralisation have been estimated at: pH 6.3-8.4, with log fO_2 from -50 to -70 at 25°C. The reduction is essentially bacterial (negative $\delta^{34}S$) and require the consumption of organic matter (commonly observed in the mudstone). Uranium reduction by H_2S was ineffective in Beverley. The uranium mineralisation formed by reduction of uranyl-bearing groundwaters by organic matter and methane. The ore and coffinite nodules show *m*REE enriched PAAS-normalized patterns, which can be explained by fluid interaction on REE-bearing minerals in the source-rock of uranium. This information indicates that the uranium source is REE-rich.

The upper part of the mineralisation at Beverley has a different mineralogy, which records acidic oxidising conditions (carnotite, no coffinite, alunite, kaolinite, goethite, gypsum). The prevailing conditions were between *p*H 3.9 and 4.5 and with log fO_2 from -0 to -30 at 25°C. This physico-chemical environment of the Beverley Clays is interpreted to postdate the main mineralisation event and to be the result of an exposure of pyrite-rich mudstones to the surface by uplift of the some basement blocks along fault structures (e.g. Poontana fault).

The U-Pb geochronology ages obtained on coffinite and carnotite (6.7 to 3.4 Ma) indicate the mineralisation to have occurred mostly or fully, prior the Pliocene-Quaternary Willawortina deposition (from 3.5 to 0.7 Ma). The paleoenvironment reconstitutions obtained from the sedimentological data help to understand the Paralana High Plains substratum geometry as a succession of basement blocks uplifted relative to each others and providing Cretaceous materials to the Beverley Sands. The 3D projection favour to possible ways to the uranium–bearing solutions towards Beverley: (1) from the MPD through Four Mile deposit area and (2) along a NNE to SSW corridor following a paleo-shoreline due to the uplift of the Paralana High Plains to the West.

There are six possible sources of uranium for the Beverley ore genesis: (1) Namba Beverley Sands (2) Namba Beverley Clays alunite soils, (3) Willawortina formation, (4) Paralana High Plains substratum, (5) Four Mile uranium mineralisations upstream and (6) the MPD basement. From these sources, mass-balance calculations indicate that only the (3) Willawortina, (6) MPD basement and to some extend (5) Four Mile mineralisations could have brought enough uranium to form the Beverley deposit. For the geochronological, geochemical and sedimentological reasons mentioned early on, the Willawortina is not considered to be the source of uranium for Beverley, although its uranium release potential remains extremely high. The source hence is necessarily the crystalline basement of the MPD.

8.1 Implications for new uranium deposits findings and recommendations

The reconstitution of the genesis of the Beverley was made possible using a range of different techniques: heavy minerals assemblages from the ore and the nearby sediments, whole-rock and mineral geochemistry and finally the integration of the regional geology to link the data collected at the deposit location.

The Beverley deposit has already proven its economic viability. The active prospecting around the mine, which leads to the discovery of the Four Mile deposit, proves the exceptional potential of the Paralana High Plains district. For the future prospecting programs, a few data are going to be essential to compare the different mineralisations and to understand their links:

- U-Pb dating of the mineralisation (includes U mineralogy identification).
- Whole-rock geochemistry of ore (REE, Cu, Mo, Se, As, V and S) to recognise the uranium sources characteristics (possibly more Cu, Mo and Se for the Four Mile deposit).

- Recognition of paleosoils or paleosurfaces with alunite-jarosite minerals or oxidation features, roots, etc… to understand the secondary uranium remobilisations and transportation (if present).
- Recognising the substratum structures and faults propagated into the sedimentary succession and following these lineaments in the direction of the paleoslopes toward the source of the uranium (uranium traps).
- For the search of new uranium deposits on the west and the north of the MPD, the presence of "key" heavy minerals like corundum, alkaline zircons or "hydrothermal" zircons can provide the proof that an ancient drainage issued from the MPD existed in there. This knowledge will become particularly important for assessing the potentiality of the Mesozoic formations of the Eromanga basin.

Some of the results of this research such like the REE pattern of the ore and its age would have directed the exploration towards the hill ranges. Similarly, the mineralisation age (Pliocene or older) would have helped to understand the formation of the deposit and lead the explorers to look under the thick Willawortina Formation closer to the ranges decades ago.

The uranium sources in the MPD can be considered as unlimited for providing uranium to the neighbouring basins. The near surface MPD rocks from the Paralana High Plains watershed and the Willawortina formation contain ~ 120'000 tonnes U_3O_8 using only 10% U availability from a near-unconformity layer. Similar settings (vicinity to the MPD, presence of Post-Mesozoic faults, presence of porous Cenozoic formation, presence of organic matter) can be found to the East of the Mt Neill – Mt Adams block, as well as to the North of the Mt Babbage inlier. If additional geochronology data on uranium mineralisations could match the Pliocene age found at Beverley (e.g. at Four Mile), a precise reconstruction of the paleoenvironment around the MPD at this time would bring a powerful tool to direct the future exploration, especially along paleolittoral features.

The sedimentary province close to the MPD can be considered as an exceptional setting because of its vicinity to exceptionally uranium-rich basement rocks. It remains highly prospective for finding new uranium mineralisations and it is not aberrant to think the province hosts more uranium resources than the entire surficial calcrete-hosted uranium province of Western Australia. Taking into account the feasibility of using ISL technique to mine uranium at Beverley but also Four Mile (recently announced), the environmental impact of developing such a uranium province is clearly the lowest and provides a lot of advantages. However, the application of the ISL technique relies on the occurrences of a very "unlikely" set of perfect sedimentological features (lacustrine shores, high porosity angular sands from glacial origin, presence of an exceptionally rich uranium province). This seriously restricts its application.